Infiltration from the pedon to global grid scales: An overview and outlook for land surface modelling

Harry Vereecken[1,2], Lutz Weihermüller[1], Shmuel Assouline[3], Jirka Šimůnek[4], Anne Verhoef[5], Michael Herbst[1], Nicole Archer[6], Binayak Mohanty[7], Carsten Montzka[1], Jan Vanderborght[1], Gianpaolo Balsamo[8], Michel Bechtold[9], Aaron Boone[10], Sarah Chadburn[11, 12], Matthias Cuntz[13], Bertrand Decharme[10], Agnès Ducharne[14], Michael Ek[15], Sebastien Garrigues[16], Klaus Goergen[1, 18], Joachim Ingwersen[19], Stefan Kollet[1], David M. Lawrence[20], Qian Li[21], Dani Or[22], Sean Swenson[23], Philipp de Vrese[24], Robert Walko[25], Yihuan Wu[26], Yongkang Xue[27]

[1] Agrosphere Institute IBG-3, Forschungszentrum Jülich GmbH, 52425 Jülich, Germany

[2] International Soil Modeling Consortium (ISMC), Forschungszentrum Jülich GmbH, Jülich, Germany

[3] Dept. of Environmental Physics and Irrigation, Institute of Soils, Water and Environment Sciences A.R.O - Volcani Center, ISRAEL

[4] Dep. of Environmental Sciences, Univ. of California Riverside, Riverside, CA 92521.
[5] University of Reading, Department of Geography and Environmental Science, Reading, UK

[6] British Geological Survey, The Lyell Centre, Research Avenue South, Edinburgh, EH14 4AP, Scottland

[7]Texas A&M University, Department of Biological and Agricultural Engineering, Texas USA

[8] European Centre for Medium-range Weather Forecasts, ECMWF, Reading, UK

[9] KU Leuven, Dept of Earth and Environmental Sciences and Dept of Computer Science, 3001 Heverlee, Belgium

[10] CNRM, UMR3589 (Météo-France, CNRS), Toulouse, France

[11] University of Leeds, School of Earth and Environment, Leeds LS2 9JT, UK

[12] University of Exeter, Laver Building, Exeter EX4 4QE, UK

[13] INRA, Université de Lorraine, AgroParisTech, UMR Silva, 54000 Nancy, France

[14] Sorbonne Université, CNRS, EPHE, UMR 7619 METIS, Paris, France

[15] National Centers for Environmental Prediction/Environmental Modeling Center, College Park, Maryland

[16] French National Institute for Agricultural Research (INRA) INRA, CESBIO, Toulouse, France

[17] Centre for Ecology and Hydrology, CEH, Wallingford, UK

[18] Centre for High-Performance Scientific Computing in Terrestrial Systems, Geoverbund ABC/J, 52425 Jülich, Germany

[19] Institute of Soil Science and Land Evaluation, Biogeophysics, University Hohenheim, 70599 Stuttgart, Germany

[20] National Center for Atmospheric Research, Boulder, CO, USA

[21] Center for Monsoon Research, Institute of Atmospheric Physics, Chinese Academy of Sciences,Beijing, China.

[22] ETH Zurich, Institut für Biogeochemie und Schadstoffdynamik, 8092 Zürich, Switzerland

[23] Climate and Global Dynamics Laboratory, Terrestrial Sciences, NCAR Bolder Colorado, USA

[24] Max-Planck Institut for Meteorology, The Land in the Earth System, Hamburg, Germany

[25] University of Miami, RSMAS; 33149 Miami, FL, USA

[26] National Centers for Environmental Prediction/Environmental Modeling Center, and I. M. System Group at NCEP/EMC, College Park, Maryland

[27] Department of Atmospheric and Oceanic Sciences, Department of Geography, University of California, Los Angeles, Los Angeles, California, USA

Core ideas:

Land surface models (LSM) show a large variety in describing and upscaling infiltration

Soil structural effects on infiltration in LSM are mostly neglected

New soil databases may help to parametrize infiltration processes in LSM

Keywords: land surface models, infiltration, soil structure, upscaling, soil databases

Content

Abstract

Infiltration in soils is a key process that partitions precipitation at the land surface in surface runoff and water that enters the soil profile. We reviewed the basic principles of water infiltration in soils and we analyzed approaches commonly used in Land Surface Models (LSMs) to quantify infiltration as well as its numerical implementation and sensitivity to model parameters. We reviewed methods to upscale infiltration from the point to the field, hill slope, and grid cell scale of LSMs. Despite the progress that has been made, upscaling of local scale infiltration processes to the grid scale used in LSMs is still far from being treated rigorously. We still lack a consistent theoretical framework to predict effective fluxes and parameters that control infiltration in LSMs. Our analysis shows, that there is a large variety in approaches used to estimate soil hydraulic properties. Novel, highly resolved soil information at higher resolutions than the grid scale of LSMs may help in better quantifying subgrid variability of key infiltration parameters. Currently, only a few land surface models consider the impact of soil structure on soil hydraulic properties. Finally, we identified several processes not yet considered in LSMs that are known to strongly influence infiltration. Especially, the impact of soil structure on infiltration requires further research. In order to tackle the above challenges and integrate current knowledge on soil processes affecting infiltration processes on land surface models, we advocate a stronger exchange and scientific interaction between the soil and the land surface modelling communities.

1. General Introduction

Infiltration or water entry into the soil profile is a key process in the hydrological cycle. Its rate and dynamics affect the partitioning of precipitation at the land surface and determines the onset of ponding and consequently, the formation of overland flow and runoff. Infiltration affects irrigation efficiency over managed lands and the resulting stored soil water available to vegetation (e.g., Verhoef and Egea-Cegarra, 2013), overland flow and soil erosion processes (e.g., Assouline and Ben-Hur, 2006, Garrote and Bras, 1995, Poesen et al., 2003), groundwater recharge (e.g., Dahan et al., 2008), the exchange of water and energy between the soil and atmosphere by controlling soil water content at the surface (Kim et al., 2017, MacDonald et al., 2017), and with this the flux partitioning into latent and sensible heat flux with multiple atmospheric feedbacks (e.g., Keune et al., 2016, Seneviratne et al., 2010), stream flow and flooding events (Garrote and Bras, 1995), and various soil physical processes such as the onset of landslides (Lehmann and Or, 2012) and soil mechanical stress-strain behavior. The spatial distribution of infiltration rates is affected by soil type, local topography and attributes of surface cover. Infiltration feedbacks have been shown to drive the formation of vegetation patterns. Infiltration rates are crucial inputs to design any irrigation system and many soil and water conservation practices. The significance of infiltration made it a subject of studies in many domains ranging from hydrology, agricultural, environmental and civil engineering.

Even at the single profile scale, infiltration exhibits strong dynamics that are dependent on soil properties, rainfall characteristics, wetting rates, vegetation cover and type, soil and crop management, and initial and boundary conditions within the soil flow domain. Based on the definition of Hillel (1980) and Brutsaert (2005) infiltration is defined as "the entry of water into the soil surface and its subsequent movement through the soil profile". The sources of liquid water for infiltration include direct precipitation (rainfall, dewfall, and snow melt), leaf drip and stem flow, irrigation, or runoff that was routed over the land surface and re-infiltrates (a process termed *runon*). A detailed understanding of the primary controls on infiltration rates and the onset of ponding with subsequent runoff, and their translation into model equations, is of great importance at all scales. The accurate process representation of infiltration is also essential for crop water use studies, the design of irrigation systems, and the optimal management of water resources. Different approaches have thus been developed over the past decades to provide quantitative tools able to describe and predict infiltration into porous media in soils, ranging from empirical expressions, to analytical and numerical solutions of the basic flow equations.

Infiltration dynamics are determined by soil properties (hydraulic conductivity, sorptivity), the hydraulic gradients that drive flow, and initial and boundary conditions (Philip, 1957). Depending on the initial soil water content in the soil profile, the water supply rate and the corresponding soil wetting dynamics, all the available water can infiltrate in different amounts into the soil. Hence, these factors will influence the infiltration curve (the change with time of the infiltration rate during a wetting event) (Mein and Larson, 1973).

The infiltration capacity or potential infiltration rate of a soil, $q_{cap}(t)$, is the maximum rate at which the soil surface can take up water for given initial conditions (Horton, 1940). The actual infiltration capacity is also affected by the initial soil water content of the soil, but for practical considerations it may be considered a time-dependent soil property where water inputs in excess of this maximum infiltration rate will pond and likely generate runoff. For surface fluxes at rates lower than the soil's infiltration capacity, the realized infiltration rate will depend upon the state of the soil (as shaped by the temporal history of the application rates and the consecutive sequences of wetting and drying). Two infiltration regimes in unsaturated soils can be distinguished and lead to different occurrence times of ponding and thus runoff generation: constant water supply (occuring during irrigation or simulated rainfall) and variable rate supply (during natural rainfall) as is shown in Figures 1 and 2, in terms of rates (top panel) or cumulative depths (bottom panel; in this case capital symbols are used).

The dashed curves in Figure 1 and 2 represent the infiltration capacity, $q_{cap}(t)$ [L T^{-1}] or $Q_{cap}(t)$ [L], of a given soil profile, the dotted line depicts the water supply rate, $r(t)$ [L T^{-1}] or $R(t)$ [L], for the constant precipitation rate (Fig. 1) or for the variable precipitation rate one, as it is often the case during natural rainfall (Fig. 2), and the solid line shows the actual infiltration rate, $q(t)$ [L T^{-1}] or $Q(t)$ [L], during these events. In case of the constant $r(t)$, all the applied water can infiltrate in the first stage of wetting (Fig. 1), and $q(t) = r(t)$. Compared to $q_{cap}(t)$ corresponding to an unlimited water application rate, $q(t)$ can be higher than q_{cap}(t) because the hydraulic gradients resulting from the unsaturated condition generated by the limited wetting rate, $r(t)$, are larger than the ones that result from the saturated condition inherent to the unlimited wetting rate. However, both curves tend towards a similar "quasi-steady" infiltration rate corresponding to a gradient of unity, but approach it at different rates resulting from the difference in the rate of decrease of the hydraulic gradients corresponding to each wetting condition. As wetting progresses, $q(t)$ begins to decrease, and at the time of ponding, t_p, where the infiltration rate, $q(t_p)$ is smaller than the wetting rate, $r(t_p)$, ponding occurs at the soil surface.

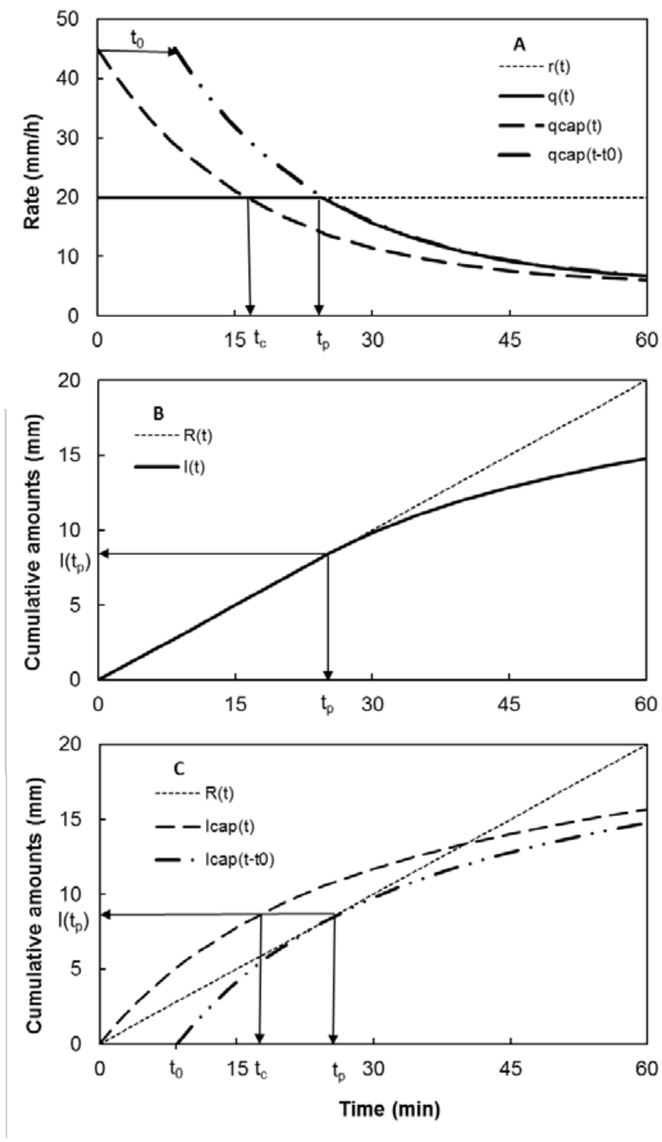

Figure 1: *(A) Illustrative representation of the infiltration capacity rate, $q_{cap}(t)$ (dashed curve) and the actual infiltration rate, $q(t)$ (solid line) of a soil profile exposed to a rainfall event with constant intensity $r(t)$ (dotted line). The time t_c denotes the moment where $q_{cap}(t)=r(t)$, while the time t_p denotes the ponding time where $q(t)=r(t)$. Shifting the representation of $q_{cap}(t)$ by $t_0=(t_p-t_c)$ (dashed-dotted line) allows to estimate t_p. (B) Illustration of t_p in terms of the cumulative infiltration, with $I(t_p)=R(t_p)$. (C) Cumulative infiltration capacity $I_{cap}(t)$ (dashed line) and cumulative rainfall $R(t)$ (dotted line). The ponding time t_p can be estimated by means of $I_{cap}(t-t_0)$ (dashed-dotted line).*

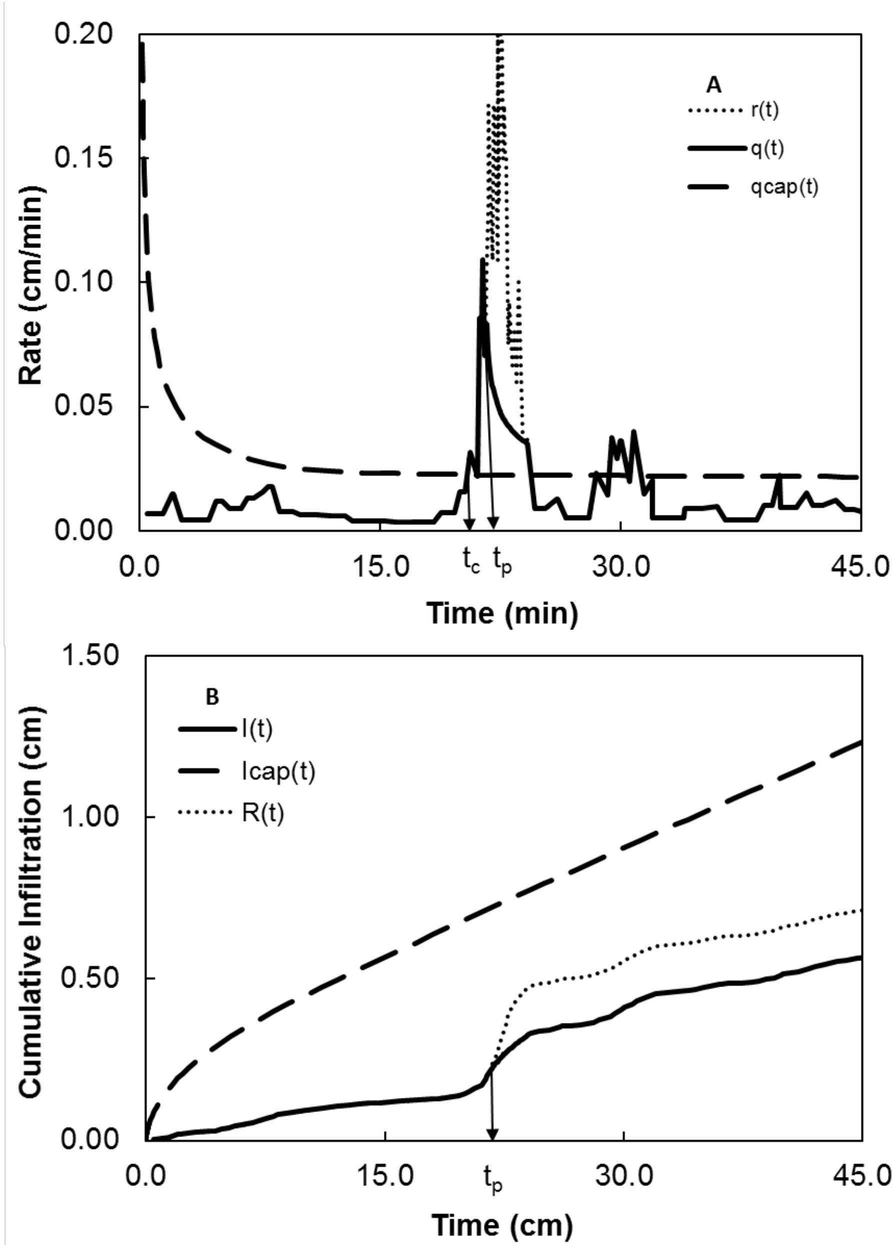

Figure 2: *(A) Illustrative representation of the infiltration capacity rate, $q_{cap}(t)$ (dashed curve) and the actual infiltration rate, $q(t)$ (solid line) of a soil profile exposed to a rainfall event with variable intensity $r(t)$ (dotted line). For low $r(t)$ values below $q_{cap}(t)$, $q(t)=r(t)$, and the result is that t_c is close to t_p. (B) Cumulative infiltration capacity $I_{cap}(t)$ (dashed line), cumulative actual infiltration, $I(t)$ (solid line), and cumulative rainfall $R(t)$ (dotted line). In this case, t_p cannot be estimated by means of $I_{cap}(t_p\text{-}t_0)$. The figure was adapted from Assouline et al. (2007).*

In terms of cumulative infiltrating volumes of water (or water depths, which are volumes per unit area). (Fig. 1-lower) $Q(t)$ is always smaller than $Q_{cap}(t)$ even when $q(t)$ was higher than $q_{cap}(t)$, indicating that the concept of infiltration capacity corresponds to cumulative infiltration rather than to infiltration rates. Since the wetting rate is constant, the picture in terms of infiltration rates (Fig. 1, upper) and cumulative depths (Fig. 1, lower) provide similar condition for t_p. Corresponding to the time where $Q(t)$ departs from $R(t)$. It is interesting to note; that if it is assumed that ponding occurs when $r(t)$ exceeds $q_{cap}(t)$, t_p is underestimated (Fig. 1, upper). The infiltration regime under variable $r(t)$ and the prediction of t_p is much more complicated as $q(t)$ depends on the pattern of $r(t)$ (Fig. 2, upper). The picture is much simpler when expressed in terms of cumulative depths (Fig. 2, lower). Assouline et al. (2007) have proposed a simple method to estimate $t_p$under variable $r(t)$.

The cases described in Figs. 1 and 2 represent one mechanism of runoff formation termed infiltration excess or Hortonian overland flow (Horton, 1933). Another important mechanism corresponds to the formation of a saturated topsoil layer that enhances runoff formation. This mechanism is termed saturation excess or Dunne overland flow (Dunne, 1978, Freeze, 1980). Dunne overland flow occurs when the soil reaches saturation from above, via direct precipitation, or below and no additional water supplied from the top can be stored in the soil profile. This can happen, for example, when the local water table is high or a hydraulically impeding layer close to the soil surface exists (causing a so-called 'perched' water table). In general, the Dunne mechanism occurs in areas close to the channels of the drainage network of a catchment or in areas in the low lying parts of a catchment where the depth to the water table is shallow. It is therefore more common in humid climates. These saturated runoff source areas vary in size, seasonally and during individual storm events. Therefore, they are often referred to as variable source areas (VSA) (Dunne and Black, 1970), and the runoff generated on them as VSA runoff (as e.g. in the TOPMODEL (Beven and Kirkby, 1979), which is implemented (sometimes in modified form) in many land surface models. On the other hand, Hortonian overland flow is more common in semi-arid climates (Entekhabi and Eagleson, 1989).

Infiltration theory, and related numerical and analytical solutions, was originally the domain of soil physicists. Several reviews on different aspects of infiltration into soils have been published (Assouline, 2013, Barry et al., 2007, Clothier, 2001, Gardner, 1960, Hopmans et al., 2007, Parlange, 1980, Parlange et al., 1999, Philip, 1969, Philip and Knight, 1974, Raats, 2001, Raats et al., 2002, Skaggs, 1982) and also constitute key chapters in textbooks (e.g., Bear, 1972, Brutsaert, 2005, Childs, 1969, Chow et al., 1988, Delleur, 2006, Hillel, 1998, Warrick, 2003). The fundamental concepts of infiltration have been applied in hydrology to deal with the prediction of infiltration at the field scale (Corradini et al., 2011, Govindaraju et al., 2012, Morbidelli et al., 2006),on hillslopes (e.g., Morbidelli et al., 2018), for heterogeneous soil systems (Govindaraju et al., 2001), and to handle the impact of complex precipitation events and patterns on infiltration (Corradini et al., 1994, Corradini et al., 1997).

With the advent of efforts to model the global water and energy cycles at the large-scale, infiltration theory was taken up by the climate and hydrological modelling community. Largely due to the (originally) limited computing power and the difficulty in defining spatially distributed and appropriately upscaled soil parameters, simplifications and approximations of the infiltration process were introduced into the land surface models (LSMs) embedded in weather and climate models. The main role of a LSM is to compute the energy partitioning at the interface between land surface and atmosphere. At the land surface, net radiation is converted into latent heat, sensible heat and ground heat flux, where the latent heat flux is the equivalent of the evapotranspiration flux in the water balance, but in this case expressed in energy units. The energy partitioning at the land surface directly affects the state of the atmosphere. For example, the relative magnitude of the latent and sensible heat flux will modify atmospheric state variables such as relative humidity and the height of the atmospheric boundary layer, which in turn will affect cloud forming processes, and ultimately rainfall. Infiltration acts on this energy partitioning indirectly via its control on soil moisture content. Near-surface soil moisture content is an important state variable in both the water and energy balance. For example, it affects net radiation due to its effects on land surface radiative properties, albedo and emissivity. Also, both soil evaporation and transpiration depend strongly on soil moisture content. A reduction in soil moisture content will lower evaporation via a reduced soil-atmosphere vapour gradient, and decreased replenishment of water to the evaporation front due to reduced hydraulic conductivity, whereas transpiration is affected via a decrease in root water uptake during drought conditions. Finally, because soil thermal conductivity and heat capacity are functions of soil moisture, infiltration also indirectly affects the soil heat regime. Anwar et al. (2018) showed that the choice of the infiltration scheme had a significant effect on the simulated regional climate. The infiltration scheme with the lower soil infiltration rate yielded a lower topsoil soil moisture that led to a lower latent heat flux and a higher sensible heat flux resulting in a net warming effect within the simulation domain.

With regard to the simulation of infiltration a range of approaches at different levels of complexity currently exists in these models.

Paniconi and Putti (2015) reviewed the last five decades of physically based numerical models in hydrology and addressed the treatment of infiltration from local via hillslope to catchment scale. They focused on the flow path heterogeneity, whereby the analysis has been focused on the non-linearity and upscaling in hydrology with a specific focus on numerical methods used in hydrological models and related computational challenges. They briefly discussed the seminal work of Horton (1933), Betson and Marius (1969), and Dunne and Black (1970) in identifying the main mechanisms of runoff generation, which is closely related to the infiltration process.

Zhao and Li (2015) reviewed the different approaches to model land surface processes over complex terrain. The main focus was on the role of grid scale spatial heterogeneity of land surface variables and parameters (e.g., soil moisture content, net primary productivity, leaf area index (LAI), fraction of vegetation cover) and the topographic impact on key atmospheric controls (e.g., precipitation, air temperature, wind speed, air pressure). The role of infiltration and its different parameterization was briefly addressed in relation to the spatial variability of soil hydraulic properties in complex terrains.

Clark et al. (2015) analyzed the state-of-the-art of infiltration processes in land surface models. They concluded that the main challenges are in the appropriate treatment of the small-scale heterogeneity to describe the large-scale fluxes of infiltration and surface runoff, and the need for an improved description of wetting front dynamics, which may lead to improved simulations of infiltration and surface runoff during heavy rainfall. More recently, Mueller et al. (2016) examined the potential of the land surface models SWAP, JULES, and CH-TESSEL to produce surface runoff for intense rainfall events. Based on the results, they recommend that future work should consider a correction of the maximum infiltration rate in JULES and to investigate its numerical scheme in order to make it suitable for high vertical resolution. Recently, Morbidelli et al. (2018) reviewed the role of slope on infiltration. They pointed out the need to further develop upscaling approaches up to catchment and subgrid scale and to establish a theoretical framework to describe infiltration on hillslopes to better explain experimental observations that have become available in the recent years.

In this review, we will briefly recapitulate the main approaches and solutions derived from soil physical theory to describe infiltration processes at the point and field scale and the techniques used to numerically solve the infiltration processes, and finally to quantify the impact of spatial variability on infiltration. Hereby, we will focus on infiltration processes in non-frozen soils. We will present the infiltration approaches used in various land surface models and address how maximum infiltration capacity is quantified, how soil moisture and spatial variability of soil properties are parameterized, and how the areal saturation fraction, F_{sat}, important for Hortonian runoff, is estimated. We will also identify key soil parameters that affect the soil infiltration and runoff and present upscaling approaches for soil hydraulic parameters applicable to the grid scale of land surface models. Finally, we will present an outlook and future perspectives on modeling infiltration in land surface models.

2. Quantitative Expression of the Infiltration Process at the Point Scale

2.1. Basic Physical Models of Soil Water Flow and Infiltration

The chronological development of three main approaches in the conceptual modeling of infiltration in porous media is presented in the following.

Darcy (1856) formulated the first quantitative description of flow through a saturated porous medium, known as *Darcy's Law*:

$$\boldsymbol{J = -K_s \frac{\partial H}{\partial z}} \qquad [1]$$

where J is the Darcian flux of water [L T^{-1}] at time t [T], K_s is a proportionality constant characterizing the medium and named “the saturated hydraulic conductivity” [L T^{-1}], and $\frac{\partial H}{\partial z}$ [-] is the hydraulic gradient calculated form the differences in total hydraulic head (H) and the (vertical) distance z [L] within the saturated porous medium (in saturated soils, the total head H is the sum of pressure (h) and elevation heads (z)).

Buckingham (1907) proposed to extend Darcy's law to unsaturated water flow, where the actual water content in the porous medium, θ, is lower than its maximum value at saturation, θ_s. The main assumption is that the constant saturated hydraulic conductivity value, K_s, could be replaced by a function of soil water content, θ, or matrix potential, h, as the characteristic of the unsaturated porous medium. That function was named “the unsaturated hydraulic conductivity function”, and given the symbol $K(\theta)$ or $K(h)$. Following the notation of Eq. (1), the resulting unsaturated flow equation resulting from Buckingham’s assumptions is:

$$\boldsymbol{J = -K(h)\frac{\partial H}{\partial z} = -K(h)\left(\frac{\partial h}{\partial z} + 1\right)} \qquad [2]$$

where z [L] is the vertical coordinate being positive upward and $z = 0$ representing a prescribed reference level. In this case, the total head H is the sum of the matrix potential in head units, h, and the gravitational head z.

Finally, Richards (1931) combined the flow equation of Buckingham (1907) (Eq. 2) and the principle of continuity assuming an infinitely mobile air phase in the soil (zero resistance to air flow). The resulting well-known and widely used one-dimensional expression for the vertical water flow is given by:

$$\frac{\partial \boldsymbol{\theta}}{\partial \boldsymbol{t}} = \frac{\partial}{\partial \boldsymbol{z}}\left[\boldsymbol{K}(\boldsymbol{h})\left(\frac{\partial \boldsymbol{h}}{\partial \boldsymbol{z}} + \mathbf{1}\right)\right] \qquad [3]$$

Eq. 3 requires the definition of an additional characteristic of the porous medium, this is the soil water retention curve (WRC), where the actual water content is a function of the matrix potential, $\theta(h)$.

The $\theta(h)$ and $K(h)$ functions represent the hydraulic properties of the porous medium. An up-to-date presentation of the mathematical expressions (e.g., Brooks and Corey, 1964, Van Genuchten, 1980) used to quantify these properties in soils can be found in the review of Assouline and Or (2013).

The Brooks and Corey (1964) retention function is given by:

$$S_e(h) = \left(\frac{h}{h_c}\right)^{-\lambda_p} ; h < h_c \qquad [4]$$

$$S_e(h) = 1 \qquad ; h \geq h_c$$

where h_c is the matric potential at air entry value [L^{-1}], λ_p is a dimensionless pore size distribution index [-], h is the pressure head [L], and S_e is the effective saturation [-] given by:

$$S_e = \frac{\theta - \theta_r}{\phi - \theta_r} \qquad [5]$$

where S_e is the effective saturation [-], θ is the actual water content [$L^3 L^{-3}$], θ_r is the residual water content [$L^3 L^{-3}$], and ϕ is the porosity [$L^3 L^{-3}$], which can be related to θ_s as the saturated water content.

The corresponding unsaturated hydraulic conductivity function is expressed by:

$$K = K_s S_e^{(3+2/\lambda_p)} \qquad [6]$$

where K_s is the saturated hydraulic conductivity [$L\ T^{-1}$].

The water retention function proposed by Van Genuchten (1980) is given by:

$$\theta(h) = \theta_r - \frac{\theta_s - \theta_r}{\left(1 + |h/h_c|^{n_{vg}}\right)^m} \qquad [7]$$

where *m* is a shape factor [-] often assumed to be related to n_{vg} by $m = 1 - 1/n_{vg}$. This function is continuous in *h* and present an inflection point, making it more appropriate for application in numerical solutions.

Applying the model of Mualem (1976) to Eq. 7 leads to the following unsaturated hydraulic conductivity function:

$$K(h) = K_s S_e^l \left[1 - \left(1 - S_e^{1/m}\right)^m\right]^2 \qquad [8]$$

where *l* is a fitting parameter depending on the soil type [-].

The Richards equation (Eq. [3]) represents the actual physical model that can be used to simulate and illustrate the infiltration process in porous media. It addresses only the macroscale behavior and is valid for a representative volume for which the prescribed hydraulic properties can be applied. The solution of the Richards equation requires the definition of initial and boundary conditions. When water is ponding at the soil surface, infiltration is governed by the hydraulic head at the soil surface, a concentration type boundary condition known also as a Dirichlet boundary condition. When the water application rate is below the soil infiltration capacity, a flux or Neumann boundary condition can be applied at the soil surface. Since Eq. [3] is highly nonlinear due to the non-linear character of the hydraulic conductivity function [$K(h)$ or $K(\theta)$], analytical solutions can only be derived for specific initial and boundary conditions, and with knowledge of the soil hydraulic properties. Consequently, solutions to practical soil water flow problems generally require the use of numerical schemes designed to solve partial differential equations.

2.2. Empirical Infiltration Equations

The necessity to describe quantitatively such a crucial hydrological process as infiltration combined with the complexity of the solution of the flow equation (Eq. [3]) led to the development of empirical expressions relating infiltration rate, *q*, to time *t*. From Fig. 1 it can be seen that, for a constant water supply, *r(t),* infiltration rate *q(t)* gradually decreases and tends towards a steady final infiltration rate, q_f. Consequently, the different forms of the suggested empirical equations describing infiltration are all monotonically decreasing functions based on exponential or power law decays, for which the parameters do not generally have a physical meaning and are evaluated by fitting to experimental data.

In general, there are two main families of equations used to describe the infiltration process, whereby one is based on the original formulation of Horton (1941) and the other on those presented by Kostiakov (1932). Over time, both equations were modified and extended by various authors such as the Kostiakov model by Lewis (1937), Mezencev (1948), Smith (1972), Parhi et al. (2007), and Furman et al. (2006) to account for different initial and boundary conditions. The original formulation proposed by Horton (1941) predicts an exponential decay of the infiltration flux q over time t by:

$$q(t) = q_f + (q_i - q_f)e^{-\alpha_K t} \qquad [9]$$

where q is the infiltration rate [L T^{-1}], q_f is the final (constant) infiltration rate [L T^{-1}], q_i is the initial infiltration rate [L T^{-1}], and α_K is the decay constant (T^{-1}). For $t \to \infty$, q_f can be related to the hydraulic conductivity of the wetted soil layer.

On the other hand, Kostiakov (1932) introduced a power law equation with two fitting parameters n_K and β_K in the form of:

$$q(t) = q_f + n_K \beta_K t^{(\beta_K - 1)} \qquad [10]$$

where n_K and β_K depend on initial and boundary conditions of the soil system.

2.3. Analytical and Semi-analytical Infiltration Description

Compared to the empirical models, analytical and semi-analytical equations based on Richards equation were also developed, wereby Philip (1957) and Philip (1969) presented the first analytical solution to the Richards equation. It considers infiltration as a sorption process with a perturbation generated by the presence of gravity. Therefore, this method corresponds by definition to the first stages of infiltration into a relatively dry soil profile where gravity plays only a minor role. It can therefore be expected to be applicable for small and intermediate values of time (Brutsaert, 2005, Hillel, 1998). Because the original solution, in the form of a power series, diverges for large values of time, Philip (1957) proposed to use a truncated version of the original solution, considering the first two terms of the series:

$$q(t) = \frac{1}{2} S_{op} t^{-\frac{1}{2}} + A \qquad [11]$$

where S_{op} is defined as the soil sorptivity [L T^{-2}], t is time [T], and A is a fitting parameter [-]. Note that Eq. [11] is equivalent to Eq. [10] for β_K = 1/2, n_K= S_{op}, and q_f = A. For long infiltration times (during ponded infiltration), the term A approaches the value of K_s. Philip (1969) and Talsma and Parlange (1972) have shown that even for long infiltration times (of practical interest), the inequality: $\frac{1}{3}K_s \le A \le \frac{2}{3}K_s$ holds. The spatial vertical water content distribution in the soil profile following infiltration and wetting is quite complex and can be illustrated by Fig. 3. Experimental results from Davidson J et al. (1963) and Rubin and Steinhardt (1964) have shown the sigmoid-like nature of the distribution of $\theta(z)$ (here, the data of Davidson J et al. (1963) are depicted in Fig. 4).

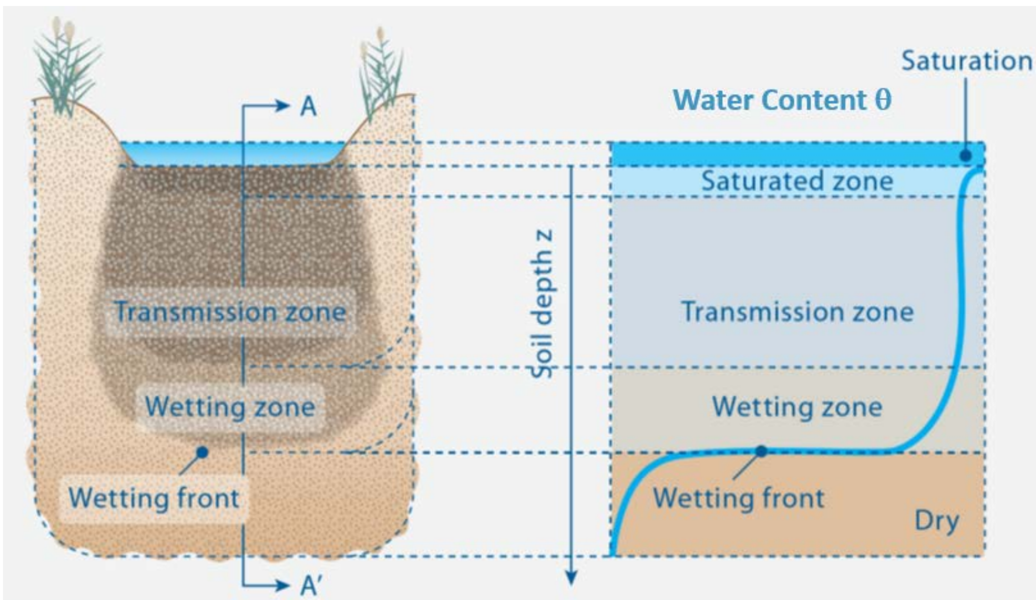

Figure 3: *Illustration of the 2-D spatial distribution of soil moisture content within a wetted soil profile during infiltration (left panel) and its corresponding soil moisture profile (right panel). AA' refers to a vertical transect depicted on the right hand side of the left panel. Or et al. Classnotes with permission.*

Green and Ampt (1911) presented an approach that is based on fundamental physics but make strong assumptions about the soil hydraulic properties and the shape of $\theta(z)$. Their key assumption is the presence of a sharp infiltration front moving downward with time, instead of the sigmoid distribution of water content with depth representing a more realistic wetting front as shown in Fig. 3 and 4. The presented infiltration function integrated macroscale physical entities such as pressure head differences over depth, soil porosity, and saturated hydraulic conductivity over the wetter soil layer. The Green-Ampt model, for the case of ponding infiltration with a negligible ponded water depth at the surface, is represented by an implicit expression for the infiltration rate, $q(t)$, which needs to be solved iteratively for the cumulative infiltration $Q(t)$:

$$q(t) = K_s\left(\frac{h_f(\theta_s-\theta_i)}{Q(t)} + 1\right) \quad [12]$$

where $Q(t)$ is the cumulative infiltration [L] at time t [T], h_f is the capillary head at the wetting front [L], K_s is the soil saturated hydraulic conductivity [L T^{-1}], and θ_ι is the initial water content of the soil profile. The matrix head h_f is related to soil hydraulic properties (Bouwer, 1964, Neuman, 1976).

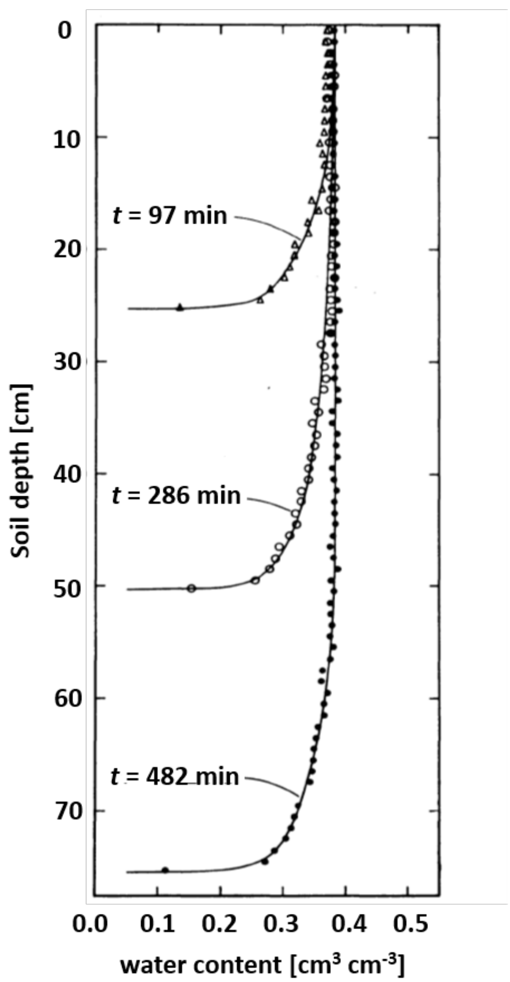

Figure 4: *Infiltration into Hesperia sandy loam soil (inially air-dry) showing the soil water content θ with depth, and the propagation of the wetting front with time during infiltration (reprinted with permission from (Davidson J et al., 1963).*

Generalized and exact solutions for $Q(t)$ were developed by Parlange et al. (1985), Parlange et al. (1982), Haverkamp et al. (1990), Swartzendruber (1987), Ross et al. (1996), Barry et al. (1995), and Barry et al. (2005). Selker and Assouline (2017) present a simple explicit solution for the position of the wetting front in time based on approximating the term describing early infiltration behavior by means of the sum of gravitational flow and the exact solution for capillary imbibition.

$$q(t) = K_s \frac{A_f K_s + \sqrt{\frac{n_f K_s h_f}{2t}}}{1 + A_f \frac{K_s t}{n_f h_f} + \sqrt{\frac{2}{n_f h_f} K_s t}} \qquad [13]$$

with A_f being a fitting parameter that can be approximated by ($^2/_3$). For infiltration into a completely dry soil profile $n_f = \theta_s - \theta_r$, whereas for a profile with known initial water content θ_i, $n_f = \theta_s - \theta_i$. The result of Eq. [13] is within 1% of the exact implicit solution of vertical Green and Ampt infiltration Eq. [12]. Hence, the proposed approximation adds essentially no error to the Green and Ampt approach, but greatly simplifies computation of infiltration by allowing an explicit expression that is in theory easy to implement in LSMs.

For near-constant rainfall rates, *q(Q)* is independent of the applied rate *r* (Skaggs, 1982, Smith et al., 2002), and infiltration capacity at any given time depends only on the cumulative infiltration volume, regardless of the previous rainfall history. The time invariance of *q(Q)* holds true also when a layered profile or a sealed soil surface is considered (Mualem and Assouline, 1996, Smith 1990). This is an important characteristic of the infiltration process and the basis of the so-called Time Compression Analysis (TCA) for predicting the timing of ponding and runoff (Assouline et al., 2007, Brutsaert, 2005).

2.4. Numerical Solutions of Profile Scale Infiltration Processes

While the empirical, analytical, and semi-analytical models discussed above provide descriptions of the infiltration process for relatively simple conditions (e.g., a homogeneous soil profile, constant initial saturation with depth, constant ponding at the soil surface), the quantitative analysis of real-world infiltration problems (e.g., a layered soil profile, variable initial saturation, time-variable rainfall, limited ponding) can be obtained only using numerical solutions of the water flow equation (i.e., Richards equation (Eq. [3])). The reason lies in the fact that the highly nonlinear eliptic parabolic Richards equation cannot be solved analytically, apart from for a very limited number of cases.

Since the 1960s soil water balance models have been developed that quantify and predict infiltration in soil by numerically solving the Richards equation for different boundary conditions and resulted in a wide range of software tools such as HYDRUS (Šimůnek et al., 2008), COUP (Jansson, 2012), DAISY (Hansen et al., 2012), and SWAP (van Dam et al., 2008), amongst many others. By using such models based on the Richards equation along with sufficient vertical and temporal discretization, the infiltration rate and occurrence of ponding should be a direct outcome of the numerical solution in the spatio-temporal domain and do not have to be calculated 'externally' using any of the introduced empirical or (semi-) analytical models above. Various simulations have been performed using HYDRUS-1D to demonstrate the water infiltration into a 1D soil profile under natural boundary conditions (Šimůnek and van Genuchten, 2008, Šimůnek et al., 2008, Šimůnek et al., 2016). The HYDRUS-1D model was selected for this purpose since it is one of the most widely used and verified codes for unsaturated flow and solute transport modeling (Scanlon, 2004) and the full set of simulations can be found at https://www.pc-progress.com/Downloads/Public_Lib_H1D/Using_HYDRUS-1D_to_Simulate_Infiltration.pdf.

Depending on the intensity of precipitation, both discretization in space and time need to be adapted to the rainfall flux, whereby most current models rely on a predefined vertical discretization and only the time discretization will be changed by an adaptive time stepping routine. In general, the typical size of the vertical discretization is often smaller than one centimeter close to the soil surface in order to adequately solve the Richards equation for rainfall events with high intensities. In some models the upper boundary condition can be automatically switched from a flux boundary condition to a fixed pressure head (Dirichlet) boundary condition during evaporation conditions to avoid the development of extreme pressure head gradients close to the soil surface. This approach stabilizes the numerical solution of the Richards equation. Additionally, the appropriate choice of temporal resolution of precipitation data is extremely important to capture the generation of excess water (Hortonian excess). Finally, using daily accumulated rainfall fluxes will lead to an under estimation of the generated excess water compared to the use of highly resolved rainfall data (Mertens et al., 2002).

2.4.1. Numerical Methods

Most early applications of numerical methods for solving variably-saturated flow problems usually used the classical finite differences method (e.g., Bresler, 1973, Bresler and Hanks, 1969, Hanks et al., 1969, Rubin and Steinhardt, 1964). Integrated finite difference, finite volumes, and especially finite element methods became increasingly popular in the seventies and thereafter (e.g., Huyakorn et al., 1986, Neuman, 1973, Paniconi and Putti, 1994, Šimůnek et al., 2008), accompanying the fast development of computers with increasing computational speed and memory. While finite difference methods are still used today in the majority of one-dimensional models, finite volume methods and/or finite element methods coupled with mass lumping of the mass balance term are usually used in two- and three-dimensional models (e.g., Healy, 2008, Pruess, 1991, Šimůnek et al., 2008). An overview of these developments with respect to infiltration prediction is given in the review of Assouline (2013).

Furthermore, a number of LSMs use *semi implicit* numerical solutions to Richards one-dimensional partial differential equation (PDE) such as in Best et al. (2011), OLAM-SOIL (Walko and Avissar, 2008a), ORCHIDEE (de Rosnay et al., 2002), and ISBA-SURFEX (Boone et al., 2000, Decharme et al., 2011). Conventional methods for solving this highly non-linear equation inevitably lead to numerical and accuracy challenges that impact their hydrological performance.

2.4.2. Governing Flow Equations

In general, the Richards equation can be formulated, and thus solved numerically, in three different ways: water content (θ) based (often also denoted as the diffusivity form), pressure head (h) based, and in terms of a mixed formulation, when both θ and h appear simultaneously in the governing equation as shown in Eq. [3]. The most popularly used vadose zone flow models currently utilize the mixed formulation of the Richards equation and solve this equation using the mass-conservative method proposed by Celia et al. (1990).

2.4.3. Boundary Conditions

Infiltration rates for a point source infiltration process can be obtained by numerically solving the Richards equation for an appropriate upper (soil surface) boundary condition (BC). In general, two types of BCs can be used to simulate the infiltration process, i.e., the Dirichlet or Neumann BC. The Dirichlet (pressure head based) BC fixes the pressure head, h, at the soil surface ($z = 0$) to a value h_0 [L], which can be either constant or variable with time:

$$h(z,t) = h_o(t) \quad at \quad z = 0 \qquad [14]$$

The value for h_0 can either be negative (e.g., for tension disk infiltration), zero, or positive (ponded infiltration). The majority of empirical, analytical, and semi-analytical models discussed above represent conditions with zero (or slightly positive) pressure head at the soil surface. The Neumann (flux based) BC fixes the water flux (infiltration), q, at the soil surface to a required water flux, q_0 [LT^{-1}], which can again be either constant or variable with time:

$$-K\left(\frac{\partial h}{\partial z}+1\right)=q_0(t) \qquad [15]$$

where q_0 is negative for infiltration and positive for evaporation when the z-axis is defined positive upward if z is defined negative over depth. If water is allowed to build up on the soil surface after the onset of soil surface ponding, a "surface reservoir" boundary condition may be applied (Mis, 1982, Šimůnek et al., 2008, van Dam et al., 2008):

$$-K\left(\frac{\partial h}{\partial z}+1\right)=q_0(t)-\frac{dh}{dt} \qquad [16]$$

The flux q_0 in Eq. [16] is the net infiltration rate, i.e., the difference between precipitation and evaporation. Based on Eq. (16) the height $h(0,t)$ of the surface water layer (ponding height) increases due to precipitation and reduces because of infiltration and evaporation of the ponding layer.

Kollet and Maxwell (2006) closed the problem of variably saturated groundwater flow, infiltration, and surface water flow by applying flux and pressure continuity conditions at the top boundary leading to a free surface overland flow boundary condition

$$-K\left(\frac{\partial h}{\partial z}+1\right)=\frac{\partial\|h,0\|}{\partial t}-\nabla\vec{v}\|h,0\|+q_0(t) \qquad [17]$$

where $\vec{v}$ is the depth averaged velocity vector [LT^{-1}], that can be expressed in terms of Manning's equation (e.g., in Chow et al., 1988) to establish a flow depth-discharge relationship.

The Dirichlet (Eq. 14) and Neuman (Eq. 15) boundary conditions are system-independent boundary conditions for which prescribed quantities (i.e., pressure heads or water fluxes) do not depend on the conditions of the soil profile, its saturation status, or its infiltration capacity. These boundary conditions thus may not properly describe real-world conditions, in which infiltration or actual soil evaporation rates depend on the conditions of the soil profile and its saturation status, which may limit infiltration or evaporation. In many applications, neither the flux across nor the pressure head at a boundary is known a priori but follows from interactions between the vadose zone and its surroundings (e.g., the atmosphere). External meteorological conditions thus control only the potential water flux across the soil surface, while the actual flux also depends on the prevailing (transient) soil moisture conditions near the surface. This occurs, for example, when the precipitation rate exceeds the infiltration capacity of the soil, resulting in accumulation of excess water on top of the soil surface and surface runoff, depending upon soil properties and on topographic conditions (for 2 and 3-D representation). Subsequently, the infiltration rate is no longer controlled by the precipitation rate, but instead by the soil infiltration capacity.

Such conditions may be best described using system-dependent boundary conditions, which take soil moisture conditions and the hydraulic conductivity of the soil near the soil surface into consideration. For example, in HYDRUS-1D, such a system-dependent BC is called an "atmospheric" BC. For these conditions, the soil surface boundary condition may change from a prescribed flux to a prescribed head type condition (and vice-versa). The numerical solution of Eq. 3 is then obtained by limiting the absolute value of the surface flux by the following two conditions (Neuman et al., 1974):

$$\left|-K\frac{\partial h}{\partial z}-K\right| \leq i_p \qquad [18]$$

and

$$h_A \leq h \leq h_s \qquad [19]$$

where i_p is the maximum potential rate of infiltration or evaporation under the current atmospheric conditions [LT^{-1}], and h_A and h_S are, respectively, minimum (i.e., for evaporation) and maximum (i.e., for infiltration) pressure heads at the soil surface allowed under the prevailing soil conditions [L]. When one of the endpoints of Eq. 19 is reached, a prescribed head boundary condition will be used to calculate the actual surface infiltration or evaporation flux.

The value for h_A is determined from the equilibrium conditions between soil water and atmospheric water vapor (e.g., Feddes et al., 1974). The value of h_S is usually set equal to zero, which represents conditions when any excess water on the soil surface is immediately removed via runoff once ponding is reached. In this case, the Neumann BC (Eq. 15) is switched internally in the model to the Dirichlet BC (Eq. 14) with h=0 once ponding is reached and then back to the Neumann BC once rainfall stops (during redistribution) and the pressure head decreases below zero. When h_S is allowed to be positive, it then represents a layer of water, which can form on top of the soil surface during heavy rains before initiation of runoff. In such case, the Neumann BC (Eq. 15) needs to be switched to the Dirichlet BC (Eq. 14) similarly as above, but the surface pressure head value h is calculated using the surface reservoir BC. Once rainfall stops, infiltration (calculated for a Dirichlet BC) continues until all water from the accumulated water layer has infiltrated when the BC is switched back to the Neumann BC.

2.4.4. Vertical and Temporal Discretization

The numerical solution of the highly nonlinear Richards equation requires relatively fine spatial (on the order of cm) (Vogel and Ippisch, 2008) and temporal (on the order of minutes) discretization. Optimal spatial and temporal discretization depends strongly on the intensity of precipitation/evaporation/infiltration and the nonlinearity of soil hydraulic properties, as well as on numerical stability criteria, involving hydraulic or thermal diffusivity (see e.g., Best et al., 2005). Simulations with high flux rates and strong nonlinearity of soil hydraulic properties require finer discretization in both space and time. Most current vadose zone, including land surface, models rely on a predefined vertical discretization, which is constant in time, while only the time discretization changes during simulations by an adaptive time stepping routine.

Spatial discretization should be made relatively small at locations where large hydraulic gradients are expected. Such a region is usually located close to the soil surface where highly variable meteorological factors can cause rapid changes in soil water contents and corresponding pressure heads. Hence, it is generally recommended to use relatively thin soil layers (small discretization) near the soil surface and then to gradually increase their thickness with depth to reflect much slower changes in pressure heads at deeper depths.

3. Upscaling Approaches Towards Larger Scales

Infiltration considered at larger scales is heavily affected by the heterogeneity of the soils and the land surface. Assouline and Mualem (2002, 2006) explicitly demonstrate the impact of heterogeneity, introduced by a combined effect of impervious areas and spatial variability in soil properties, on infiltration. Figure 5 shows the results in terms of the infiltration rate ($q(t)$) curves for a homogeneous and a heterogeneous field exposed to a constant rainfall rate.

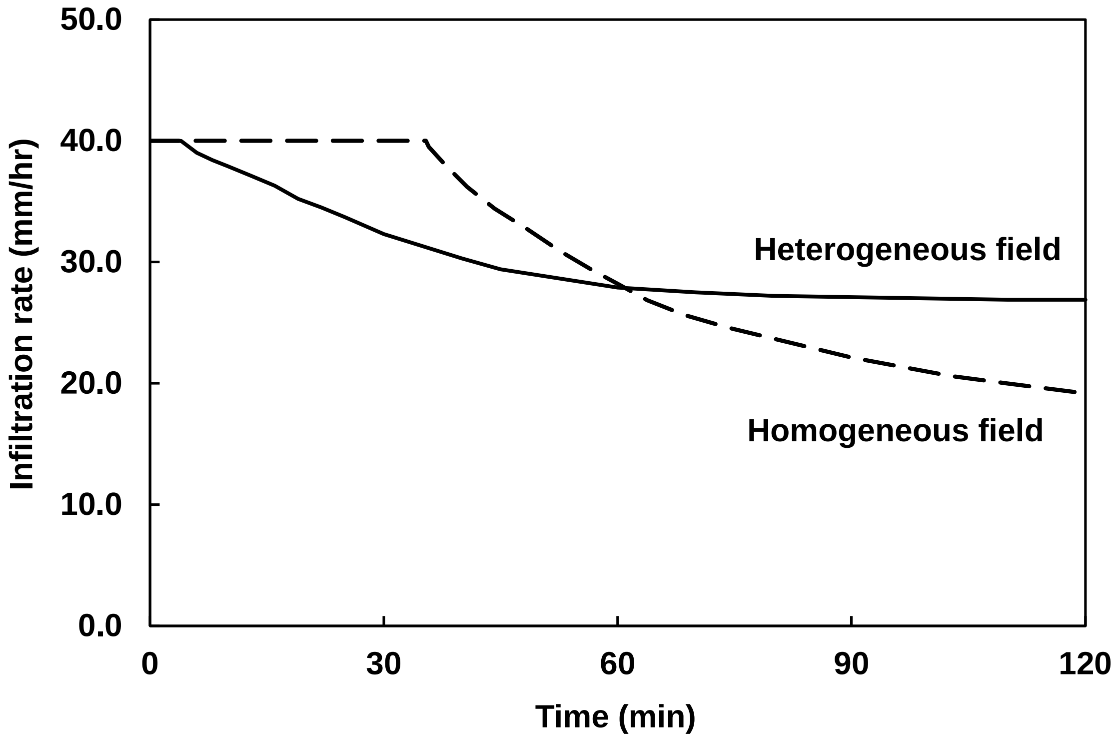

Figure 5: *Mean infiltration in a heterogeneous (solid line) vs. a homogeneous (dashed line) field.*

Accounting for field spatial variability leads to shorter ponding times and to a more gradual decrease of the infiltration flux with time (Smith and Hebbert, 1979). Consequently, surface runoff will appear earlier in heterogeneous fields than in homogeneous ones. This results from the fact that part of the heterogeneous field has much lower hydraulic conductivity than that of the homogeneous one and this generates the early runoff. As LSMs typically incorporate infiltration at grid sizes from meters to hundreds of kilometers, scaling approaches are necessary to account for sub-grid heterogeneity at the model resolution. Also, parameters relevant for infiltration, as well as experiments for direct infiltration measurements, are typically observed and performed at the point-scale (see Section 2). Therefore, scaling approaches are needed to translate the measurements to adequately address infiltration characteristics at larger scales. Two general strategies are discussed in the following, (i) the scaling of infiltration-related properties and (ii) the scaling of infiltration fluxes themselves. We have chosen this categorization rather than a scale based categorization as several of the methods proposed below, such as e.g. similarity scaling, aggregation, and Bayesian upscaling, can be applied at a range of scales. Figure 6 shows the different upscaling approaches to obtain effective parameters at the scale of LSMs. We distinguish four different categories: i) the LSM upscaling approaches that either assign uniform soil properties to a dominant soil class or use pdfs of parameters that reflect subgrid variability, ii) parameter upscaling methods, iii) similarity upscaling methods, and iv) stochastic upscaling methods. The last three approaches have been mainly developed for upscaling from the field to catchment scale, while the first one involves downscaling the parameters from grid to point scale, before upscaling the resulting infiltration from point to grid scale. Within the LSM upscaling approaches, three main methods can be distinguished: (1) Uniform upscaling assuming the soil hydraulic parameters are constant (2) Empirical upscaling that use pdfs to define F_{sat} and I_{max} that are then further used to calculate grid-cale infiltration, and (3) Physical upscaling in which infiltration is calculated at point-scale and pdfs are used used to upscale it at grid-scale.

3.1. Upscaling Spatially Heterogenous Parameters Relevant for Infiltration

LSMs need input parameters at the grid scale, i.e. estimates of effective parameters to quantify hydrological and energy balance fluxes, and to generate soil infiltration-related properties such as water storage at the grid cell level (see Section 2). In order to adequately represent nonlinear relationships between model parameters and states and fluxes, it is generally agreed upon that spatial scaling ideally should take place after the model has been run. However, this is also a matter of computational resources, which are limited and generally do not afford simulations at the support, which is the area or volume over which a measurement is made or a state variable defined. LSMs driven for global or continental applications typically require upscaling of information that is available at higher resolution to scales of a few to tens of kilometers. Here, a simplification of the landscape heterogeneity by dominant class selection (e.g., USDA soil classes) or simple parameter averaging typically does not account for nonlinear relationships of sub-grid processes and may introduce important biases on specific LSM variables, including infiltration and runoff (Boone and Wetzel, 1999).

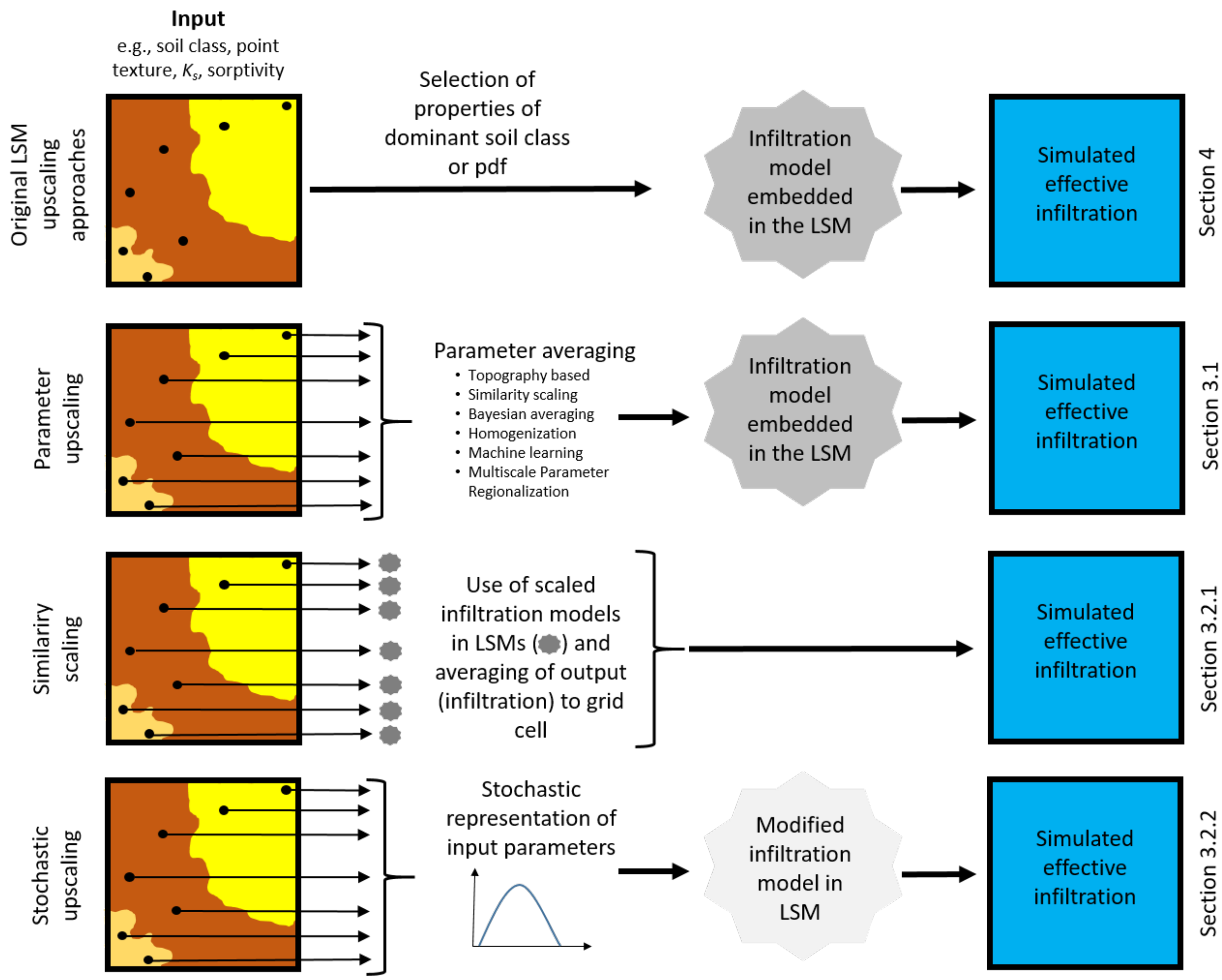

Figure 6*: Schematic overview of different upscaling methods of soil parameters (Original LSM upscaling approach, Parameter upscaling, Similarity scaling, and Stochastic upscaling) described in section 4., 3.1, 3.21, and 3.2.2.). Differences in the infiltration model used are indicated by different colors.*

Another method proposed by Noilhan and Lacarrère (1995) consists to compute grid-scale land surface parameters according to observed soil textures (sand and clay) aggregated from the high resolution and using continuous relationship derived from textural classification of Clapp and Hornberger (1978) or Cosby et al. (1984). The scaled effective parameters are often dependent on the spatiotemporal patterns of the unsaturated system at the smaller scale and are not simply a function of the average parameter values obtained from measurements.

General focus was placed on upscaling soil hydraulic parameters, because significant spatial variability of these properties has been reported earlier by Nielsen et al. (1973), Warrick and Nielsen (1980), Peck (1983), and Logsdon and Jaynes (1996). In most of these cases, the field saturated hydraulic conductivity,

K_s, was log-normally distributed (Reynolds and Eldrick, 1985, Russo et al., 1997, White and Sully, 1992). However, steady-state infiltration fluxes and soil surface water content are distributed either normally or log-normally (Cosh et al., 2004, Kutilek et al., 1993, Loague and Gander, 1990, Sisson and Wierenga, 1981, Vieira et al., 1981). Several studies have dealt with modeling the effect of spatial variability of soil hydraulic properties on infiltration (Assouline and Mualem, 2002, Dagan and Bresler, 1983, Govindaraju et al., 2006, Milly and Eagleson, 1988, Sivapalan and Wood, 1986, Smith and Hebbert, 1979, Warrick and Nielsen, 1980, Woolhiser et al., 1996).

While heterogeneity in soil hydrology properties, parameters, and boundary conditions is ubiqoutous, understanding of sensitivity to different aggregation/upscaling methods is limited. Zhu and Mohanty (2002a, 2002b, 2003, 2004, 2006), Zhu et al. (2006, 2004), and Mohanty and Zhu (2007) investigated in a series of studies the suitability of various soil hydraulic parameter upscaling schemes by matching their prediction performances with ensemble vadose zone fluxes (infiltration and evaporation) under different hydroclimatic scenarios for horizontally and vertically heterogeneous soil systems. Their synthetic experimental results showed that soil texture, geological layering, groundwater depth, surface/profile soil moisture status, vertical flux direction (infiltration versus evaporation), hydraulic parameter statistics (correlations and spatial structures), root distribution in the soil profile, and topographic features/arrangements conjointly determine the “upscaled” pixel-scale soil hydraulic parameters for the equivalent homogeneous medium that delivers the same amount of flux (infiltration or evaporation) as the natural heterogeneous medium. Thus, different homogenization algorithms (rules) for different hydrologic scenarios and land attribute complexities were suggested for parameter upscaling. Several approaches have been proposed in the literature to upscale soil hydraulic properties from the point to larger scales in order to obtain effective properties (Vereecken et al., 2007a), which are discussed in the following.

3.1.1. Topography-based Aggregation

Expanding the power average operator of Yager (2001), Jana and Mohanty (2012a, 2012b, c) coarsened the soil hydraulic parameters to the model grid scale in the attempt to study remote sensing based soil moisture distribution at the watershed scale (Little Washita). Two types of aggregating methods were combined in this topography-based aggregation technique. By combining the features of both mode-like and mean-type aggregating methods, the power average technique provided an ideal tool in scaling of soil hydraulic parameters for soil pedons. Power averaging operator across a number of spatial nodes use a support function based on linear distances in different Cartesian coordinates allowing data clustered around a particular value to combine nonlinearly while being aggregated. Generally, soil pedons clustered around a location tend to have similar properties, that correlation decreases as the distance between two points increases. In other words, the aggregating method considers the mutual support the pedons extend to each other when clustered.

3.1.2. Homogenization

Homogenization by spatially averaging the soil hydraulic parameters is a simple way of upscaling. Numerical studies such as those presented by Zhu and Mohanty (2002b) and Mohanty and Zhu (2007), and observational studies such as those of Jana and Mohanty (2012b) examined the impact of areal heterogeneity of soil hydraulic parameters at the model grid scale on the ensemble response of hydrologic fluxes. In particular, arithmetic, geometric, and harmonic averages of the soil hydraulic parameters were tested with different parameter correlation structures. Findings of these studies suggested that different averaging schemes should be used for different soil hydraulic conductivity parameters and functional forms.

3.1.3. Similarity Scaling

Another method for scaling is based on the theoretical framework of geometric similarity for porous media introduced by Miller and Miller (1956). The basic idea is, that porous media, which are geometrically similar in their microscopic arrangement of particles, differ only in terms of their characteristic length scale λ_{SC}. The underlying assumption is that the hydraulic behavior of a porous medium can be transformed to the behavior of a reference medium by scaling (Nielsen et al., 1998). This scaling factor α_{sc} is defined as the ratio between the characteristic length λ_{SC} of a geometrically similar soil and the characteristic length of the reference soil λ_r:

$$\alpha_{SC} = \frac{\lambda_{SC}}{\lambda_r} \qquad [20]$$

This approach can also be used for spatial scaling of soil hydraulic properties (Mohanty, 1999, Shouse and Mohanty, 1998). Zhu and Mohanty (2006) used Miller-Miller scaling in combination with a one-dimensional infiltration equation based on the Haverkamp et al. (1990) model to derive effective hydraulic parameters at the grid scale of LSM and global climate models (GCMs). Heterogeneity of soil hydraulic parameters was considered in the horizontal dimension and the infiltration process was described using the concept of parallel stream tubes without lateral interaction. They found that the variability in Miller-Miller scaling factors had a strong influence on the effective grid cell infiltration than the saturated water content and the ponding depth, which reflects micro-topography. This approach was also implemented by Montzka et al. (2017) to generate an optimized soil hydraulic properties data base at coarse global grid resolution of 0.25° from the soil texture information system SoilGrids1km of Hengl et al. (2014). Further information about similarity and Miller-Miller scaling in terms of scaling infiltration processes is given in Section 3.2.1.

3.1.4. Bayesian Upscaling

Considered as a calibration method at the remote sensing footprint scale, the Markov Chain Monte Carlo (MCMC) based upscaling algorithm introduced by Das et al. (2008) provides an alternative to derive the upscaled effective soil hydraulic parameters from a time-series of soil moisture observations and stochastic information of the fine scale soil hydraulic parameter variability. The Bayesian framework produces probability distributions of the effective (pixel-scale) soil hydraulic parameters, where pre-existing knowledge about the local scale soil parameters (e.g., from Soil Survey Geographic (SSURGO) database) can be combined with dynamic hydrologic observations and model outputs.

Kim and Mohanty (2017) proposed a more general approach by accounting for the effects of mixed (weighted) physical controls (covariates) as well as the interactions between the controls on soil moisture distribution and subsurface flow including lateral flow between grid cells. They used a Bayesian averaging scheme for effectively estimating the contributing ratios (weights) for the physical controls and their interactions. This scheme provide proper weights that show how the controls contribute to describing the spatial variability of soil moisture and thus effective soil hydraulic properties. This approach underpins the concept of hydrologic connectivity, based on probability of connected local pathways of surface and subsurface flow, by which emergent catchment-scale behavior is depicted. The physical control based connectivity index approach can be easily adopted in land surface hydrologic and biogeochemical models leading to an Earth System Modelling (ESM) framework, where geophysical attributes such as geology, ecotones, and topography are (will be) the primary drivers for water, carbon, and energy cycle.

3.1.5 Machine Learning Based Upscaling

Pedotransfer functions have been used as inexpensive alternatives for estimating soil infiltration and hydraulic properties using soil textural and bulk density information at the local scale. Expanding the concept of pedotransfer function to estimate landscape-scale soil hydraulic properties, Sharma et al. (2006) developed Artificial Neural Networks (ANN)-based pedo-topo-vegetation transfer functions with good success by adding topographic and vegetation characteristics to soil textural and bulk density information. Advancing the idea within a Bayesian framework, Jana et al. (2008) and Jana and Mohanty (2011) developed multi-scale Bayesian Neural Network (BNN) based pedotransfter functions. Using BNN, they upscaled/downscaled soil hydraulic parameters using soil texture and structure data at one scale, to simulate the key soil moisture contents related to soil water retention at another. In that study, training inputs to the BNN consisted of the percentage of sand, silt, and clay, and the bulk density of the soil, and DEM and vegetation data, while the targets were the soil water content at 0 (saturation), 0.33 (field capacity), and 15 (wilting point) bar. Using MCMC techniques, the BNN provides a distribution of the output parameter instead of a single deterministic value. Recently, Montzka et al. (2017) used pedotransfer functions to derive effective spatial distribution of scaling factors and mean properties of soil hydraulic properties that can be used in LSMs to quantify the effect of spatial variability on infiltration fluxes.

3.1.6 Multiscale Parameter Regionalization

The Multiscale Parameter Regionalization (MPR) method proposed by Samaniego et al. (2010) is a two-step approach with initial regionalization and subsequent upscaling. The regionalization establishes a priori relationships between model parameters and distributed basin predictors at the fine scale, leading to linear or nonlinear transfer functions. These functions are used as global parameters to reduce overparameterization and ease transferability. Soil texture and land cover can be used as predictors for infiltration (Samaniego et al., 2010). The upscaling towards coarser scales is performed by a selection or combination of upscaling operators such as arithmetic mean, maximum difference, geometric mean, harmonic mean, and majority. With this approach, the sub-grid variability is used for facilitating transferability towards ungauged and uncalibrated regions for improved model parameterization. Samaniego et al. (2017) analyzed the applicability of the MPR approach for several LSMs.

3.1.7 Other Parameter Scaling Approaches

Other parameter scaling methods are fractal approaches (e.g., Tyler and Wheatcraft, 1990) and the scaleway approach (e.g., Vogel and Roth, 1998). Although, they have been used over small watersheds, they have strong limitations (Meng et al., 2006). Stochastic upscaling or aggregation methods statistically allow to better account for landscape heterogeneity conditions. Stochastic upscaling makes use of geostatistical descriptors of spatial variables and quantify a probability distribution for each state variable at larger scales by stochastic perturbation rather than a deterministic quantity (see Section 3.2.2).

Govindaraju et al. (2006) suggested a semi-analytical model to compute the space-averaged infiltration at the hillslope scale when spatial variability in both soil properties and rainfall intensity are accounted for. The soil spatial heterogeneity was characterized by a log-normal distribution of the saturated hydraulic conductivity, while the rainfall spatial heterogeneity was simulated by a uniform distribution between two extreme rainfall intensities (low and high). At each location, the soil saturated hydraulic conductivity, K_s, and the rainfall intensity was assumed to remain constant during the rainfall event. The main finding was that ponding time decreases with the increase in the coefficient of variation of K_s (see also Figure 5). Other researchers also developed and evaluated methods that are potentially applicable for transfering infiltration parameterizations across scales. Hailegeorgis et al. (2015) evaluated four regionalization methods for continuous streamflow simulation. Their regional calibration method uses the maximum weighted average of a performance measure such as Nash-Sutcliff Efficiency to identify specific parameter sets per sub-pixel by the DREAM algorithm (Vrugt et al., 2009). Another method uses the regional median of each parameter for regionalization, where a limitation is that the correlation structure between parameters is lost. Scaling by the nearest neighbor approach includes the assumption that spatial proximity in terms of Euclidian distance explains parameter similarity. The physical similarity approach assumes that similarity of regions in physical attributes such as land use, cumulative distribution functions of terrain slopes, and/or soil types can explain their response in the hydrological variable.

The potential of most of these upscaling methods has not yet been tested in currently used land surface models. As highly resolved soil information becomes available that allows to parametrize subgrid variability, several of the above presented methods may prove to be valuable in estimating effective soil properties controlling infiltration processes at the pixel scale of land surface models. First results using e.g. the multi-scale parameterization method and similarity approach show great potential in parameterizing key hydraulic properties at the grid scale of LSM.

3.2. Upscaling Infiltration Processes

In order to upscale infiltration processes themselves rather than providing a method for the averaging of infiltration-related parameters as discussed above, besides scaling the Richards equation for infiltration (Sadeghi et al., 2012, Warrick and Hussen, 1993), the Miller-Miller similarity can be applied. The stochastic upscaling of infiltration is based on the frequency distribution of infiltration-related parameters and allows for a computation of effective infiltration fluxes using semi-analytical approximations.

3.2.1 Similarity Scaling

Besides providing a method for the averaging of infiltration-related parameters as presented in Section 3.1.3 similarity scaling can also be applied for a reduction of the number of parameters in the analytical or semi-analytical infiltration equations, which in turn also reduces the data requirement. Within the similarity scaling approach for infiltration, the infiltration data consists of a set of scaling factors, one for each location or grid cell, and an average infiltration function. In the following, mainly two examples of similarity scaling for infiltration are presented. The first example Sharma et al. (1980). is based on the similiraty scaling of cumulative infiltration Q [L], which is estimated over time t (Philip and de Vries, 1957):

$$Q(t) = S_{op}t^{1/2} + ACt. \qquad [21]$$

where $S_{op,i}$ and AC_i are the parameters fitted to each of the infiltration measurements, i, within a region. Sharma et al. (1980) use two alternative approaches to realize the scaling of cumulative infiltration: i) either by determination of two separate scaling factors for the sorptivity and steady state infiltration, or ii) by determination of a single optimized scaling factor. For the first approach, the two scaling factors α_{Sop} and α_{AC} [-], for sorptivity S_{op} [L T$^{-0.5}$] and steady state infiltration AC [L T^{-1}], respectively, were calculated according to

$$\alpha_{Sop,i} = \left(\frac{S_{op,i}}{\langle S_{op}\rangle}\right)^2 \qquad [22]$$

and

$$\alpha_{AC,i} = \left(\frac{AC_i}{\langle AC\rangle}\right)^{1/2}, \qquad [23]$$

where $\langle S_{op}\rangle$and $\langle AC\rangle$ represent the respective mean values of those fitted infiltration parameters. The scaling of the infiltration data was subsequently performed by:

$$Q^* = \alpha Q \qquad [24]$$

and

$$t^* = \alpha^3 t, \qquad [25]$$

where Q^* and t^* identify the scaled cumulative infiltration [L] and time [T], respectively, and scaling factor α is either α_{Sop} or α_{AC}. At this point, both scaling factors α_{opt} and α_{AC} can be used to scale the cumulative infiltration data. However, both attempts, using either α_{opt} or α_{AC}, fail to arrange the scaled infiltration data near the reference cumulative infiltration curve $\langle Q \rangle$ defined by $\langle S_{op} \rangle$ and $\langle AC \rangle$. For the second scaling approach, a single scaling factor α_{opt} was derived by least-squares fitting (using Eqs. [24] and [25]). The sum of squares, *SS*, between scaled cumulative infiltration and reference cumulative infiltration, given by

$$SS = \sum_{t_i^*} \left(Q_{t_i^*}^* - \langle Q \rangle_{t_i} \right)^2 \qquad [26]$$

was minimized by adjusting α_{opt} based on the cumulative infiltration measurements available at each timestep t_i for each of the multiple measurements. Finally, with this second scaling approach all the measurements reasonably coalesced about the reference cumulative infiltration curve.

By using Eq. [26], Sharma et al. (1980) depart from the geometric similarity proposed by Miller and Miller (1956), which would require that $\alpha_{S_{op}}$ and α_{AC} are identical. A scaling methodology following the second approach (Eq. 26) is empirical in nature and usually referred to as functional normalization (Tillotson and Nielsen, 1984). Nonetheless, it is still relevant since it provides a mathematical framework for the handling of Philips' infiltration in terms of spatial variability. Eqs. [24] to [26] can be used to account for the variability in infiltration, when only the variance of the scaling factors and the mean infiltration curve are known. Furthermore, this approach provides an opportunity to lump both infiltration parameters AC_i and $S_{op,i}$ into a single scaling parameter $\alpha_{SC,i}$ for each soil. Yet, to the best of our knowledge, such an approach has not been implemented in any land surface or hydrological model. However, for the spatial scales of LSMs, it remains unclear how appropriate scaling parameters could be derived and implemented in practice.

The frequency distribution of α_{opt} determined by Sharma et al. (1980) had a mean of about 1, as expected, and a standard deviation of 0.58. The spatial distribution of α_{opt} did not show a distinct pattern, which was explained by Loague and Gander (1990) later on, as they determined a spatial autocorrelation length of less than 20 m for infiltration in the catchment under consideration. This in turn would support a purely stochastic approach to the variability of infiltration. However, this conclusion is based on the assumption of the occurrence of vertical fluxes only.

Hopmans (1989) simplified the scaling of Philips' infiltration suggested by Sharma et al. (1980) by substituting Eqs. [22] and [23] into Eq. [21]. Accordingly, the scaled instantaneous infiltration $q*$ [L T^{-1}] yields:

$$q^{*}(t) = {\alpha_{SC}}^{1/2}\langle S_{op}\rangle t^{-1/2} + {\alpha_{SC}}^{2}\langle AC\rangle \qquad [27]$$

where $q*$ is the scaled infiltration rate [L T^{-1}], and $\langle S_{op}\rangle$ [L T$^{-0.5}$] and $\langle AC\rangle$ [L T^{-1}] represent the parameters of the reference infiltration curve, now determined by non-linear regression to all infiltration measurements available. Hopmans (1989) also performed functional normalization according to Tillotson and Nielsen (1984) with the modified empirical three-parameter infiltration equation of Kostiakov (see Eq. [10]). Both scaling approaches were successful and the author stressed that the attractiveness of this lies in the potential to lump the spatial variability of infiltration into a single parameter, which, for example, allows for correlation with other environmental variables. Furthermore, it potentially removes any inter-correlations between the infiltration parameters.

Haverkamp et al. (1998) provide inspectional analyses of Miller-Miller similarity scaling for infiltration according to the theories provided by Green and Ampt (1911), Philip (1957), and Talsma and Parlange (1972). However, the analyses presented by Haverkamp et al. (1998) remain at a theoretical level and were not tested in any practical application.

3.2.2 Stochastic Upscaling

A stochastic approach to upscale infiltration can be implemented via Monte-Carlo simulations for any type of infiltration equation and any given distribution of relevant parameters. This has been demonstrated, e.g., by Smith and Hebbert (1979) and Sharma and Seely (1979). A sufficient number of random samples needs to be drawn from a given distribution of infiltration parameters and after computation of every Monte-Carlo model realization the average and/or standard deviation of predicted infiltration can be obtained. However, due to the assumption that the infiltration process is ergodic, large sample sizes are usually required resulting in a rather large computational demand, which in reality prohibits any practical application in large-scale studies involving hydrological models or LSMs. Notwithstanding, many semi-analytical solutions to infiltration problems are still validated against Monte Carlo results (e.g., Corradini et al., 2002, Craig et al., 2010, Govindaraju et al., 2001).

Starting with the infiltration theory according to Philip (1957), while making some considerable approximations, Sivapalan and Wood (1986) provided semi-analytical solutions to calculate average infiltration over a gridbox for two cases. For the first case, a spatially constant rainfall rate, and a log-normal distribution of saturated hydraulic conductivity K_s were assumed. In the second case, a spatially variable rainfall rate and spatially uniform distribution of K_s were considered. In both cases, run-on was not accounted for and the soil profiles were assumed to be vertically homogeneous. The approximations derived by Sivapalan and Wood (1986) were tested against Monte-Carlo simulations, but an in-depth analysis of the uncertainties was not presented. Moreover, due to the mathematical complexity of the approximations, practical application was not feasible.

Smith and Goodrich (2000) simulated the ensemble behavior of infiltration according to Parlange et al. (1982) by making use of Latin hypercube sampling. They assumed that the log-normal probability density functions of K_s and capillary parameter G were divided into n equal sub-areas and infiltration was computed using the average of each sub-area. The areal average infiltration was then given as the equally weighted sum of all subdivisions. This method does not involve any analytical solution and has the advantage of a significantly reduced computational demand as compared to the Monte Carlo technique. Govindaraju et al. (2001) assume spatial autocorrelation of log-normally distributed saturated hydraulic conductivity and provide semi-analytical solutions to the Green-Ampt equation based on series expansion. As a follow-up, the semi-analytical solutions of Govindaraju et al. (2001) were combined by Corradini et al. (2002) with a kinematic wave expression to account for run-on effects.

Craig et al. (2010) provide approximations for the estimation of average infiltration rate $\langle q \rangle$ [L T^{-1}] according to the Green-Ampt approach as a function of precipitation rate J_w [L T^{-1}] and mean saturated hydraulic conductivity, $\langle K_s \rangle$, and standard deviation, σ_{Ks}, of a standard log-normal distribution, $f_k(K_s)$, of saturated hydraulic conductivity, K_s. They estimated a dimensionless error term ε for J_w, K_s, and X, whereby X represents a dimensionless time parameter computed from time t, J_w, and α_{wf}. This last variable α_{wf} is defined as the product of the absolute value of wetting front suction head and the difference between saturated water content and initial water content at the beginning of the infiltration event. Finally, the averaged infiltration rate, $\langle q \rangle$, is approximated by:

$$\langle q \rangle = \frac{J_w}{2} erfc\left(\frac{\ln(J_w X) - \langle K_s \rangle}{\sigma_{ks}\sqrt{2}}\right) + \frac{1}{2X} exp\left(\langle K_s \rangle + \frac{\sigma_{ks}^2}{2}\right) erfc\left(\frac{\sigma_{ks}}{\sqrt{2}} - \frac{\ln(J_w X) - \langle K_s \rangle}{\sigma_{ks}\sqrt{2}}\right) + J_w \int_0^{X(t)} \varepsilon(X(t), k_s) \cdot f_k(k_s) dk_s \qquad [28]$$

According to the authors a comparison between the semi-analytical upscaling approach given in Eq. [28] with Monte-Carlo simulations revealed errors of less than 3%, which appears to be acceptable for any practical purpose. The authors also provide approximations of infiltration for a given normal distribution of aggregate parameter α_{wf}. From Monte-Carlo simulations Craig et al. (2010) concluded that the heterogeneity in K_s is of much greater relevance than the heterogeneity in α_{wf}.

Craig et al. (2010) upscaled the Green and Ampt equation to a basin or (LSM) grid cell. Thereby, the upscaled Green Ampt equation is based on the information of the distributions of saturated hydraulic conductivity, K_s, and/or the initial soil water deficit of the basin or grid cell. Additionally, preferential flow, which is defined as the uneven and rapid movement of water through the soil, characterized by regions of enhanced flux e.g., wormholes, root holes, cracks, can be also incorporated by considering a bimodal distribution of K_s by:

$$\langle q \rangle = \int_0^\infty \int_0^\infty (X(t, \alpha_{GA}), K_s) f_{k\alpha_{GA}}(K_s, \alpha_{GA}) d\alpha_{GA} dK_s \qquad [29]$$

with

$$X = 1/\left(1 + 1\left(\frac{J_w}{\alpha_{GA}}\right) t\right) \qquad [30]$$

with $\alpha_{GA} = |h_f|(\theta_s - \theta_i)$, where h_f is the pressure head at the wetting front [L], θ_s is the saturated water content and θ_i is the water content at the wetting front [L^3 L^{-3}]. The ponding time can be calculated as:

$$t_p = \frac{\alpha_{wf} K_s}{J_w(J_w - K_s)} \qquad [31]$$

This approach also allows calculating of the saturated land surface fraction in a basin or LSM grid cell. To our knowledge, none of the proposed methods related to stochastic upscaling have been tested or used in full LSM/hydrological models.

Finally, Choi et al. (2007) developed a three-dimensional volume-averaged soil moisture transport model (VAST) based on Richards equation to account for local scale variation of topographic attributes such as elevation, slope, and curvature on subsurface soil moisture fluxes and thus also the infiltration flux. In this approach, the coordinate system $x_i \in \{x, y, z\}$ is replaced by $x_i^* \in \{x, y, z^*\}$ where z^* follows the terrain elevation defined as:

$$z^* = Z_g - z \qquad [32]$$

with Z_g as the ground surface elevation [L]. The local terrain surface slopes, $S_{x_l}^*$, are defined as:

$$S_{x_l}^* = \left(\frac{\partial Z_g}{\partial x}\frac{\partial Z_g}{\partial y} - 1\right) \qquad [33]$$

Second-order Taylor expansion of the hydraulic conductivity and diffusivity with respect to soil moisture were formulated and substituted in a diffusion, pressure based Richards equation and the soil water content and terrain slope at any point were approximated by a first-order perturbation approach. Scale dependent functions are used to characterize sub-grid variability incorporating statistical properties that relate the dependence of soil moisture variability to terrain attributes. The covariance between soil water content and terrain slopes is defined as:

$$\langle \theta' S'_{x_l} \rangle = \rho \sigma_\theta \sigma_{S_{x_l}} \quad [34]$$

where ρ is the correlation coefficient between the terrain slope and the soil water content. The correlation coefficient was expressed by Choi et al. (2007) as:

$$\rho = \gamma_1 + \gamma_2 \left(\frac{\langle \theta \rangle}{\theta_s} \right) + \gamma_3 \left(\frac{\langle \theta \rangle}{\theta_s} \right)^2 \quad [35]$$

where γ_1, γ_2, and γ_3 are fitting parameters estimated from observations. Note, that other approaches are available to estimate the variance of soil water content (e.g., Choi et al., 2007, Qu et al., 2015, Vereecken et al., 2007a).

Choi et al. (2007) combined this modelling approach with a 1D diffusion wave model for surface overland flow, called it the conjunctive surface-subsurface flow model (CSSF) and proposed it for use in mesoscale climate simulations. CSSF was tested through implementation in the common land model (CLM) (Oleson et al., 2008) using a set of offline simulations for catchment scale basins around the Ohio Valley region. They showed that CSSF simulated a strong contribution of the effects of surface or overland flow depths of water on infiltration estimates that led to an increased baseflow generation. In addition, a better representation of the surface subsurface flow processes improved the representation of soil moisture spatial variability and may improve the partitioning of energy at the land surface.

4. Infiltration Processes in Land Surface Models

In the following, we provide an overview of how widely used land surface models (LSMs) represent infiltration processes at the global scale. Therefore, we selected 12 LSMs, namely: (1) OLAM-SOIL (Walko et al., 2000), (2) ParFlow-CLM (Kollet and Maxwell, 2006, 2008a), (3) ORCHIDEE rev4783 (d'Orgeval et al., 2008, Ducharne et al., 2017), (4) Catchment land surface model (CLSM) (de Lannoy et al., 2014, Ducharne et al., 2000, Koster et al., 2000), (5) ISBA-SURFEX (Boone et al., 2000, Decharme et al., 2011, Decharme et al., 2016, Decharme and Douville, 2006), (6) Noah-MP version 3.0 (Niu et al., 2011a, Schaake et al., 1996),

(7) JULES version 4.6 (Best et al., 2011, Clark et al., 2011), (8) CLM4.5 (Oleson et al., 2013), (9) CABLE (Decker, 2015, Kowalczyk et al., 2013, Kowalczyk et al., 2006a, Wang et al., 2011), (10) SSiB (Li et al., 2010, Sun and Xue, 2001b, Xue et al., 1991, Xue et al., 1996, Zhan et al., 2003), (11) CH-TESSEL (Balsamo et al., 2009, Entekhabi and Eagleson, 1989), and (12) JSBach version 3.0 (Hagemann and Stacke, 2015, Roeckner et al., 2003). All models are listed in Table 1 and the labeling is used throughout the appendix for consistency.

First, we review how these LSMs address the challenge of treating infiltration processes in a large grid cell, and associated runoff generation. Second, we review how infiltration processes are treated numerically in different LSMs, considering approaches ranging from empirical to analytical equations or direct solution of the Richards equation with appropriate numerical schemes, boundary conditions, and vertical discretization. These approaches have been introduced in the previous sections.

4.1. Grid Scale Infiltration Processes

In this section, we focus on parameterization of infiltration and runoff generation processes and their definition at the grid scale. These include the maximum infiltration rate, the characterization of the soil water content distribution at the grid cell level, the characterization of grid cell heterogeneity with respect to infiltration controls, and the saturated surface fraction. Although, most LSMs use a Richards' type formulation to describe the soil water flow at the grid scale, it is used primarily to redistribute soil water vertically in the profile rather than for calculation of infiltration rates at each time step. This is justified by the computationally demanding solution of the pressure head at the land surface required for obtaining accurate and stable solutions of the Richards equation. This calculation is particularly demanding during high intensity rainfall events, where accurate solutions require very small spatial and temporal discretization (see Section 2.4.4) leading to very high computational demand. Various parametric approaches have been devised in LSMs to handle the process of infiltration efficiently within the constraints of data availability (e.g., spatially available K_s values), to avoid such computational burden. However, the implementation of Richards based solution for infiltration allows for: 1) direct calculation of excess water flux (e.g., rainfall) that cannot infiltrate, 2) a physically-based determination of the time to ponding, and 3) direct accounting for the effect of variable soil properties on infiltration at the grid cell (when such information is available). Table 1 gives an overview of twelve different LSMs and their numerical treatment of infiltration processes. Four of the twelve LSMs derive infiltration rates directly from solving the Richards equation in its mixed form (ISBA-SURFEX, OLAM-SOIL, CLSM, and ParFlow-CLM) and thus do appear only in some of the following sections dealing with specific issues of grid-scale parameterization of infiltration and runoff generation. Here, it has to be noted that most reviewed LSMs (except OLAM-SOIL and Parflow-CLM) are designed to be used globally, with typical grid-cell size of 0.5° or more. These models first define uniform soil parameters at the grid-cell (Table 3), used to calculate either infiltration, or Hortonian and Dunne runoff, at the point-scale. In the latter case, grid-scale infiltration is defined as the as the incoming water that does not run off.

4.1.1. The Maximum Infiltration Rate in LSM

In LSMs, the maximum infiltration rate is used to partition the water flux reaching the land surface into infiltrable flux and excess water that generates surface runoff. In the subsequent, we will focus on infiltration of vegetated or bare land surfaces and exclude glaciers, lakes, and urban areas. An interesting example is provided by Entekhabi and Eagleson (1989), who used a Darcy based approach to estimate the maximum infiltration rate or infiltrability for a heterogenous grid cell in a land surface model. They defined surface runoff, q_s, as the sum of Hortonian infiltration excess ($P_x - f^* \text{ for } P_x > f^* \text{ and } s < 1$, i.e., the first term on the right hand side in Eq. [36]) and Dunne saturation excess (the second term on the right hand side of Eq. [36]) where saturation excess is equal to P_x when $s \geq 1$:

$$q_s = \frac{1}{\kappa}\left[\int_0^1 \int_{f^*}^{\infty} (P_x - f^*) f_{P_x}(P_x) dP_x f_s(s) ds + \int_1^{\infty} \int_0^{\infty} (P_x) f_{P_x}(P_x) dP_x f_s(s) ds\right] \quad [36]$$

where, P_x (ML^2T^{-1}) is the flux of water incident at the soil surface, f^* the infiltrability of the first soil layer, s is effective relative saturation, κ is a scaling factor needed to redistribute the global climate model (GCM) grid scale precipitation over the scale of precipitation events, and $f_.$ represents the spatial probability density function (pdf) of the respective variables (rainfall and relative saturation). The first term on the right hand refers to the amount of point precipitation intensity that exceeds the infiltration rate of the soil, f^*, and therefore, represents the maximum infiltration rate at that moment in time. The second term on the right hand side refers to the rainfall that falls on saturated surfaces and cannot infiltrate.

Based on Buckingham-Darcy equation they derived f^* as:

$$f^* = K_s v s + K_s(1 - v) \quad [37]$$

where $v = \left.\frac{dh}{ds}\right|_{s=1} \frac{1}{\Delta z}$ and h is the matric potential [L], Δz the thickness of the first soil layer [L], s refers to to the effective relative saturation $((\theta/\theta_s)$, and K_s is the saturated hydraulic conductivity ($L\ T^{-1}$). For gravitational flow $v = 0$ and hence $f^* \approx K_s$. It is important to state that K_s is assumed to be uniform for a grid cell.

Other, more empirically based approaches have been implemented in LSMs to quantify the maximum infiltration rate to determine the excess water for surface runoff. LSMs differ in the way they define this maximum infiltration rate and the input parameter needed to estimate the infiltration flux. An overview of the different equations used in LSMs to estimate I_{max} is given in Table 2. Appendix A2 provides a more detailed presentation of the concepts and equations. In general, all LSMs that use I_{max} require, in some way or another, information about the actual soil water status of the land surface. In Noah-MP and CLM this is embedded in the saturated water fraction, Fsat (see Section 4.1.4). H-TESSEL and CH-TESSEL require knowledge about the actual and maximum water content of the first 50 cm of the soil profile to calculate Hortonian infiltration. ORCHIDEE, JULES and ISBA-SURFEX require information on the soil hydraulic conductivity to estimate I_{max}. CLSM does not use the concept of a maximum infiltration rate but assumes that the amount of water that can infiltrate over a certain time at the catchment scale is a function of the model's dynamically varying spatial moisture fields.

Based on the detailed description provided in Appendix A2 on how maximum infiltration rate is estimated in LSMs, and the information provided in Table 1 on the numerical simulation of soil water flow at grid cell scale, we conclude that currently used LSMs parameterize infiltration processes by 1) estimating the saturated area in a grid cell to calculate Dunne saturation excess. All precipitation that falls on the saturated surface fraction of a grid cell becomes immediately available for runoff and does not infiltrate into the soil profile. 2) calculating the unsaturated land surface area available for Hortonian infiltration excess, and 3) using different approaches to simulate the maximum amount of water that can enter the soil during a certain time step, any excess being Hortonian infiltration excess.

No	LSM	Key References	Model time stepping	Vertical resolutionof the first compartment	Temporal resolution of precipitation input	Form of Richards equation used for 1D water movement	Infiltration rate from solution of Richards equation	Is ponding allowed based on pressure head?	Impact of lower boundary (LB) on infiltration	Approaches to point-scale infiltration	Approaches to grid-scale infiltration
1	**OLAM-SOIL**	1	less than a day (approx. 1 min to 6 hr)	2 to 5 cm	minutes	diffusivity form	Yes	Yes	LB of soil model is impermeable but > 100 meters deep. Water table governed by Richards Eqn.	Richards Eqn. is coupled with surface water (ponding) upper boundary condition. Infiltration occurs when infiltration capacity will be exceeded	Uniform upscaling of infiltration
2	**ParFlow-CLM**	2, 3	variable	10 layers for first 3 m, additional 5 layer for next 100 m[§]	variable	mixed form	Yes	Yes	Richards equation is solved globally (saturated and variably saturated conditions); different types of BCs can be used (Dirichlet, Neumann, gravity drainage)	runoff occurs if precipitation exceeds K_s	Uniform upscaling of infiltration
3	**ORCHIDEE rev4783**	4, 5	less than a day (30 min)	1 mm top layer, 11 layers in total	30 minutes	diffusivity form	No	No	By controling the soil moisture profile and therefore infiltration capacity	runoff occurs if precipitation exceeds K_s	exponential pdf on K_s
4	**Catchment land surface model (CLSM)**	6, 7, 8	less than a day (typically set to <1 hr)	1 cm for Richards equation in off-line simulations, 2 to 5 cm for catchment scale simulations.	hourly	mixed form	Yes[b]	No	Water table depth influences the soil moisture profile and therefore infiltration rates	runoff occurs if water table depth aboce surface or precipitation exceeds infiltration capacity	Richards Eqn. combined with TOPMODEL formulations to derive parameters for catchment-scale vertical moisture transfer
5	**ISBA-SURFEX**	9, 10, 11, 12	less than a day (down to 5 min)	0.01 m (by default but user can modify this)	maximum 3 hours but can be smaller depending on available data	mixed form	Yes[#]	No	the default is free drainage (hydraulic conductivity in lowest model layer) except when ISBA is coupled to a ground water model, in which capillary rise can occur into the soil from GW.	runoff occurs if precipitation exceeds Ks (Horton) or soil is saturated (Dunne)	F_{sat} based on reflected power pdf on soil moisture capacity (Dümenil and Todini, 1992) or TOPMODEL approach
6	**Noah-MP version 3.0**	13, 14	Less than a day	four layers: 0.1 m, 0.3 m, 0.6 m und 1.0 m	offline mode 30 min to 1 hour. In coupled mode down to seconds	diffusivity form	No	No	no impact due to free drainage LB	runoff occurs if precipitation exceeds Ks (Horton) or soil is saturated (Dunne)	exponential pdf on precipitation, and Topmodel approach for F_{sat}
7	**JULES version 4.6**	15, 16	less than a day (typically 1hour but set by user)	flexible, set by user. Standard top layer = 10 cm.	flexible but never longer than 1 day. Usually between 1 to 6 hours	diffusivity form	No	No	When topmodel approach is used, there is an additional deep water store below the soil column, in which saturated conductivity is assumed to reduce exponentially with depth.	runoff occurs if precipitation exceeds Imax=βKs (Horton) or soil is saturated (Dunne)	TOPMODEL approach for F_{sat}
8	**CLM4.5**	17	less than a day (30 min)	increasing layer thickness with depth, upper layer = 1.75 cm	3 to 6 hours	(form is not provided)	No	Yes	no impact of LB	runoff occurs if precipitation exceeds Ks (Horton) or soil is saturated (Dunne)	TOPMODEL approach for F_{sat}
9	**CABLE**	18, 19, 20, 21	Fixed, depending on forcing data or coupling model time step.	Increasing layer thickness with depth; first layer 2.2 cm; soil thickness 4.6 m.	depending on forcing data or coupling model time step.	diffusivity form	No	No	Infiltration depends on vertically averaged relative saturation over the grid cell, which includes the lowest soil layer.	air space in first three soil layers is filled from the top with infiltration water at the beginning of timestep.	gamma pdf on soil moisture
10	**SSiB**	22, 23, 24, 25, 26	less than a day	increasing layer thickness with depth, upper layer = 1.75 cm	30 min or hourly	diffusivity formn	No	No	by interaction of baseflow and the overlying soil layers	runoff occurs if precipitation exceeds K_s	exponential pdf on precipitation
11	**CH-TESSEL**	27, 28	one hour or less	increasing layer thickness with depth, upper layer = 7 cm	flexible but never longer than 6 h offline. Typically 3-hourly or hourly offline and shorter/equal to atmospheric timestep when coupled	diffusivity form	No	No	no impact of LB	runoff occurs if soil moisture exceeds capacity	F_{sat} based on reflected power pdf on soil moisture capacity (Dümenil and Todini, 1992)
12	**JSBACH version 3.0**	29, 30	less than a day (hourly)	6.5 cm	hourly, daily	diffusivity form	No	No	no impact of LB	runoff occurs if soil moisture exceeds capacity	F_{sat} based on reflected power pdf on soil moisture capacity (Dümenil and Todini, 1992)

[#] Calculation of infiltration rate from solution of Richards equation is done only for small time steps. For large time steps and intense rain events, a Green Ampt based approach can permit infiltrated water to attain several layers during a time step.

[b] parameters for catchment-scale vertical moisture transfer between surface and root zone, and root zone and catchment deficit, are derived from detailed Richards equation simulations conducted off-line combined with TOPMODEL formulations.

[§] ParFlow-CLM vertical discretization is in general flexible and can be set by the user, given example is used as standard setting in TerrSysMP

[1] Walko et al. (2000), [2] Kollet and Maxwell (2006), [3] Kollet and Maxwell (2008),), [4] d'Orgeval et al (2008), [5] Ducharne (2017), [6] Koster et al. (2000), [7] Ducharne et al. (2000), [8] De Lannoy et al. (2014), [9] Boone et al. (2000), [10] Decharme and Douville (2006), [11] Decharme et al. (2011), [12] Decharme et al. (2016), [13] Niu et al. (2011), [14] Schaake et al. (1996), [15] Best et al. (2011), [16] Clark et al. (2011), [17] Oleson et al. (2013), [18] Kowalczyk et al. (2006), [19] Kowalczyk et al. (2013), [20] Wang et al. (2011), [21] Decker (2015), [22] Xue et al. (1991), [23] Xue et al. (1996), [24] Zhan et al. (2003), [25] Sun and Xue (2001), [26] Li et al. (2010), [27] Balsamo et al. (2009), [28] Entekhabi and Eagleson (1989), [29] Roeckner et al. (2003), [30] Hagemann and Stacke (2015),

Table 1: *Overview of LSMs and their numerical treatment of infiltration process.*

With respect to Hortonian infiltration excess, the majority of the LSMs use an empirical parameterization of I_{max}. The vertical redistribution of the amount of infiltrated water in most LSMs is based on a diffusion form of the Richards equation. A primary consideration in using the simplified infiltration parameterization presented above is the large computational burden of solving the more accurate pressure head based Richards equation. Such a direct approach, however, has the advantage of obviating the need for defining maximum infiltration capacity, and that the amount of Hortonian infiltration excess and Dunne saturation excess are immediate outcomes of solving the Richards equation (albeit subgrid information and runoff-runon processes must be represented). CLSM overcomes the computational burden of the mixed form of the Richards equation by running detailed Richards equation simulations solely off-line prior to LSM runs in order to derive parameters of catchment-scale vertical moisture transfer using an amended TOPMODEL approach. Also, Walko et al. (2000) developed a global LSM (part of OLAM-SOIL) capable of calculating infiltration processes using a pressure head based Richards equations and highly resolved spatial information of soil properties.

4.1.2. Spatial Heterogeneity in Soil Water Content Using Probability Densities

Characterization of subgrid soil moisture variability in LSMs is especially important to estimate the generation of Dunne saturation excess. In this section, we will focus on the different approaches used in land surface models to quantify heterogeneity in soil water content in respect of quantifying infiltration-runoff processes at the grid scale level. These approaches are based on the underlying assumption that spatial variability in soil water content and derived properties such as soil water storage or soil water deficit can be described by probability density functions (pdf) without considering their spatial patterns nor specific locations. Different types of pdfs have been proposed and used in land surface models such as standard reflected power distribution functions, Gamma functions, and exponential functions.

Several researchers used standard reflection power distributions functions to describe spatial variability of soil water content and soil water content dependent variables that affect infiltration. These functions are a special case of the more general beta distribution function written as:

$$f(x;\alpha_G,\beta_G) = \frac{\Gamma(\alpha_g+\beta_G)}{\Gamma(\alpha_G)\Gamma(\beta_G)} x^{\alpha_G-1}(1-x)^{\beta_G-1} \qquad 0 \le x \le 1;\ \alpha_G,\beta_G > 0 \qquad [38]$$

where $\Gamma(\ldots)$ Is the Gamma function and α_G,β_G the parameters of the Gamma function. Moore (1985) was among the first to propose the probability-distributed model (PDM) as a concept to characterize spatial variability of soil water content related variables at the catchment scale. He used a standard reflected power cumulative distribution function to characterize the spatial variation of the storage capacity, *c*, written as:

$$F(c) = 1 - \left(1 - \frac{c}{c_{max}}\right)^{b} \qquad 0 \le c \le c_{max}; b > 0 \tag{39}$$

with the corresponding density function

$$f(c) = \frac{dF(c)}{dc} = \frac{b}{c_{max}}\left(1 - \frac{c}{c_{max}}\right)^{b-1} \tag{40}$$

where *c* is the water storage capacity at a certain location defined as the depth of water that can be stored [L], c_{max} is the maximum water storage capacity [L], and *b* controls the spatial variability of storage capacity over the basin, whereby *b* = 0 indicates a constant value of the storage capacity and *b* = 1 means a capacity that follows a uniform distribution between 0 and c_{max}. Moore (1985) did not specify how to calculate the storage capacity from basic soil properties. Based on Eq. [40] we can derive the maximum water depth S_{max} (L) over the basin as:

$$S_{max} = \int_0^{c_{max}} \left(1 - F(c)\right) dc = \frac{c_{max}}{b+1} \tag{41}$$

The concept proposed by Moore (1985) has been used in many land surface models using a bucket type of soil water model to characterize spatial variability of infiltration and storage capacity such as in VIC (Liang et al., 1994) or HD (Hagemann and Gates, 2003), or Richards equation based LSM (e.g., JULES, H-TESSEL/CH-TESSEL). Clark and Gedney (2008) compared the PDM approach of Moore (1985) and a modified TOPMODEL approach in generating surface runoff using the MOSES (now JULES) LSM, by comparing model output against the observed stream flows in three catchments. TOPMODEL performed best as it allowed a better response to subsurface flow contributing to peak flows but also capturing slower changes in recession times. PDM only improved the calculation of the surface runoff without improving subsurface flow. In Appendix A1 we briefly describe the PDM scheme of Moore (1985).

Rather than using a reflected power density function, Entekhabi and Eagleson (1989) proposed a two-parameter gamma pdf to characterize spatial heterogeneity of soil water content at the level of the grid cell:

$$f_s(s; \alpha_c, \lambda_s) = \frac{{\lambda_s}^{\alpha_c}}{\Gamma(\alpha_c)} s^{\alpha_c - 1} e^{-\lambda s}, \;\; \alpha_c, \lambda_s, s > 0 \tag{42}$$

where *s* is the mean surface layer point soil water saturation defined by

$$s = \frac{\theta}{\theta_s} \quad [43]$$

with θ as the actual and θ_s defined as the saturated volumetric soil water contents [L^3 L^{-3}], respectively. The two parameter Gamma distribution, Γ, in Eq. [42] is related to *s* via:

$$\lambda = \frac{\alpha_c}{\langle s \rangle} \quad [44]$$

where <*f*(*s*)> is the grid mean relative saturation of the surface soil layer [L^3 L^{-3}]. This concept has been implemented for example in the CABLE model (Decker, 2015).

For the CLSM, the basic land element is the (irregularly shaped) hydrological catchment rather than the GCM grid cell. A number of these catchments lie within a given cell, and grid-cell fluxes are computed through areal weighting of the component catchment fluxes. Within an individual catchment element, CLSM simulates a dynamic water table depth of which the distribution is related to catchment topography characteristics using the TOPMODEL formulation (Beven and Kirkby, 1979):

$$d = \bar{d} - \frac{1}{v_K}\left(ln\frac{\alpha_T}{\tan\beta_T} - \bar{x}\right) \quad [45]$$

where *d* is water table depth [L] (negative for ponding layers caused by rising groundwater), $ln(\alpha_T/tan\beta_T)$ is the 'topographic index' at the point in question, $\bar{d}$ is the mean water table depth [L], $\bar{x}$ is the mean catchment value of $ln(\alpha_T/tan\beta_T)$, α_T is the upstream area that contributes flow through a unit contour positioned at the point, and v_K is a parameter describing the decrease of saturated hydraulic conductivity with depth. Each catchment is characterized by its topographic index distribution, which in effect is used to diagnose the spatial variability of soil moisture within the catchment. The information on soil moisture variability is used to define three distinct hydrological regimes: i) the wilting area, ii) the sub-saturated-but-transpiring area, and iii) the saturated fraction. The definition of these three regimes is key to CSLM as different evaporation and runoff physics are applied to each.

4.1.3. Representing Spatial Heterogeneity of Surface Properties that Control Infiltration in a Single Parameter

Several land surface models use a single parameter in combination with pdfs in order to characterize the spatial heterogeneity of infiltration processes. Many of these pdfs, presented above, can be derived from Eq. [38], which was used in Section 4.1.2. to describe the spatial variability of soil water content and related variables. The estimation of this exponent (denoted as *B* or *b*) in such pdfs remains an open question as it cannot be immediately derived from available soil properties. Please note that this exponent has received sometimes a different notation in some LSMs. Liang and Xie (2001) used the “*b*” notation to describe the variability of soil and grid cell properties affecting Dunne excess saturation in the VIC model and the “*B*” parameter to describe the variability of soil and grid cell properties affecting Hortonian infiltration excess in the VIC model. Three main approaches have been reported in the literature to determine this exponent, from here on referred to as the *b* parameter, for simplicity.

In the first approach, the *b* parameter is obtained by model calibration to available hydrological time series. Huang et al. (2003) present a brief discussion of the literature dealing with the estimation of the *b* parameter in the VIC model. They showed that the calibration approach suffers from the problem of equifinality, as so many other LSM calibration exercises. Furthermore, they did not manage to establish meaningful relationships between model parameters and physical characteristics of the catchment or regions.

In the second approach, the *b* parameter is derived from available soil and/or topographic information. For example, Dümenil and Todini (1992) suggested to calculate the *b* parameter from the subgrid standard deviation of topography by

$$b = max\left[\frac{\sigma_h - \sigma_{min}}{\sigma_h - \sigma_{max}}; 0.01\right] \quad [46]$$

where σ_h refers to the standard deviation of the topography within a model grid cell. Balsamo et al. (2009) stated that $\sigma_h$varies between 0.01and 0.5 and σ_{min} and σ_{max} can be set to values proposed by van den Hurk and Viterbo (2003). On the other hand, Habets et al. (1999), in this case for the ISBA model, assumed the *b* parameter to be constant.

The third option fits a pdf to the observed cumulative distributions of soil properties as a function of the occupied space in a grid cell or basin. Sivapalan and Woods (1995) fitted the so-called *Xinanjiang* distribution to data of soil profile depth to estimate the *b* parameter in the following equation:

$$F_S(z^*) = 1 - (1 - Z/Zm)^b \quad [47]$$

where F_s is the cumulative distribution function of the scaled infiltration capacity (scaled by its maximum value); *Z* is the soil profile depth to the bedrock [L] and *Zm* its maximum value of the bedrock depth within the gridcell [L]. Here, it is assumed that the available porosity is constant in space and time. To prove their concept, Sivapalan and Woods (1995) used a regionalized cumulative soil depth distribution for six landforms observed in the Serpentine catchment and obtained the best fit with a value of *b* = 4.03 and *Zm* = 10 m.

Huang et al. (2003) used a method based on a self-organizing neural network map combined with a *K*-means clustering method to develop transfer functions that are able to transfer *b*-values of data rich to data poor areas. The data rich area was used to fit the relation to values of soil water capacity data derived from soil map information to the surface areas of catchments by:

$$w = w_{max}\left[1 - (1 - A)^{1/b}\right] \quad [48]$$

where *w* and w_{max} are the point and maximum point soil water capacity, *A* is the area for which the soil water capacity is less than or equal to *w*, and *b* is defined as a soil water capacity shape parameter. In their study, Huang et al. (2003) used the STATSGO (Digital General Soil Map of the United States) database to represent the data rich areas. Here, it has to be noted that appropriate soil information at resolutions finer than 1 km is presently available, whereby the global SoilGrids1km 250m database of Hengl et al. (2014) is only one example. These new developments will allow estimating the value of the *b* parameter at high resolution globally, without the need of applying transfer approaches as proposed by Huang et al. (2003). Additionally, such highly resolved global map information combined with pedotransfer functions would allow to directly relate the *b* parameter to soil properties to be determined, as well as the subgrid variability depending on the size of the grid cells used in LSMs. This will be explained later on in Section 4.1.5.3.

4.1.4. Estimating the Areal Saturation Fraction F_{sat}

Estimation of the areal saturation fraction, F_{sat}, as used for example in the equations listed in Appendix A2 Eqs. [A24 A35, A36, A40, A58, A50, A52, A56], is key in determining the contribution of Dunne saturation excess runoff and Hortonian infiltration excess runoff to the overall runoff generation of a grid cell in many LSM. In this section, we will discuss briefly the different approaches used in various LSMs. A correct representation of F_{sat} typically requires a good knowledge about subsurface properties like the depth to bedrock, the location of the groundwater table, soil porosity, and the actual state of the soil water content in the profile. One approach that is frequently used in LSMs is based on the assumption that the saturated fraction of a grid cell can be determined from topographical characteristics and the soil moisture status of a grid cell. This approach is closely related to the concept introduced in the TOPMODEL and adopted in many studies of infiltration runoff generation. It has been used in LSMs such as CLM, JULES, Noah-MP, CSLM and ISBA-SURFEX amongst others. Some LSMs only require information on the soil moisture distribution such as CABLE. O ORCHIDEE does not use the concept of F_{sat} but introduces the notion of a ponded fraction which serves the opposite of F_{sat}. Instead of increasing runoff, it does enhance infiltration since it allows the latter to develop over several time steps. JSBACH uses the Arno-Scheme to calculate surface runoff and infiltration and uses soil water capacity to determine F_{sat}. The equations used calculate F_{sat} are listed in Table 2 and a more extensive description of the use F_{sat} in various LSMs, including the concepts used in the TOPMODEL are presented in Appendix A2.

LSM	Distribution of soil moisture	Distribution of precipitation	Distribution of Ks	Saturated fraction of grid cell	Description/Formulation of grid-scale I_{max}	Grid cell soil moisture variability Equation used	*b*-parameter
OLAM-SOIL	No	No	No	Ponding is permitted, and the hydraulic head at the bottom of the pond is the Dirichlet upper boundary condition for Richards Eqn. in the soil layers. Infiltration is the direct solution of Richards Eqn.	Homogeneous within grid box	N.A.	N.A.
ParFlow-CLM	No	No	No	No	No	N.A.	N.A.
ORCHIDEE rev4783	No	No	Exponential pdf	No F_{sat}, i.e. no saturation excess runoff; but ponding can occur because of infiltration-excess runoff (see A3.9)	Maximum infiltration rate not imposed per se in the model concept. It is the outcome Ks distribution and infiltration from top to bottom via a modified Green-Ampt model (see A2.6)	Not described for the horizontal variability	N.A.
Catchment land surface model (CLSM)	Amended TOPMODEL approach: Grid cell soil moisture variability is tied to the catchment water table depth distribution. Moisture distribution is shifted by root zone water in excess (or deficit) of equilibrium conditions.	No	No	Amended TOPMODEL approach:local water table depth *d* is related to local topographic index, mean topographic index and mean water table depth. Saturated fraction equals the fraction of d>0	Maximum infiltration rate not imposed per se in the model concept. It is a complex outcome of off-line Richards equation simulations, TOPMODEL formulations and the model's dynamically varying spatial moisture fields (see A2.7)	Amended TOPMODEL approach: Grid cell soil moisture variability is tied to the catchment water table depth distribution. Moisture distribution is shifted by root zone water in excess (or deficit) of equilibrium conditions.	N.A.
ISBA-SURFEX	Reflected power pdf, or TOPMODEL approach	No	No	Two options available: 1. F_{sat} is based on a Topmodel type approach $\sim 1 f(D_t = (\theta_{sat} - \langle\theta\rangle)\langle d_z\rangle)$ 2. Arno scheme following Dumenil and Todini (1992)	see A2.7	reflected power density function	Can be set to value 0.2 or 0.5 depending on model application
Noah-MP version 3.0	TOPMODEL approach	Exponential pdf	No	$F_{sat} = (1 - F_{frz}) F_{max} e^{-0.5 f_d (z_{wt} - z_{bot})} + F_{frz}$	$P_d \frac{D_x(1-e^{-kdt \Delta t})}{P_d + D_x(1-e^{-kdt \Delta t})}$	N.A.	N.A.
JULES version 4.6	Modified TOPMODEL approach based on local topographic index $\lambda_{local} = ln(T(z_{local})/T(z_T)) + \lambda_m$	No	No	$F_{sat} = a_s exp(-c_s \lambda_{crit})$	$(1 - F_{sat})\beta_s K_s$	Modified TOPMODEL approach based on local topographic index $\lambda_{local} = ln(T(z_{local})/T(z_T)) + \lambda_m$	N.A.
CLM4.5	TOPMODEL approach	No	No		$(1 - F_{sat})K_s C_{ice}$	homogeneous within gridbox	N.A.
CABLE	Gamma pdf (Entekhabi and Eagleson, 1989) $f_s(s) = \frac{\lambda_s^{\alpha_s}}{\Gamma(\alpha_s)} s^{\alpha_s - 1} e^{-\lambda s}$	No	No	$F_{sat} = 1 - erf\left(\sqrt{\frac{K_p}{\lambda_s}}\right)$	N.A.	Entekhabi and Eagleson (1989). $f_s(s) = \frac{\lambda_s^{\alpha_s}}{\Gamma(\alpha_s)} s^{\alpha_s - 1} e^{-\lambda s}$	N.A.
SSiB	No	Exponential pdf	No	$F_{sat} = \frac{1}{b_{SSiB}} log\left(\frac{K_s \Delta t}{P_{drop} c_{SSiB}}\right) - \frac{c_{SSiB}}{a_{SSiB}}$	N.A.	Homogeneous within gridbox	constants based on different plant functional type (Xue et al., 1996)
CH-TESSEL / H-TESSEL	Reflected power pdf	No	No	$F_{sat} = 1 - \left(1 - \frac{W}{W_{sat}}\right)^{b/(b+1)}$	$(W_{sat} - W) + max\left(0, W_{sat}\left[\left(1 - \frac{W}{W_{sat}}\right)^{\frac{1}{b+1}} - \left(\frac{P_T + P_M}{(b+1)W_{sat}}\right)\right]^{b+1}\right)$	reflected power density function	$max\left[\frac{\sigma_o - \sigma_{min}}{\sigma_o + \sigma_{max}}\right]$
JSBACH version 3.0	Reflected power pdf	No	No	Arno scheme following Dümenil and Todini (1992)	For each timestep, infiltration is limited to the the difference between water holding capacity of the rootzone and the water content of the rootzone at the beginning of the timestep.	Homogeneous within gridbox	N.A.

Table 2: *Overview of definition of parameters and properties affecting infiltration in the different LSM.*

4.1.5. Characterizing the Surface Saturated Hydraulic Conductivity, K_s

The saturated hydraulic conductivity, K_s, is a key soil hydraulic property that controls soil water fluxes and thus the infiltration of water in soils. However, K_s is a scale dependent parameter that strongly depends on the support size of the measurement (Ghanbarian et al., 2015), and it exhibits anisotropic behavior (Pachepsky and Hill, 2017). Despite its importance, point scale K_s is a parameter that is still very difficult to estimate from pedotransfer functions that are typically based on simple basic soil information such a soil texture and bulk density. However, this information only partly explains the variability observed in point scale K_s values. In the widely employed ROSETTA software (Schaap et al., 2001), that contains soil hydraulic properties and basic soil information for various soils and is used to estimate soil hydraulic properties, the logarithmicly transferred point scale K_s value is estimated with a coefficient of determination (R^2) equal to 53.5 % when using bulk density, sand, silt, and clay percentages. Including soil moisture content at field capacity and wilting point, the R^2 increased up to 64.7 %. The HYPRES database of soil hydraulic properties for European soils developed by Wösten et al. (1999) that contains information of 1136 horizons for hydraulic conductivity provided a PTF to estimate point scale K_s with an R^2 of 19 %. This function uses silt and clay content, bulk density, percentage organic matter, and whether the soil sample to derive the properties originated from the top soil or subsoil. A similar R^2 value was obtained by Vereecken et al. (1990) using clay, sand and carbon content, as well as bulk density, for 127 undisturbed point scale samples. In order to further increase the prediction of point scale K_s structural properties in addition to currently used soil properties need to be considered (Vereecken et al., 2010).

Currently, pedotransfer functions for point scale K_s are based on relatively small sample volumes. In addition, point scale saturated hydraulic conductivity shows a high spatial variability as it is not only controlled by textural properties but also by soil structural properties and by the management of soils (Strudley et al., 2008, Van Looy et al., 2017). Some of these aspects will be elaborated in more detail in Section 4.1.5.1. In this section, we review the different approaches that currently are being used in LSM to estimate K_s and to represent its spatial distribution at the grid scale.

4.1.5.1. Spatial Distribution of K_s

Table 3 provides an overview of the approaches used to quantify grid scale K_s in 12 different LSMs. It must be stressed, that theses estimations of grid scale K_s are based on PTFs (using the textural class as input for prediction), although the support scale for the development of these PTFs is in all cases the point scale.

In all models studied in the analysis, K_s is considered horizontally uniform across the grid cell except for ORCHIDEE and ISBA-SURFEX. ORCHIDEE considers an exponential distribution of the infiltrability across the grid cell and with depth. Infiltrability is defined as the arithmetic mean of K_s in the deepest fully saturated layer and the hydraulic conductivity in the topmost unsaturated layer. ISBA-SURFEX also considers an exponential distribution of K_s within a grid cell but only for Hortonian runoff (Decharme and Douville, 2006). As already mentioned in Section 3, heterogeneous soil surfaces will generate runoff earlier on than homogeneous soil surfaces, which is partly caused by the heterogeneity in saturated hydraulic conductivity.

With respect to the vertical heterogeneity, JSBACH, Noah-MP, and CABLE assume a constant K_s value with depth. CLSM, JULES, ISBA, ORCHIDEE, and OLAM-SOIL allow for both constant and depth variable K_s values. Vertical heterogeneity of K_s in CLM is derived directly from vertical heterogeneity in soil texture. In ORCHIDEE, K_s decreases exponentially with depth using the K_s value defined at 30 cm depth as a reference value. The extent of the exponential decrease depends on an extinction factor. Furthermore, the K_s profile may be modified depending on root density. For example, CLSM differentiates between surface and root zone layer hydraulic properties (including K_s) in the Richards equation simulations that are used in the derivation of time scale parameters of catchment-scale vertical moisture transfer. For subsurface runoff, CLSM uses a TOPMODEL based approach with a depth-dependent K_s. ISBA can consider up to 14 soil layers with a varying K_s value.

4.1.5.2. Estimators for K_s

In all LSMs, the estimation of grid scale Ks is typically based on soil textural information, but using classical PTFs developed for the point scale (details on these PTFs are provided in Appendix A4). These estimations are often completed with specific estimation functions for organic rich soils (e.g., CLM 4.5, ISBA, JULES, see details in Section 4.1.5.4 and Table 3).

Rahmati et al. (2018) compared the K_s values for the point scale provided by Clapp and Hornberger (1978) with K_s estimates derived from field scale infiltration experiments using the global soil infiltration database SWIG. The K_s derived from these experiments did not show a dependence on soil textural properties. Only for sand and loamy sand the values of Clapp and Hornberger (1978) and the SWIG data were of the same order of magnitude. For all other textural classes SWIG values were larger by a factor two to a factor of more than one thousand. Weynants et al. (2009) pointed out that improved estimates of point scale K_s may be obtained by including structure-related information such as pedologic data and information about land use and crop management, which strongly affect surface soil properties, as a result of tillage, root growth, soil trampling by cattle etc. (see Section 6.1.).

A notable advance is offred by OLAM-SOIL (Walko and Avissar, 2008b, Walko et al., 2000), which uses the pedotransfer functions developed by Weynants et al. (2009) or de Boer (2016) to estimate K_s. The PTFs of Weynants et al. (2009) are based on a dataset of 182 point scale soil samples of Belgian soils (Vereecken et al., 1990, Vereecken et al., 1989). They estimated the texture-dependent K_s value by extrapolating the unsaturated soil hydraulic conductivity data to saturation and then calculated the ratio between the textural dependent K_s and the measured K_s value, which was also available. This ratio is a measure for the effect of structural related properties on measured K_s and was shown to depend on the sand fraction in the soil.

Soil classes in CLSM are parameterized by Campbell (1974) equations and the corresponding hydraulic parameters including K_s are based on lookup tables for twelve different soil textural classes or using the PTFs of Wösten et al. (2001), which are both developed on point scale. Campbell's method used the Brooks-Corey parameterization of the soil water retention curve and a single point measurement of K at a given water content to calculate the complete hydraulic conductivity function.

None of the models directly considers the effect of soil structure on saturated hydraulic conductivity. Only the OLAM-SOIL considers implicitly the impact of structural properties on K_s by linearly interpolating between the measured K_s value and the value of the hydraulic conductivity obtained at a pressure head of about -6 cm as proposed by Weynants et al. (2009). Based on the work of Jarvis (2007) this value was considered to delineate the saturation range that is controlled by structural properties.

In JSBACH, K_s values are assigned to 11 textural classes based on data presented in Beringer et al. (2001). However, the origin of the tabulated K_s values that appear to be mean measured values for a specific textural class is not clear. Most likely, they were derived from the dataset of Clapp and Hornberger (1978).

JULES uses sand and clay content to estimate the saturated hydraulic conductivity for the main soil column. Below the soil column is an additional `deep water store', within which K_s decreases exponentially with depth with a dampening factor set equal to 3 as proposed by Clark and Gedney (2008). K_s values can also be defined for each soil layer and can account for the presence of soil organic matter (Chadburn et al., 2015a). Rahman and Rosolem (2017) incorporated the effect of preferential flow into JULES (but note that this has not yet been adopted in the current 'official' UKMO version of JULES), to allow simulation of highly fractured unsaturated Chalk soils. Their bulk conductivity (BC) model introduces only two additional parameters (namely the macroporosity factor and the soil wetness threshold parameter for fracture flow activation) and uses the saturated hydraulic conductivity from the chalk matrix. The BC model was implemented into JULES and applied to a study area encompassing the Kennet catchment in the southern UK and the model performance at the catchment scale was evaluated against independent data sets (e.g., runoff and latent heat flux). The results demonstrated that the inclusion of the BC model in JULES improved the simulations of land surface water and energy fluxes over the chalk-dominated Kennet catchment. This simple approach to account for soil structure has potential for large-scale land surface modelling applications. ORCHIDEE uses VG soil parameters (K_s, n, α, θ_r, and θ_s) for each USDA class. In addition, a decay of K_s with depth is imposed (as also in JULES), as written in Section 4.1.1. With respect to the horizontal variability, ORCHIDEE uses an exponential PDF to describe horizontal heterogeneity.

4.1.5.3. Use of Soil Maps to Estimate K_s

The previous section shows that the basic soil information that is used to derive the soil properties needed to estimate point scale K_s differs amongst the models. Importantly, each LSM, in particular when employed for weather forecasting or GCM studies, can use different soil maps to inform the model on soil hydraulic parameters (so called ancillary data). For example, CABLE uses the Zobler soil class information (Zobler, 1986). The version used by Decker (2015) uses the soil texture from the Harmonized World Soil Database (FAO, 2009), and so does JULES. OLAM-SOIL uses the SoilGrids data published by Hengl et al. (2014) and Hengl et al. (2017) The SoilGrids databases provide information on basic soil properties at seven depths in the soil profile up to 2m. They also provide estimates of the depth to bedrock and the distribution of soil classes. The gridded predictions were based on approx. 150.000 soil profiles and remotely sensed data. The input data used to estimate the soil hydraulic properties by CLSM or ISBA-SURFEX are obtained from the Harmonized World Soil Database version 1.21 (HWSD1.21) and the State Soil Geographic (STATSGO2) project (de Lannoy et al., 2014). PARFLOW-CLM uses the UNESCO soil map of the world (FAO, 1988) to provide a global coverage of K_s values.

The default soil texture map used in ORCHIDEE is the map presented by Zobler (1986) at 1° and it is used in the currently ongoing CMIP6 simulations. CMIP6 refers to the coupled model intercomparison project phase 6 that aims to address 1) how the Earth System is responding to forcing, 2) origins and consequences of systematic model biases and 3) the assessment of future climate change in the contect of internal climate variability, predictability and scenario uncertainty (Eyring et al., 2016). ORCHIDEE can also use two other soil texture maps. The first one is the map developed by Reynolds et al. (2000) at 1/12° and the second one is the surface SoilGrids maps at 1 km (Hengl et al., 2014). All these maps are used to define the dominant texture at the model resolution, using the USDA texture classification.

CLM 4.5 uses the soil dataset produced by the Global Soil Data Task 2000 that comprises 4931 soil mapping units and contains the textural composition (sand and clay content). These data were used by Bonan et al. (2002b) to create a global soil map of mineral soil textural data. The global data on soil carbon content are obtained from ISRIC-WISE (Batjes, 2006), whereas the soil carbon content for the higher latitudes are obtained from the Northern Circumpolar Soil Carbon Database (Hugelius et al., 2013).

4.1.5.4. K_s and Infiltration in Organic Soils

Four models listed in Table 3 adjust the calculation of K_s for soils rich in organic manner as these soils typically show higher K_s than mineral soils. Organic soils mostly refer to soils in the Northern latitude and tropical areas and include permafrost and peat soils. The first few centimeters of these soils typically have a soil organic carbon content of up to 100% (Lawrence and Slater, 2008). CLM 4.5 use the approach proposed by Lawrence and Slater (2008) to calculate K_s as

$$K_{s,i} = \left(1 - f_{sc,i}\right)K_{s,min,i} + f_{sc,i}K_{s,sc,i} \qquad [49]$$

where $f_{sc,i}$ is the soil carbon density of a soil normalized by the soil carbon density of peat in layer *I*, $K_{s,sc,i}$ is the saturated hydraulic conductivity [L T^{-1}] of the organic carbon fraction in layer *i*,. $K_{s,min,i}$ is the saturated hydraulic conductivity of the mineral fraction [L T^{-1}], whereby $K_{s,min}$ is obtained from the point scale PTFs of Clapp and Hornberger (1978) and Cosby et al. (1984) and given by

$$K_{s,min,i} = 0.0070556 \times 10^{-0.884+0.0153(\%sand)_i} \qquad [50]$$

Values for $K_{s,sc}$were given by Letts et al. (2000).

In JULES and ISBA-SURFEX a geometric average of the point scale K_s is used to account for the effect of soil carbon following the approach of Chadburn et al. (2015b) and Decharme et al. (2016), respectively, with:

$$K_s = {K_{s,min}}^{(1-f_{sc})} \times {K_{s,sc}}^{f_{sc}} \qquad [51]$$

For CLM 4.5, soil organic matter data are obtained from the Harmonized World Soil Database, except for the northern high latitudes which come from the Northern Circumpolar Soil Carbon Database (Hugelius et al., 2013). In ISBA, the soil organic carbon content is determinated from two soil horizons (0-30cm and 30-100cm) of the HWSD1.21.

In JSBACH three additional classes are added to the 11 soil textural classes, namely peat, moss, and lichen, each with an average value of K_s according to Beringer et al. (2001).

In CLSM, soils are stratified into four levels of organic carbon content (de Lannoy et al., 2014), with the highest one (>8.72% C, i.e. >15% organic matter) representing peat. Peat parameters were taken from the point scale information provided by Wösten et al. (2001) that represent highly decomposed peat. In a recently developed peatland module for CLSM, parameters and model structure were further revised, i.a. accounting for the high macropore fraction of undecomposed peat by allowing direct infiltration to the water table when the top soil layer becomes saturated, i.e. effectively turning off the Hortonian runoff mechanism over peatlands (Bechtold et al., under review).

LSM	PTF to estimate for grid-scale K_s	Underlying soil maps to provide coverage of K_s	Use of soil structural information	K_s constant in grid cell	Variation of K_s with depth
OLAM-SOIL	Weynants et al. (2009) or de Boer (2016)	Soil Grids (Hengl et al., 2014)	Yes	Yes	Yes
ParFlow-CLM	Schaap and Leij (1998) for the first 10 soil layers and Gleeson et al. (2011) for deeper layers	FAO (1988) and Gleeson et al. (2011)	No	Yes	Yes
ORCHIDEE rev4783	lookup tables for van Genuchten soil parameters for each USDA class	Zobler (1986) at 1° is the default soil texture map, but other soil maps can be used alternatively: Reynolds et al. (2000) at 1/12° and the SoilGrids maps at 1km (Hengl et al., 2014)	No	No[b]	Yes
Catchment land surface model (CLSM)	Campbell (1974) or Woesten et al. (2001)	Harmonized World Soil Database version 1.21 (HWSD1.21) and the State Soil Geographic (STATSGO2 project) (De Lannoy et al. 2014).	No	Yes	Yes
ISBA-SURFEX	from Clapp and Hornberger (1978) or Cosby et al. (1984) (optional) ; for organic soils (Decharme et al., 2016)	Harmonized World Soil Database (HWSD; http://webarchive.iiasa.ac.at/ Research/LUC/External-World-soil-database/HTML/), (FAO/IIASA/ISRIC/ISSCAS/JRC, 2012) at a 1 km resolution from the Food and Agricultural Organization (FAO/IIASA/ISRIC/ISSCAS/JRC, 2012).	No	Yes	Yes
Noah-MP version 3.0	from Clapp and Hornberger (1978)	Harmonized World Soil Database (FAO, 2009) or Milovac et al. (2014)	No	Yes	No
JULES version 4.6	from Clark and Gedney (2008); for organic soils Chadburn et al. (2015)	The default configurations of JULES use soil ancillaries based on sand/silt/clay fractions from the harmonised world soil database (HWSD), using function of Cosby et al 1984.	No	Yes	Yes
CLM4.5	from Clapp and Hornberger (1978) and Cosby (1984), for organic soils Lawrence and Slater (2008)	Based on IGBP soil data set for mineral soils (IGBP, 2000), with organic soil described from ISRIC-WISE (Batjes, 2006) and the Northern Circumpolar Soil Carbon Database (Hugelius et al., 2013)[a]	No	Yes	Yes
CABLE	same as horizontal	CABLE rev 2.0 uses the Zobler soil class information [Zobler, 1986, 1999]. Decker [2015] uses sand/clay/silt fractions from the Harmonized World Soil Database [FAO, 2009], calculating soil properties from the textures as in CABLE rev 2.0 from Zobler [1986].	No	Yes	No
SSiB	from Clapp and Hornberger (1978) and Sellers et al. (1986)	Harmonized World Soil Database v.1.1 (FAO et al., 2009)	No	Yes	No
CH-TESSEL	Based on tabulated values for 7 textural classes including organic soils (Balsam et al., 2009)	FAO (2003) soil texture map	No	Yes	yes
JSBACH version 3.0	from Beringer et al. (2001)	Based on an improved FAO soil type dataset (Hagemann and Stacke, 2015)	No	Yes	No

[a] The International Geosphere-Biosphere Programme (IGBP) soil dataset (Global Soil Data Task 2000) of 4931 soil mapping units and their sand and clay content for each soil layer were used to create a mineral soil texture dataset (Bonan et al. 2002b). Soil organic matter data is merged from two sources. The majority of the globe is from ISRIC-WISE (Batjes, 2006). The high latitudes come from the 0.25o version of the

[b] based on exponential pdf (see Table 2 and A2.6)

Table 3: *Overview of approaches used for the spatial distribution of saturated hydraulic conductivity, K_s in the LSMs. References for Table 3: Weynants et al. (2009), de Boer (2016), Hengl et al. (2014), Schaap and Leij (1998), Gleeson et al. (2011), FAO (1988), Zobler (1986), Reynolds et al. (2000), Campbell (1974), Wösten et al. (2001), de Lannoy et al. (2014), Clapp and Hornberger (1978), Cosby et al. (1984), Decharme et al. (2016), FAO (2009), Milovac et al. (2014), Clark and Gedney (2008), Chadburn et al. (2015b), Lawrence and Slater (2008), Batjes (2006), Hugelius et al. (2013), Zobler (1999), Decker (2015), Sellers et al. (1986), FAO (2003), Beringer et al. (2001), Hagemann and Stacke (2015), IGBP (2000), Bonan et al. (2002a), Batjes (2006).*

4.2. Numerical Treatment of Infiltration in LSM

The precipitation simulated in LSMs either infiltrates into the soil or becomes runoff when the soil is saturated (Dunne overland flow) or if the precipitation rate exceeds the infiltration capacity of the soil (Hortonian runoff). As have been discussed above, various modeling approaches have been developed to describe infiltration and transition to surface runoff. In the following, we provide an overview of the numerical treatments used by the LSMs listed in Table 1.

The version of ORCHIDEE described here (Ducharne et al., 2017) solves water infiltration and redistribution based on the diffusivity form of the Richards equation, using an 11-layer vertical discretization (de Rosnay et al., 2002). Since d'Orgeval et al. (2008), point (profile) scale infiltration is no longer calculated based on the Richards equation, instead, it invokes a piston-like wetting front inspired by the Green and Ampt (1911) formulation to simplify the boundary conditions under time-varying rainfall rates and soil moisture profiles. In ORCHIDEE, the speed of the wetting front propagation is simplified in two ways, which both tend to reduce infiltration compared to the classical Green and Ampt formulation: (i) the suction at the front is neglected, (ii) the hydraulic conductivity at the wetting front is not the soil K_s, but an arithmetic mean of K_s in the lowest fully saturated layer and $K(\theta)$ in the topmost unsaturated layer (the resulting value is termed K_i). An iterative procedure is used to account for saturation of a soil layer after the other, and infiltration-excess (Hortonian) runoff results when the rainfall rate cannot infiltrate over a single ORCHIDEE time step of 30 minutes. In this framework, infiltrability depends on the profiles of K_s and $K_{(\theta)}$, which itself depends on K_s and θ based on the Mualem-van Genuchten model (Eq. [7] and [8]). The value of K_s at 30 cm depth is taken from Carsel and Parrish (1988) for the 12 USDA soil textural classes, but K_s exponentially decreases with depth following Beven and Kirkby (1979).

In the original JULES version listed in Table 1, soil water fluxes are calculated by numerically solving the diffusivity form of the Richards equation, for the soil water content increment $\Delta\theta$, where $K(\theta)$ and $h(\theta)$ are given by either Brooks Corey (Eqs [4] – [6]) or van Genuchten (Eqs [7] and [8]) parametric models. The choice of parametric model is set by the user. Note that currently the JULES van Genuchten scheme uses parameters (h_c and n_{vg}) that are directly derived from the Brooks Corey soil ancillary parameters as used for the Cosby et al. (1984) $K(\theta)$ and $h(\theta)$ equations, rather than employing van Genuchten-specific PTFs given by Wösten et al. (1999), for example. The numerical scheme uses an implicit 'forward timestep weighting' for numerical stability, in which the water fluxes are first calculated as a first order finite difference scheme using Eq. [3], but then the moisture increments are recalculated with K and h given by the water contents after the timestep, effectively solving Eq. [52] (see Best et al., 2011 for detail):

$$\frac{\partial\theta}{\partial t} = \frac{\partial}{\partial z}\left(K(\theta+\delta\theta)(\frac{\partial h(\theta+\delta\theta)}{\partial z}+1\right) \quad [52]$$

The vertical discretisation in JULES is flexible and set by the user. For the standard operational configurations and current Earth System Model only four soil layers are used, with thicknesses of 0.1, 0.25, 0.65, and 2 m. For greater numerical accuracy, a finer discretisation has been applied (e.g., Chadburn et al., 2015b). Model time stepping in JULES is typically less than an hour but set also by the user. Recently, Haverd et al. (2016) and Cuntz and Haverd (2018) implemented a new soil (Haverd and Cuntz, 2010a) and snow model with physically accurate freeze-thaw processes within CABLE, which solved the Richards equation in the mixed form.

In JSBach (Hagemann and Stacke, 2015, Roeckner et al., 2003) the diffusive form of Richards equation is used with hourly model time stepping. The soil profile is disretized in the first compartment with 6.5 cm layer thickness and vertical infiltration is calculated based on the ARNO scheme according to Dümenil and Todini (1992), whereby water will infiltrate while precipitation is below the difference between local storage capacity and the initial water content within the root zone. In JSBach no ponding is allowed and the lower boundary has no impact on the infiltration rate.

In SSiB (Sun and Xue, 2001a, Xue et al., 1991, Zhan et al., 2003) the water flow is solved by the diffusivity form of the Richards equation, whereby the soil is discretized non-uniformely with smaller layer thicknesses close to the surface (upper layer = 1.75 cm). Time stepping is less than an hour and runoff will occur if precipitation exceeds the saturated hydraulic conductivity, K_s. No ponding of water is allowed at the soil surface.

Noah-MP (Niu et al., 2011b, Schaake et al., 1996), JULES (Best et al., 2011), and CABLE (Decker, 2015, Kowalczyk et al., 2013, Kowalczyk et al., 2006b) also solve the Richards equation in its diffisivity form and none of these models calculate the infiltration rate directly from Richards equation. Vertical discretization varies between 2.2 cm (CABLE) to 10 cm (Noah-MP and JULES) for the upper layer and time stepping is less than a day for all models (see Table 1). No ponding is allowed for any of these three models and for Noah-MP and JULES the lower boundary does not affect infiltration, whereas for CABLE the infiltration will be modified by changes in the soil moisture profile due to groundwater influence.

Another set of LSMs solve the Richards equation in its mixed form such as Parflow-CLM (Kollet and Maxwell, 2006, 2008b), OLAM-SOIL (Walko et al., 2000), and ISBA (Boone et al., 2000, Decharme and Douville, 2006), the Catchment-Land Surface Model (CLSM) (Ducharne et al., 2000, Koster et al., 2000), and CABLE enhanced by Haverd et al. (2016) and Cuntz and Haverd (2018). Because these models solve the Richards equation in the mixed form the infiltration rate can be directly computed from solving Richards equation. Nevertheless, ponding is only allowed in OLAM-SOIL, Parflow-CLM, and enhanced CABLE.

In CLSM, infiltration rates are not solely an outcome of the Richards equation simulations. They are one component of an overall catchment-scale model concept with other processes affecting infiltration rates. CLSM uses a non-traditional framework that strongly emphasizes the subgrid horizontal variability of the land surface hydrological processes. The results of the one-dimensional Richards equation simulations are combined with TOPMODEL formulations that control the varying water table depth and moisture fields at the catchment scale. From this combination, time scale parameters of catchment-scale vertical moisture transfer are derived. It is to be emphasized that in this approach the spatial water table depth distribution is an important factor influencing catchment-scale infiltration rates.

5. Sensitivity of Infiltration-runoff Process to Model Parameters

Most sensitivity studies that have been performed with LSM models with respect to infiltration-runoff processes have focused more on the analysis of runoff and river discharge (e.g., Huang et al., 2017, Materia et al., 2010, Zhang et al., 2016) and less on the sensitivity of the infiltration process to model parameters. In this section, we will review the results from sensitivity studies on LSMs that provide information on key parameters controlling infiltration processes and thus ultimately the whole water and energy balance.

One of the first studies to analyze the sensitivity of LSM to infiltration processes was conducted by Dirmeyer and Zeng (1999). They analyzed the sensitivity of infiltration to the treatment of convective precipitation and the choices made with respect to the vertical resolution of the soil profile and soil properties. They found that the choice of the thickness of the surface soil layer impacts the simulation of the infiltration, with thinner surface layers causing infiltration excess to be more likely as the thinner surface layer has a much smaller capacity. Basic information about the impact of the vertical discretization of the hydrological components is also provided in this review in Section 2.4.4. Unfortunately, in most LSMs the discretization is predefined and often fairly coarse. In addition, Dirmeyer and Zeng (1999) found that a “realistic” distribution of convective rainfall in space and time at the grid cell scale is needed to adequately represent the infiltration, and thus, surface runoff. In addition, evaporation of intercepted canopy water will be overestimated if “unrealistic” distributions of convective rainfall will be assumed. They also analyzed in detail the impact of having a depth dependent soil porosity (here they used three layers for the SSiB model) with a higher porosity for shallow soil layers and lower porosity (more compaction) for deeper ones. By doing so, they modelled larger infiltration amounts and reduced gravitational drainage. Finally, thinner soil layers (2 instead of 5 cm) were found to generate more infiltration excess, i.e. higher surface runoff, during high insensitivity rainfall events and soil melt.

Soet et al. (2000) analyzed different conceptualizations of the land surface scheme and parameter values for three sites with contrasting soils and climate using the ECMWF TESSEL land surface model developed by Viterbo and Beljaars (1995). A sensitivity analysis, set up to explore the impact of using standard parameter values instead of site-specific ones, found that implementing site specific soil hydraulic properties had a significant effect on runoff and infiltration at all three sites. On the other hand, the use of standard soil parameters led to a systematic underestimation of evapotranspiration and biases in surface runoff that differed in sign for the three different locations.

The sensitivity of the infiltration shape parameter *b* in the VIC model (see Section 4.1.1) as well as the exponent in the Brooks Corey equation (Eg. [4] – [6]) were found to be key for correct representation of the hydrological system and the partitioning of rainfall between infiltration and runoff under dry soil conditions (Demaria et al., 2007). Ducharne et al. (1998) found a similar sensitivity to the *b* parameter for the bucket model version of ORCHIDEE. On the other hand, the impact of these parameters on surface runoff generation and stream flow simulations in wet regions was not significant. Shi et al. (2014) analyzed the sensitivity of the catchment outlet discharge rate to soil properties in the Penn State model Flux PIHM and found an important impact of the van Genuchten parameters h_c and $n_{vg}\alpha$ and n (see Eq. [7] and [8]) on both discharge rate and soil water content. Runoff simulations of ten state-of-the-art hydrological and land surface models including H-TESSEL, JULES, and ORCHIDEE were compared by Beck et al. (2017) and they argued for the need to better calibrate, parametrize, and regionalize the parameters of these macro-scale models. Most models were found to generate snowmelt runoff that occurred too early, either due to the underestimation of precipitation or incorrect description of input snowfall, snow physics, and meltwater infiltration into the soil (Bierkens, 2015). Getirana et al. (2014) calibrated river routing parameters and stated that one of the most important aspects to getting the runoff timing (by 1 or 2 months!) and runoff volumes right was the specification of the soil water threshold when runoff occurs (using the Habets and Saulnier (2001) option for runoff in ISBA). They extended the study of (Getirana et al., 2017) to a large group of LSMs including those presented here (e.g., CLSM, ISBA, H-TESSEL, JULES, ORCHIDEE) and found that this was also the case for most of the other LSMs in the ALMIP2 ensemble analysis. In another study, Gudmundsson et al. (2012) compared nine large scale LSMs including H-TESSEL/CH-TESSEL, JULES, and ORCHIDEE to predict observed runoff percentiles of 426 small catchments throughout Europe and found, that the differences in performance between the models became more pronounced for low runoff percentiles. They concluded that this might be explained by the uncertainty associated with the representation of hydrological processes, such as the depletion of soil moisture storage by rootwater uptake. It is likely that differences in the treatment of infiltration and calculation of hydraulic properties will also have played a role. The performance of three LSMs was analyzed by Sahoo et al. (2008), including HySSiB, Noah, and CLM and the authors found substantial differences in the prediction of surface and subsurface runoff for the Little River experimental watershed, Georgia (USA), which was caused by differences in the partitioning of the precipitation into infiltration, surface runoff, and evaporation. An extensive analysis was presented by Zhou et al. (2012) who compared a set of 14 land surface models (including VISA, CABLE, ISBA, CLMTOP, and Noah) and six Budyko-type models against the observed mean annual runoff from 150 large basins. They showed that the LSM biases in the prediction of the simulated mean annual runoff were caused by errors in forcing data, model parameterizations, but also by structural model errors. The largest biases between the LSM estimates and observed runoff were found in regions with low mean annual runoff, which corresponds with the findings of Gudmundsson et al. (2012). Hogue et al. (2006) evaluated the model performance and parameter sensitivity for varying levels of land surface model complexity across four different biomes using five LSMs including Noah-MP. They found a large variability amongst porosity, saturated hydraulic conductivity, K_s, and the *b* parameter used in these models. Based on the impact of these parameters on the simulation results, the authors advocate either a rigorous calibration or the development and integration of improved vadose zone water flow models. Especially, calibration of these parameters at different experimental sites led to differences with respect to the standard values. A study in the same direction was performed by Cuntz et al. (2016) who analyzed the role of hard coded model parameters (i.e., providing the user with no option to change values) on the hydrological fluxes in Noah-MP. They found that the total runoff was sensitive to both plant and soil parameters (e.g., soil porosity), and that therefore, these parameters should be considered for calibration. They also stated, that surface runoff is affected by subsurface runoff, which is dependent on available soil water in the soil profile. Yang and Niu (2003) compared three different schemes of topography-based runoff production for the LSM VISA (which is based on the LSM of Bonan (1998) and analyzed their sensitivities to key parameters using two catchments. They found that the decay factor, *f*, which controls the timing and partitioning of subsurface runoff by rescaling the saturated hydraulic conductivity, K_s, with depth, is a highly important parameter controlling water table depth and the saturated fraction of the grid cell. Shellito et al. (2016) compared calibrated soil hydraulic parameters in Noah using in-situ soil moisture network data and surface soil moisture from SMOS satellite observations obtained from seven sites in the US. Most calibrated simulations lead to higher surface runoff than simulations based on hydraulic parameters estimated from textural information using a pedotransfer function. The calibrated soil hydraulic parameters included pore size distribution index, saturated soil water content, saturated hydraulic conductivity, K_s, and the saturated matric potential (or air entry value, h_c) in the Brooks-Corey equations (Eq. [4] – [6]). Finally, Yang et al. (2005) concluded that the characterization of the vertical soil hydraulic heterogeneity is highly important to correctly describe soil water and soil temperature at the land surface and thus indirectly infiltration and surface runoff. Based on numerical simulations and experimental data, they concluded that it was not possible to replace vertical soil heterogeneity by a homogeneous soil with effective parameters.

In conclusion, there is relatively little information provided in literature on how well the infiltration process and the generation of Dunne or Hortonian overland flow are modelled using different LSMs, and which model parameters mostly impact the infiltration process. In addition, this literature review indicates that it is difficult to identify sources of errors in handling infiltration estimation due to the complexity and the different ways in which the infiltration proces is being described. One approach to address comparisons of different approaches was proposed by Clark et al. (2015) who advocated the development of models that include different paramterizations of the infiltration process so that parameters and parameterizations can be evaluated in a controlled manner.

6. Improving the Infiltration Process in LSMs

The balance between parametrization of complex heterogeneous soil structure and exogenic processes that affect infiltration with the operational performance to compute infiltration/runoff processes that are embedded within LSMs, requires an understanding towards the trade-off of adding more complex physics to describe the infiltration/runoff process and the reality of the technical aspects of computing land surface processes and the determination of related parameters. Also, infiltration/runoff are just two of many other processes impacting the land-atmosphere interaction. This section therefore, aims to provide an overview to contextualise the complexity of the derivation of soil hydraulic parameters, rather than to point out the shortcomings of LSMs in terms of modelling infiltration and runoff.

In general, there are many soil characteristics broadly related to soil composition and structure (including macro- and biopores), and also to exogenic processes, including water repellency, wetting and drying, swelling and shrinkage, air entrapment, freeze/thaw, thermal gradients, impermeable layers, and anthropogenic perturbations (e.g., tillage, harvesting) that impact infiltration and runoff at the point scale (see Young and Crawford (2004) and Hannes et al. (2016), for example).

Most of these are presently not considered in most hydrological and land surface models, or not in enough detail and there is only little ongoing work in this sense such as the implementation of soil structure in the OLAM-SOIL model (see Table 3) by the use of a dual porosity model. Unfortunately, the main challenge in implementing soil structure into the LSMs lies in the lack of PTFs considering e.g. soil structure explicitly and also the temporal change of soil structure.

In the following, we provide an overview of these processes and features and discuss the impact on infiltration and runoff generation briefly.

6.1. Soil Structure

The physical soil structure is formed by the combination of the size, shape, and arrangement of voids and solids, which ultimately affect water infiltration and runoff, mainly through the soil hydraulic properties (water retention and hydraulic conductivity curves) that are part of most LSMs and hydrological models. In general, the amount of water that infiltrates into a soil is dependent on the available void space (represented by the model soil layer porosity), which is the cross-sectional area of flow. Greater soil aggregation and pore connectivity increase bypass or preferential flow, therefore, increasing the hydraulic conductivity and movement of water to deeper soil layers (e.g., Franzluebbers, 2002, Nissen and Wander, 2003). However, the process has not been implemented in most LSMs (Le Vine et al., 2016), apart from the efforts described in Rahman and Rosolem (2017). The formation of aggregates and the stability of the intra-aggregate void spaces is dependent on the rearrangement, flocculation, and cementation of soil and is mediated by the soil organic carbon (SOC), soil biota, ionic bridging, soil clay content, and carbonates. Additionally, macro-organisms facilitate soil porosity, infiltration, and aggregate stability by ingestion of soil (Brown et al., 2000). Factors affecting soil aggregation are summarized in Fig. 7. Macropores, defined as large continuous openings formed by macro-organisms (e.g., earthworm burrows, old root channels) have also an important influence on infiltration and subsurface storm flows as reviewed by Beven and Germann (1982) and for snowmelt infiltration by Mohammed et al. (2018).

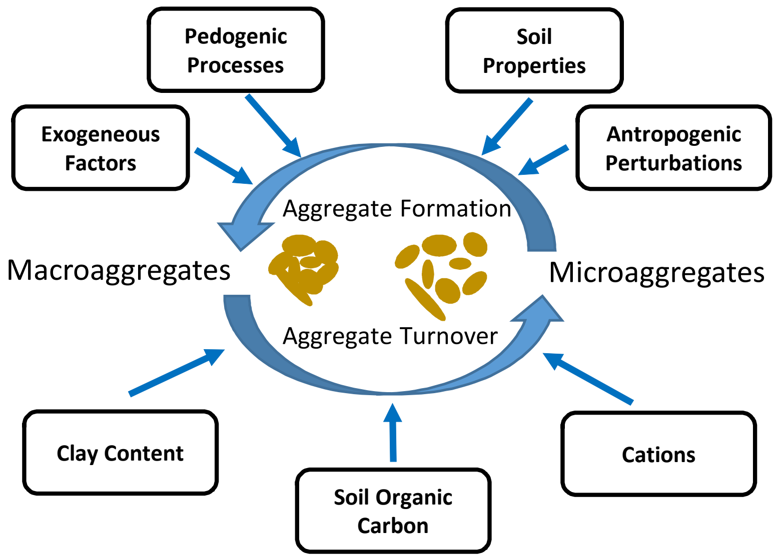

Figure 7: *Factors affecting soil aggregation (modified after Bronick and Lal (2005)).*

Growing vegetation modifies the soil matrix, affecting soil hydraulic conductivity and soil water storage. Hereby, roots alter the distribution of pore size and connectivity between pores as they push into the soil matrix, and they also release complex organic compounds into the soil (Bengough, 2012). The continuous network of branched roots that permeate the soil, with new roots frequently forming while old ones decay, causes hydrological processes to change. Root length distribution is a key property that controls connectivity and preferential flow pathways within the rooting zone and thus impacts infiltration (Lange et al., 2009).

6.2. Hysteresis in the Soil Water Retention Curve and Thermal Effects on Hydraulic Properties

Many LSM models assume that the difference between the soil water retention behaviour between wetting and drying phases in unsaturated soils (hysteresis) can be ignored and that the soil can be considered as having one unique soil water retention curve, which is used to solve Richard's equation (Eq. [3]).

However, hysteresis can play a crucial role in the accurate description of the flow processes within a soil profile (Glass et al., 1989, Hanks et al., 1969, Ibrahim and Brutsaert, 1968, Scott et al., 1983). Hysteresis is a process that describes the non-identical nature of equilibrium soil water content in relationship to matrix potential, during the wetting or drying phases. The relationship between actual soil water content and matric potential can be obtained in desorption, i.e. drying of wet soils, or sorption, i.e. gradual wetting of dry soil. The resulting desorption/sorption curves are generally not identical, because equilibrium soil water content is greater at a given suction in drying than during wetting. The relationship of actual water content and matrix potential has been extensively studied by Haines (1930), Everett (1955), Poulovassilis (1962), Topp (1971), Mualem (1974), Mualem and Dagan (1975), Parlange (1976), Hogarth et al. (1988), Nimmo (1992), Bachmann and van der Ploeg (2002), Huang et al. (2005), and Mualem and Beriozkin (2009).

Thermal gradients also induce significant changes in the estimated water fluxes as temperature affects soil hydraulic properties (Ben Neriah et al., 2014, Gardner, 1955, Grant and Bachmann, 2002, Grant and Salehzadeh, 1996, Hopmans and Dane, 1986, Nimmo and Miller, 1986, Parlange et al., 1998, Philip and de Vries, 1957, She and Sleep, 1998). For example, increasing water temperature decreases water viscosity, causing an increase in hydraulic conductivity (Levy et al., 1989), and thermal swelling of solid particles that change soil pore characteristics and the solid/liquid interface between soil particles (Gao and Shao, 2015).

The advancement of innovative modelling that includes the hysteretic nature of soil water retention curve was reviewed and further developed by Nuth and Laloui (2008) but it has to be mentioned that for large scale LSMs the inclusion of hysteretic complexity requires greater computing capability and the knowledge of input parameters from observations and databases, or availability of appropriate pedotransfer functions.

6.3. Soil Water Repellency

Soil water repellency (SWR) or hydrophobicity reduces the affinity of soils to infiltrating water such that they resist wetting for periods ranging from a few seconds to hours or even weeks (e.g., Doerr and Thomas, 2000, King, 1981). Additionally, soil water repellency is spatially and temporally very variable (Regalado and Ritter, 2008, Ritsema and Dekker, 1998, Täumer et al., 2005). SWR is mostly caused by the coating of the soil particles by hydrophobic substances, whereby different organic compounds derived from living or decomposing plants or microorganisms can be responsible for SWR. Soils below particular vegetation types (such as needle leaf trees), soils with higher soil carbon content, coarse textured soils, as well as areas with frequent wildfire are more prone to SWR compared to others. A review of factors affecting SWR is given by Doerr et al. (2000). As mentioned, SWR will reduce the soil infiltration capacity (e.g., Imeson et al., 1992, Van Dam et al., 1990), and therefore, will increase overland flow (e.g., Crockford et al., 1991, McGhie and Posner, 1981, Witter et al., 1991). Topsoil SWR may cause Hortonian overland flow (runoff) even at precipitation events with rates much smaller than saturated hydraulic conductivity.

In LSMs where K_s is derived from pedotransfer functions, and where water repellency is not included, this may lead to ovestimation of infiltration for SWR prone soils. In some areas, water repellent layers underlie highly permeable hydrophilic surface layers, and here, the infiltrating water may pond above the water-repellent layer and subsequently the infiltration water can be stored above this hydrophobic layer and be used for evapotranspiration.

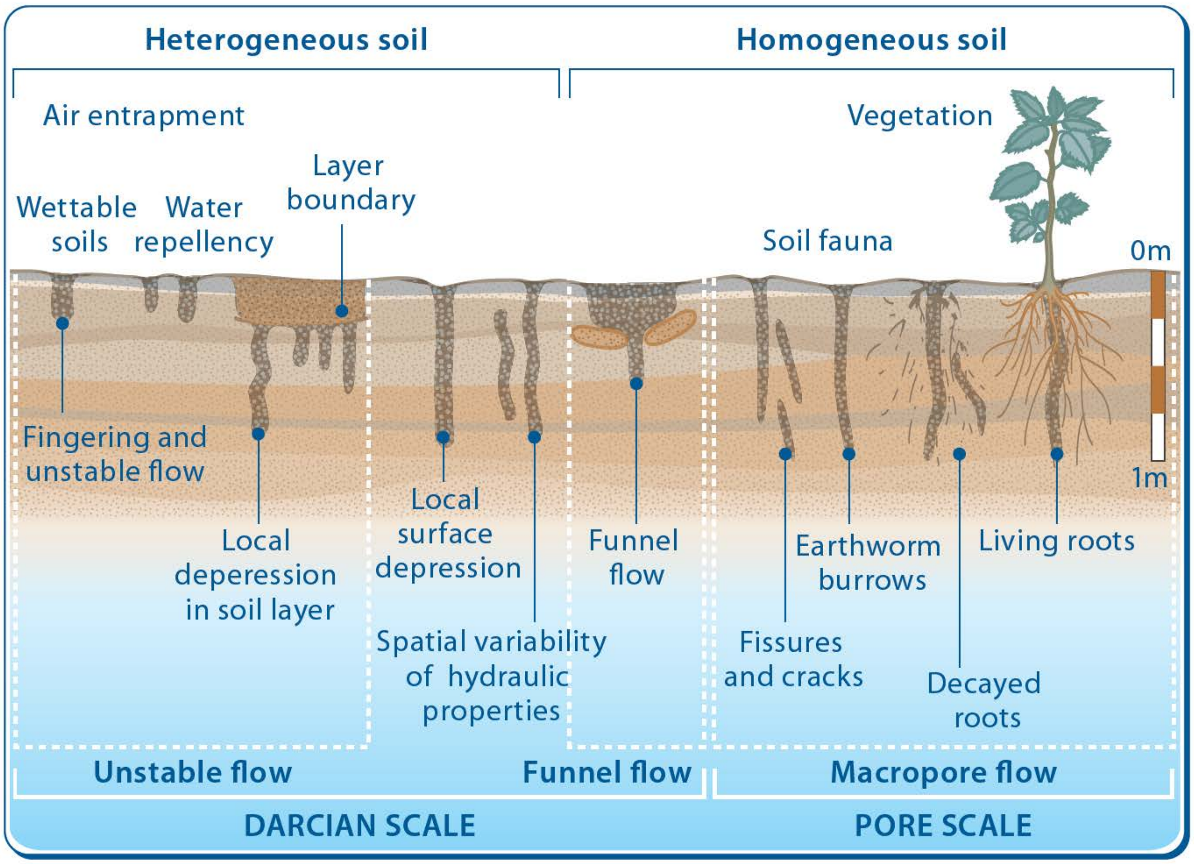

Figure 8: *Schematic illustration of possible hydrological responses of the soil under wettable and water repellent soils, layer bounds, spatial variability of soil hydraulic properties, and macropore flow induced by soil fauna and vegetation. Or et al. classnotes with permission.*

This process can also cause saturated excess overland flow if the above permeable layer becomes fully saturated, can cause lateral water flow either through structural gaps or along the slope of the hydrophilic layer, or the water can move downwards through the hydrophilic layer along preferential flow paths (Doerr et al., 2000). A schematic illustration of the possible hydrological responses caused by top and subsoil hydrophobicity is provided in Fig. 8. According to our knowledge, SWR has not yet been implemented in any LSM.

6.4. Compaction, Swelling, and Shrinkage

Compaction is the process of reducing the volume of voids in a soil, mainly those filled with air, by packing the soil particles closer together. It can result from natural processes such as soil overburden or from anthropogenic causes, such as the use of cultivation machinery or cattle grazing. Compaction is often characterized by the increase of soil bulk density. This has often been considered as an appropriate independent variable to quantify the decrease in the soil saturated hydraulic conductivity (Ahuja et al., 1989, Assouline and Or, 2008, Laliberte et al., 1966, Or et al., 2000) or the changes in the soil hydraulic functions (Ahuja et al., 1998, Assouline, 2006a, b, Stange and Horn, 2005) following compaction. These estimates can thus be applied to evaluate the impact of soil compaction on infiltration. Soil swelling during wetting and shrinking during drying induces dynamic changes in porosity with changing water content of the soil and changes in the hydraulic properties, which consequently affect infiltration (Giraldez and Sposito, 1985, Philip, 1970, Raats and Klute, 1969, Smiles, 1974, Sposito, 1975). In general, the macroporosity, and to a lesser extent the microporosity, of swelling and shrinking soils is affected by their shrinkage and swelling behaviour (Alaoui et al., 2011), whereby exactly these voids in the pore system are highly important for rapid water infiltration into the soil and the separation between infiltration and runoff. Electrolyte concentration of the applied water also can have a significant impact on soil hydraulic properties and on the infiltration process. The way the soil structure behaves to electrolyte concentration depends on pedogenic processes and the nature of the parent material. For example, a high proportion of sodium ions relative to other cations weaken the bonds between soil particles, decreasing hydraulic conductivity (Frenkel et al., 1978, McNeal and Coleman, 1966, Quirk, 1994, Rengasamy and Olsson, 1991). This process and its impacts on soil physical and chemical properties is described in several studies (Assouline and Narkis, 2011, Assouline et al., 2016, Bresler et al., 1982, Greene and Hairsine, 2004, Jury et al., 1991, Kim and Miller, 1996, Quirk and Schofield, 1955, Russo, 2005).

Additionally, expansive soils, including peat, can adsorb large quantities of water during rainfall and therefore, reduce surface runoff. According to the USDA soil classification clayey soils with clay content >30% (often Vertisols) cover around 320 million ha globally and are sensitive to swelling and shrinkage (Dinka and Lascono, 2012). Several studies have looked at the dynamics of shrinking and swelling and associated crack changes for the purpose of improving hydrological models (e.g., Arnold et al., 2005, Bronswijk, 1991, Kishné et al., 2010), but none for LSMs. An extensive review of these models is provided by Adem and Vanapalli (2015). Unfortunately, the shrink-swell properties of the Vertisols vary also as a function of soil properties, climate, topography, vegetation, cropping management, and management practices (Davidson and Page, 1956, Lin et al., 1998, Thomas et al., 2000, Vaught et al., 2006), which complicates the representation in hydrological and land surface models.

6.5. Freeze and Thaw

Many soils at higher elevation or latitudes freeze and thaw seasonally, impacting the soil physical properties, and therefore, affect the water movement in the landscape substantially. The main effect of freeze-thaw cycles (FTC) on soil properties lies in the impact on the soil structure, which, as shown earlier, regulates infiltration and runoff to a large extent (e.g., Chamberlain and Gow, 1979, Fouli et al., 2013, Qi et al., 2006). Freezing and thawing processes induce uneven stress within the soil but the conclusions in the literature about the effects on soil structure and water flow are not unanimous. There are indications that FTC decreases soil stability (Edwards, 1991, Kværnø and Øygarden, 2006), whereas Lehrsch (1998), Lehrsch et al. (1991), and Park et al. (2011) observed increasing stability after a few FTCs, while an increased number of FTCs caused a decrease in soil stability, leading to changes in soil hydraulic parameters over time. On the other hand, there seems to be more consensus that the effect of FTC on clayey soils is much larger than on coarse textured soils (Bisal and Nielsen, 1967, Kværnø and Øygarden, 2006). Unger (1991) additionally stated that FTC decrease soil bulk density.

It is also known that the hydraulic conductivity of frozen soil decreases rapidly as the temperatures fall (Williams and Burt, 1974), and some models do take this into account (e.g., CLM, Noah-MP, SSiB, SURFEX, CABLE, OLAM-SOIL, ORCHIDEE). Additionally, even water in the liquid phase is impacted by temperature changes as the viscosity of the pore water increases significantly with decreasing soil temperatures (Hillel, 1998) leading to lower fluidity and water percolation even before freezing. Finally, if the freezing front is near the soil surface, ponding is likely to occur at the soil surface after a precipitation event, resulting in runoff, because the amount of liquid water-filled pathway has reduced. Most LSMs take this effect into account. Also, as the freezing front moves down the soil profile, soil water will migrate towards the freezing front, leaving a drier soil behind, resulting in a larger matric potential gradient pulling the water towards the freezing front (Jame, 1977). Even though some LSMs account for the direct impact of freezing on the saturated hydraulic conductivity, K_s, temporal changes on the hydraulic parameters due to structural changes induced by FTC are not implemented yet. This might be problematic for regions where FTC might become more frequent in future climate as stated by Eigenbrod (1996).

6.6. Impermeable Soil Layers

Impermeable layers, or more precisely soil horizons with extremely low saturated hydraulic conductivity, frequently occur in natural or managed soils. Often these layers are denoted as hardpans, hard layers, or compacted horizons either located at the surface or subsurface (Busscher, 2011). These layers can be caused by traffic, tillage practices, trampling of livestock, or soil forming properties that result in layers with high density or cemented soil particles (Hamza and Anderson, 2005, Silva et al., 2000). For example, the extent of compacted soil is estimated worldwide at 68 million hectares of land from vehicular traffic alone (Flowers and Lal, 1998). Some of these compacted or extremely dense soil layers are relatively thin, and are therefore, often neglected in soil maps at coarser scales. Additionally, changes in the saturated hydraulic conductivity due to soil compaction is often not accounted for in pedotransfer functions, if bulk density is not used for the prediction of the hydraulic parameters (Van Looy et al., 2017). Nevertheless, these layers are of utmost importance because they control the infiltration of water into the soil, and its redistribution to greater depth. In general, presence of impermeable soil layers will lead to the same hydrological response as shown for the hydrophobic layers depicted in Fig. 8, generating more overland flow (runoff) and sub-surface storm events.

Impermeable layers complicate the naturally occurring soil vertical heterogeneity, where generally successive distinct layers of soil with different hydraulic properties occur. Several studies have proposed solutions for infiltration in layered soil systems (Childs and Bybordi, 1969, Colman and Bodman, 1945, Hanks and Bowers, 1962, Miller and Gardner, 1962, Philip, 1967, Raats, 1973, Warrick and Jim Yeh, 1990, Zaslavsky, 1964). Chu and Marino (2005) presented a solution for determining ponding conditions and simulating infiltration into a layered soil profile based on the Green and Ampt approach for unsteady rainfall. Beven (1984) and Selker et al. (1999) also extended the Green and Ampt model for infiltration into soil profiles where pore size varied with depth. A review of the applications of the Green and Ampt model to vertically heterogeneous conditions was provided by Kale and Sahoo (2011).

A special case of layered soil profile occurs when a seal layer or crust develops on the soil surface, resulting from the destructive action of raindrop impacts on the soil, which alters the soil structure and soil hydraulic properties, especially the saturated hydraulic conductivity, K_s. This process and its impacts on physical and chemical properties is described by Quirk and Schofield (1955), Bresler et al. (1982), Jury et al. (1991), Kim and Miller (1996), Greene and Hairsine (2004), Russo (2005), and Assouline et al. (2015). A review of the approaches proposed to model infiltration into sealed (or crusted) soils can be found in Mualem and Assouline (1992), Mualem and Assouline (1996), and Assouline (2004). The direct effect of the presence of the impeding seal layer at the soil surface is to reduce ponding time and infiltration rate during rainfall (Römkens et al., 1986, Romkens et al., 1986). Hillel and Gardner (1969, 1970) first addressed the problem of infiltration in the case of sealed soils. They presumed that a sealed soil can be modelled as a uniform soil profile capped with a saturated thin layer of low permeability with constant prescribed physical properties such as the saturated hydraulic conductivity. Their simplified solution was based on the Green and Ampt model, assuming a constant water content (or suction) at the interface between the seal and the soil beneath. It was further applied in different studies (Ahuja, 1974, Ahuja, 1983, Moore, 1981a, Parlange et al., 1984). Variations and extensions of this basic approach included the simulation of infiltration with time-dependent seal hydraulic conductivity functions (Ahuja, 1983, Brakensiek and Rawls, 1983, Chu et al., 1986, Farrell and Larson, 1972, Moore, 1981b, Vandervaere et al., 1998, Whisler et al., 1979). An additional conceptual model, based on the model of Corradini et al. (1997), was suggested by Smith et al. (1999). Römkens and Prasad (1992) applied the solution of Prasad and Römkens (1982) based on the spectral series approach to solve the infiltration equation in soils topped by a constant or transient crust.

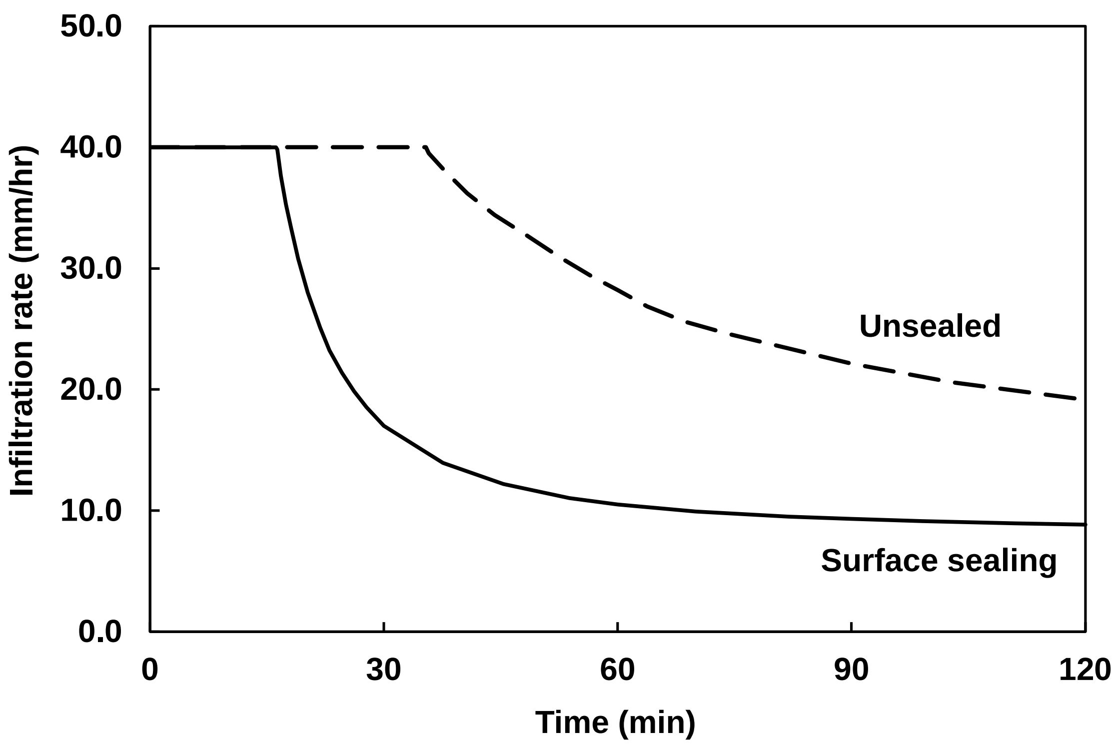

Figure 9: *The impact of soil surface sealing on infiltration.*

Here, it has to be noted that in all these studies the hydraulic properties of the seal layer were arbitrarily chosen. Mualem and Assouline (1989) as well as Baumhardt et al. (1990) have addressed the problem of infiltration into sealed and sealing soils by attributing to the seal layer hydraulic functions that evolved from those of the undisturbed soil, and that were related to the specific rainfall kinetic energy and intensity involved in the seal formation. The impact of soil surface sealing on infiltration is illustrated in Fig. 9, where it is depicted that soil surface sealing reduces the ponding time and the infiltration rates into the soil profile, including the final quasi-steady rate. As a result, much more runoff is formed by a given rainfall event when the soil surface sealing is accounted for.

6.7. Instability of Different Flow Regimes

Wetting front instability occurring under certain flow regimes can also affect significantly the infiltration process (DiCarlo, 2004, Jury et al., 2003, Or, 2008, Parlange and Hill, 1976, Philip, 1975, Raats, 1973). Wetting front instability refers to a splitting up of the infiltration front into several fingers along which water is transported downward rapidly. Since a part of the soil pore volume is bypassed by the infiltration through fingers, wetting front instability leads to considerably deeper infiltration than in case of stable wetting fronts. Raats (1973) explained that an increase of soil water pressure with depth above the wetting front in general leads to instabilities of the wetting front. Entrapment of air, the presence of layers with higher water entry values, water repellency, but also the reversal of pressure gradients during redistribution just after infiltration at the soil surface ceased can cause such an increase in pressure above the wetting front that leads to unstable wetting fronts (Wang et al., 1998, Wang et al., 2003a, Wang et al., 2003b). Another process, which orginates at the pore scale and which can explain the persistence of individual fingers due to pressure increase or pressure overshoot above the wetting front of a single finger is the dynamic pressure-water content relation that results from a rapid filling of larger pores and a subsequent redistribution (DiCarlo, 2013).

6.8. Solution of Numerical Issues

Rainfall of different rainfall intensity also affects infiltration depths and runoff ratios (Frauenfeld and Truman, 2004). For example, varying intensity rainfall simulations yield larger runoff ratios and peak runoff rates in comparison to uniform rainfall simulations (Dunkerley, 2012). Using Horton equations, predicted runoff rates were significantly improved during intra-event time variation of fluctuating rainfall simulations (Dunkerley, 2017).

Conventional solution methods to the highly non-linear Richards' one-dimensional partial differential equation (PDE) equation used in LSMs inevitably lead to numerical and accuracy issues, which impact on their hydrological performance. LSMs may consider the implementation of alternative 1-D unsaturated zone flow solution methods (such as those provided by Ogden et al. (2015). The Ogden Soil Moisture Velocity Equation (SMVE) approach uses the hodograph method to transform Richards equation into a differential equation for a velocity, and employs a discretisation of the resulting equation in the form of 'bins' containing values of the water content. The scheme is computationally efficient, although the explicit time steps are limited by stability considerations because there are no convergence limits as imposed by implicit schemes. Ogden et al. (2015) consider the transport of three regimes of soil water in detail, namely infiltration, wetting fronts disconnected from the surface, and groundwater recharge. The SMVE method offers accuracy comparable to, or in some cases exceeding, that of the numerical solution of the Richards partial differential equation method, but without the numerical complexity and in a form that is robust, continuous, and suitable for use in models of coupled climate and hydrology at a range of scales.

7. Summary and Conclusion

Infiltration processes are at the core of land surface models, representing the complex and highly dynamic coupling between precipitation and land surface properties where soil, vegetation, initial soil conditions, and topography interact. Although the formulation of infiltration representation for the soil profile scale is well established and tested by the soil physical community, there are still issues that need resolving with regards to the parameterisation of infiltration in LSMs. In particular, the extension of the concepts to the catchment and global grid cell scales remains challenging and is in some cases tentative, and with various different solutions that are currently in use. In this perspective, we reviewed and analyzed the different approaches used in current land surface models to predict soil infiltration processes. Specific attention was given to the underlying physical principles and concepts used to predict infiltration at the point and grid scale and the approaches used to describe spatial heterogeneity and upscaling of key parameters controlling the infiltration process in LSMs. We identified several topics and processes that warrant further attention in advancing the prediction of infiltration processes.

First, there is the prediction of saturated hydraulic conductivity, a key parameter in describing infiltration. Currently, K_s estimates in LSMs are derived from pedotransfer functions that are typically based on the textural composition of soils but do not consider the impact of soil structure on the infiltration process in general. Recently, Rahmati et al. (2018) published a global database of infiltration measurements that clearly shows that K_s derived from field experiments can not be predicted from soil texture alone. Therefore, research needs to be directed towards the development of pedotransfer functions that consider the effect of structural properties on *K* e.g. using land use and tillage treatment as proxies (Jorda et al., 2015). This might be even more important as a recent study of (Hirmas et al., 2018) indictates that drier climates induce the formation of greater soil macroporosity than do more humid ones, and that such climate-induced changes occur over shorter timescales than have previously been considered. Translation of the effects of these different, largely exogenic, processes to time-varying hydraulic properties (currently hydraulic properties in LSMs are kept constant in time) is one of the greatest challenges in current land surface modelling. For example, the increase of high-frequency rainfall event under future climate conditions will make crust-formation for certain soil types more likely, which will cause a decrease in infiltration and increase in surface runoff. Ignoring these aspects will add further uncertainties to predictions of future land-atmosphere interactions. This issue needs to be addressed urgently and in a coherent fashion whereby other soil properties (e.g. thermal properties) and vegetation parameters that depend on, or affect, soil properties (such as rooting depth) are changed concurrently.

Additionally, numerical simulations are needed to quantify the effect of K_s estimates considering the role of soil structure on the energy, water, and matter cycles.

Secondly, due to the availability of spatially highly resolved soil map information at the global scale with a spatial resolution of 250 m or even less, quantification of the subgrid variability is now within reach. The use of this information in combination with pedotransfer functions allows direct estimation of *b*, a lumped parameter used in several LSMs to describe the spatial variability of infiltration capacity. In addition, this highly resolved spatial information can be used to derive effective soil hydraulic parameters such as the Mualem van Genuchten parameters, which are used in the solution of Richards equation. The increasing availability of highly resolved spatial data poses questions on how to effectively and efficiently represent subgrid soil and landscape information in LSMs. The strengths and weaknesses as well as the validity and applicability of the methods presented in this review paper with respect to modelling land surface processes at the continental and global scale still has not been addressed.

The requirement to correctly represent Hortonian infiltration but also redistribution processes of water in the subsurface (e.g., due to root water uptake or capillary rise) is best fulfilled by using a Richards-equation based approach. Stochastic analyses of water flow in spatially heterogeneous soil fields (Mantoglou and Gelhar, 1987a, Mantoglou and Gelhar, 1987b, Vereecken et al., 2007b) have shown that the upscaled Richards equation at the field or larger scale has a form similar to the local scale equation.

However, the spatial variability of soil hydraulic properties introduces a hysteretic behaviour of the larger scale system, as the effective hydraulic conductivity is a function of the hydraulic gradient and of its history reflecting non-equilibrium conditions. How far this non-equilibrium behaviour is relevant for grid scale infiltration processes needs to be further studied. The definition of the effective parameters in the upscaled Richards equation, however, requires detailed knowledge of the spatial statistics of local scale hydraulic parameters. The availability of highly resolved soil maps in combination with pedotransfer functions opens up new opportunities to define subgrid variability of hydraulic parameters and thus to quantify effective hydraulic parameters at the scale of LSMs. Also for heterogeneous porous media, the solution of the Richards equation for an infiltration problem remains stable (Egorov et al., 2003). To represent the impact of soil structure, macropores, cracks, or other well connected structures on water infiltration in soils, several modifications ranging from changing the typically used uni-modal pore size distribution to a dual or multimodal pore size distribution to introducing an extra flow equation that represents the infiltration in the macropre pore network and that is coupled with the flow equation in the soil matrix have been proposed (see reviews of Jarvis (2007) and Simunek et al. (2003). These well connected and highly conductive structures could also be represented in 3D Richards models (e.g., Vogel et al., 2006). But even for such media, the solution of the Richards equation leads eventually to relatively stable infiltration profiles that could be represented fairly well by an upscaled Richards equation with effective parameters (e.g., Schlüter et al., 2012). It must be noted, though that the local water fluxes above the infiltration front can be very heterogeneous (but the wetting front is relatively homogeneous). However, the Richards equation cannot reproduce unstable infiltration fronts that are observed at the local scale as a consequence of pore scale dynamic effects. Phenomena like finger development in gravity dominated flow, which can have an important impact on the vertical distribution of the infiltrated water and how it varies with infiltration rate at the soil surface, are therefore, not represented by the Richards equation. Several approaches to account for these dynamic and non-equilibrium processes by adding additonal terms to the continuum Richards equation have been proposed (Cueto-Felgueroso and Juanes, 2009, DiCarlo, 2013, Eliassi and Glass, 2002). Although, these approaches describe experimentally observed non-uniform infiltration fronts, it still requires further investigation how the upscaled non-stable infiltration can be described by a continuum model and what its consequences are for the water distribution during an infiltration event at the LSM grid scale.

Also, correct representation of Hortonian infiltration requires consideration of vertical heterogeneity of soil hydraulic parameters, a vertically variable discretization with the finest discretization near the surface, and the use of a pressure head based Richards equation. Recently, LSMs such as Parflow/CLM, ISBA, CLSM, and OLAM-SOIL have developed approaches that allow these requirements to be fullfiled. Introducing similar approaches in other LSMs automatically avoids the need to define a maximum infiltration capacity of soils leading to a more physically consistent description of infiltration.

We observed a disparity between the approaches used at the field or small catchment scale, presented in Section 3, and the approaches applied at the grid scale in LSMs, presented in Section 4. This of course is a result of having two different scientific communities working predominantly at different spatial scales. The soil physics community mainly focuses on the field scale and typically uses semi-analytical solutions or full implementations of the Richards equation to explicitly solve for infiltration flux. This in general requires fine vertical discretization (~mm near the surface boundary) and short time steps (seconds) to calculate infiltration fluxes. Modelling of infiltration in LSMs is performed at much larger scale, which usually does not allow for a fine spatial and temporal discretization in order to keep the models computationally efficient. The majority of the LSM community has therefore taken the approach to parameterize the infiltration process at the land surface and use the Richards equation, mainly in the diffusive form, to redistribute infiltrated water in the soil profile. The common basis for both approaches is Richards equation, even though for different reasons. It is, however, the goal of this review to foster the cooperation and the exchange of ideas between the two communities. As a first step, the work of Montzka et al. (2017) provides a global concept of subgrid variability of soil hydraulic properties along the methods of similarity scaling. As the need increases to account for subgrid variability in LSMs, these above-mentioned methods provide options for incorporating this uncertainty.

Furthermore, there is a large diversity among the analyzed LSMs in estimating key properties such as soil moisture capacity and in the treatment of heterogeneity of soil moisture at the grid scale. In case of soil moisture heterogeneity three mathematical formulations have been used: i) reflection power distribution functions, ii) gamma distributions, and iii) exponential distributions with a variable number of parameters (two, three). In some cases LSMs also use different approaches to derive the saturated fraction (F_{sat}) of a grid cell, which is used to partition between Dunne saturation excess and Hortonian infiltration excess. Besides differences in concepts used to formulate the saturated fraction, there is a large divergence in the way the saturated fraction of the land surface within a pixel, F_{sat}, is being parameterized.

Differences include whether or not groundwater depth is explicitly simulated, and if so, how; and the treatment of the storage capacity of the soil between the land surface and the bedrock or groundwater table depth.

In addition, our analysis showed that basic soil information that is used to obtain spatial coverage of key soil hydraulic properties strongly differs between land surface models but also between the various version of one single LSM. The impact of using different spatial soil maps combined with the wide range of approaches used to estimate the saturated hydraulic conductivity, K_s, and other soil hydraulic properties is not yet known. Further research is needed in this direction to quantify the impact of this input variability.

Also, many LSMs use a prescribed parameterization of maximum infiltration capacity to partition precipitation between infiltrable water and runoff (exceptions being Parflow/CLM, ISBA-SURFEX, ORCHIDEE, CLSM, and OLAM-SOIL). These approaches have been heavily tuned by each LSM to ensure they fit with runoff observations. The lack of a general framework for this central hydrological process leaves a serious gap in the present LSM parameterizations and hinders simple and transparent updating of soil information when it becomes available.

Moreover, re-infiltration, called runon is ignored in most LSMs; runoff production that occurs at sites where the infiltration capacity is exceeded may reinfiltrate in the grid cell due to soil and land surface heterogeneity, so that not all of the runoff that is generated at a grid cell needs to be routed out of the cell or to a receiving water body. A classic example is the runon in vegetation patches or bands(strips) in semi-arid regions (Assouline et al., 2015). Roots can increase the local infiltration capacity so that runoff from sealed non vegetated areas can infiltrate in vegetated areas (Nimmo et al., 2009). In addition, runon leads to a scaling behavior of rainfall runoff relations with generally less runoff produced at a larger scale than what would be derived from smaller scale rainfall-runoff relations. A crucial property that defines the rainfall-runoff relations at larger scales is the connectivity of regions that generate runoff (Herbst et al., 2006).

Finally, several processes that control infiltration and thus impact the soil water balance, and ultimately the energy balance and related land-atmosphere interactions, at the grid cell scale require more attention. This includes the role of the vegetation in the infiltration process, the role of runoff-runon process at the grid cell scale and the dynamics of soil structural properties. Correct representation of the runoff-runon process will need spatially distributed information about parameters controlling Hortonian infiltration excess generation and the formulation and parameterization of redistribution mechanisms within the grid cell. The role of vegetation is related to the effect it exerts on the structural status of the vadose zone leading to soil properties that are changing over time. In addition, changes in land use and management may affect the structural status of the vadose zone and thus effect water infiltration in soils. One way forward would be to develop pedotransfer functions that consider time dependent soil properties. This, however, requires a basic understanding on how vegetation and management practices change soil hydraulic properties of soils, suggesting the need for greater integration of soil physics, plant science and land management. There is increasing evidence that spatial variability in water infiltration may also be attributed to dynamics of vegetation-driven-spatial heterogeneity (Archer et al., 2013, Archer et al., 2012, Puigdefabregas, 2005) leading to increased infiltration capcity of soils. These processes that may lead to a decrease in Hortonian infiltration have not yet been introduced in land surface models.

Currently, activities have been initiated between ISMC SoilMIP, and GEWEX (https://soil-modeling.org/activities/events/the-gewex-soilwat-initiative-first-planning-workshop-for-scope-and-interactions-advancing-integration-of-soil-and-subsurface-processes-in-climate-models) to advance the implementation of high quality soil information and the description of soil processes in LSMs. These improved LSMs, in turn, will feed into ESMs for global prediction and closure of water, energy, and carbon budgets. This review is a part of this initiative and one of the first outcomes of this joint activity based on a workshop held in Leipzig, Germany in 2016. Further activities are presently running such as the analysis of the effect of incorporating soil structure on the soil water balance of the terrestrial system and new ones are being initiated and developed.

Acknowledgments

This review emerged from discussions among GEWEX-SoilWat community held at the workshop in Leipzig (Germany) 2016, and is a product of the International Soil Modeling Consortium (ISMC) effort. We would like to thank Randal Koster (NASA-GMAO) for discussion of CLSM parts.

8. References

Abramopoulos, F., C. Rosenzweig and B. Choudhury. 1988. Improved Ground Hydrology Calculations for Global Climate Models (GCMs): Soil Water Movement and Evapotranspiration. J Climate 1: 921-941. doi:10.1175/1520-0442(1988)001<0921:ighcfg>2.0.co;2.

Adem, H.H. and S.K. Vanapalli. 2015. Review of methods for predicting in situ volume change movement of expansive soil over time. Journal of Rock Mechanics and Geotechnical Engineering 7: 73-86. doi:https://doi.org/10.1016/j.jrmge.2014.11.002.

Ahuja, L.R. 1974. Applicability of the Green-Ampt approach to water infiltration through surface crust. Soil Science 118: 283-288.

Ahuja, L.R. 1983. Modeling Infiltration into Crusted Soils by the Green—Ampt Approach. Soil Science Society of America Journal 47: 412-418. doi:doi:10.2136/sssaj1983.03615995004700030004x.

Ahuja, L.R., D.K. Cassel, R.R. Bruce and B.B. Barnes. 1989. Evaluation of spatial distribution of hydraulic conductivity using effective porosity data. Soil Science 148: 404-411.

Ahuja, L.R., F. Fiedler, G.H. Dunn, J.G. Benjamin and A. Garrison. 1998. Changes in Soil Water Retention Curves Due to Tillage and Natural Reconsolidation. Soil Science Society of America Journal 62: 1228-1233. doi:10.2136/sssaj1998.03615995006200050011x.

Alaoui, A., J. Lipiec and H.H. Gerke. 2011. A review of the changes in the soil pore system due to soil deformation: A hydrodynamic perspective. Soil and Tillage Research 115-116: 1-15. doi:https://doi.org/10.1016/j.still.2011.06.002.

Anwar, S.A., A.S. Zakey, S.M. Robaa, M.M.J.T. Abdel Wahab and A. Climatology. 2018. The influence of two land-surface hydrology schemes on the regional climate of Africa using the RegCM4 model. doi:10.1007/s00704-018-2556-8.

Archer, N.A.L., M. Bonell, N. Coles, A.M. MacDonald, C.A. Auton and R. Stevenson. 2013. Soil characteristics and landcover relationships on soil hydraulic conductivity at a hillslope scale: A view towards local flood management. J Hydrol 497: 208-222. doi:https://doi.org/10.1016/j.jhydrol.2013.05.043.

Archer, N.A.L., J.N. Quinton and T.M. Hess. 2012. Patch vegetation and water redistribution above and below ground in south-east Spain. Ecohydrology 5: 108-120. doi:10.1002/eco.210.

Arnold, J.G., K.N. Potter, K.W. King and P.M. Allen. 2005. Estimation of soil cracking and the effect on surface runoff in a Texas Blackland Prairie watershed. Hydrol Process 19: 589-603. doi:doi:10.1002/hyp.5609.

Assouline, S. 2004. Rainfall-Induced Soil Surface Sealing: A Critical Review of Observations, Conceptual Models, and Solutions.

Assouline, S. 2006a. Modeling the Relationship between Soil Bulk Density and the Hydraulic Conductivity Function. Vadose Zone Journal 5: 697-705. doi:10.2136/vzj2005.0084.

Assouline, S. 2006b. Modeling the Relationship between Soil Bulk Density and the Water Retention Curve. Vadose Zone Journal 5: 554-563. doi:10.2136/vzj2005.0083.

Assouline, S. 2013. Infiltration into soils: Conceptual approaches and solutions. Water Resour Res 49: 1755-1772. doi:10.1002/wrcr.20155.

Assouline, S. and M. Ben-Hur. 2006. Effects of rainfall intensity and slope gradient on the dynamics of interrill erosion during soil surface sealing.

Assouline, S. and Y. Mualem. 2002. Infiltration during soil sealing: The effect of areal heterogeneity of soil hydraulic properties. Water Resour Res 38: 22-21-22-29. doi:doi:10.1029/2001WR001168.

Assouline, S. and Y. Mualem. 2006. Runoff from heterogeneous small bare catchments during soil surface sealing. Water Resour Res 42. doi:doi:10.1029/2005WR004592.

Assouline, S. and K. Narkis. 2011. Effects of long-term irrigation with treated wastewater on the hydraulic properties of a clayey soil. Water Resour Res 47. doi:doi:10.1029/2011WR010498.

Assouline, S., K. Narkis, R. Gherabli and G. Sposito. 2016. Combined Effect of Sodicity and Organic Matter on Soil Properties under Long-Term Irrigation with Treated Wastewater.

Assouline, S. and D. Or. 2008. Air entry–based characteristic length for estimation of permeability of variably compacted earth materials. Water Resour Res 44. doi:doi:10.1029/2008WR006937.

Assouline, S. and D. Or. 2013. Conceptual and Parametric Representation of Soil Hydraulic Properties: A Review.

Assouline, S., J.S. Selker and J.-Y. Parlange. 2007. A simple accurate method to predict time of ponding under variable intensity rainfall. Water Resour Res 43. doi:doi:10.1029/2006WR005138.

Assouline, S., S.E. Thompson, L. Chen, T. Svoray, S. Sela and G.G. Katul. 2015. The dual role of soil crusts in desertification. Journal of Geophysical Research: Biogeosciences 120: 2108-2119. doi:doi:10.1002/2015JG003185.

Bachmann, J. and R.R. van der Ploeg. 2002. A review on recent developments in soil water retention theory: interfacial tension and temperature effects. Journal of Plant Nutrition and Soil Science 165: 468-478. doi:doi:10.1002/1522-2624(200208)165:4<468::AID-JPLN468>3.0.CO;2-G.

Balsamo, G., A. Beljaars, K. Scipal, P. Viterbo, B. van den Hurk, M. Hirschi and A.K. Betts. 2009. A Revised Hydrology for the ECMWF Model: Verification from Field Site to Terrestrial Water Storage and Impact in the Integrated Forecast System. J Hydrometeorol 10: 623-643. doi:10.1175/2008jhm1068.1.

Barry, D.A., J.-Y. Parlange, M.-C. Liu, G. C. Sander, M. B. Parlange, D. A. Lockington, F. Stagnitti, S. Assouline, J. Selker, D.-S. Jeng, T. S. Steenhuis, L. Li, R. Haverkamp and W.B. Hogarth. 2007. Infiltration and ponding, in mathematical models. In: J. A. a. J. B. K. Filar, editor Encyclopedia of Life Support Systems (EOLSS), Developed under the Auspices of the UNESCO. EOLSS Publishers, Oxford, UK.

Barry, D.A., J.-Y. Parlange, R. Haverkamp and P.J. Ross. 1995. Iinfiltration under ponded conditions: 4. Explicit predictive infiltration formula. Soil Science 160: 8-17.

Barry, D.A., J.Y. Parlange, L. Li, D.-S. Jeng and M. Crapper. 2005. Green Ampt approximations.

Batjes, N.H. 2006. ISRIC-WISE derived soil properties on a 5 by 5 arc-minutes global grid In: R. a. t. http://www.isric.org). editor.

Baumhardt, R.L., M.J.M. Römkens, F.D. Whisler and J.-Y. Parlange. 1990. Modeling infiltration into a sealing soil. Water Resour Res 26: 2497-2505. doi:doi:10.1029/WR026i010p02497.

Bear, J. 1972. Dynamics of Fluids in Porous Media. American Elsevier, New York.

Bechtold, M., G.J.M.D. Lannoy, R.D. Koster, R.H. Reichle, S. Mahanama, W. Bleuten, M.A. Bourgault, C. Brümmer, I. Burdun, A.R. Desai, K. Devito, T. Grünwald, M. Grygoruk, E.R. Humphreys, J. Klatt, J. Kurbatova, A. Lohila, T.M. Munir, M.B. Nilsson, J.S. Price, M. Röhl, A. Schneider and B. Tiemeyer. under review. PEAT-CLSM: A Specific Treatment of Peatland Hydrology in the NASA Catchment Land Surface Model. Journal of Advances in Modeling Earth System.

Beck, H.E., A. van Dijk, A. de Roo, E. Dutra, G. Fink, R. Orth and J. Schellekens. 2017. Global evaluation of runoff from 10 state-of-the-art hydrological models. Hydrology and Earth System Sciences 21: 2881-2903. doi:10.5194/hess-21-2881-2017.

Ben Neriah, A., S. Assouline, U. Shavit and N. Weisbrod. 2014. Impact of ambient conditions on evaporation from porous media.

Bengough, A. 2012. Water Dynamics of the Root Zone: Rhizosphere Biophysics and Its Control on Soil Hydrology.

Beringer, J., A.H. Lynch, F.S. Chapin, M. Mack and G.B. Bonan. 2001. The representation of arctic soils in the land surface model: The importance of mosses. J Climate 14: 3324-3335. doi:10.1175/1520-0442(2001)014<3324:Troasi>2.0.Co;2.

Best, M.J., P. Cox and D. Warrilow. 2005. Determining the optimal soil temperature scheme for atmospheric modeling applications. Boundary Layer Meteorology 114: 111-142.

Best, M.J., M. Pryor, D.B. Clark, G.G. Rooney, R.L.H. Essery, C.B. Menard, J.M. Edwards, M.A. Hendry, A. Porson, N. Gedney, L.M. Mercado, S. Sitch, E. Blyth, O. Boucher, P.M. Cox, C.S.B. Grimmond and R.J.

Harding. 2011. The Joint UK Land Environment Simulator (JULES), model description - Part 1: Energy and water fluxes. Geosci Model Dev 4: 677-699. doi:10.5194/gmd-4-677-2011.

Betson, R.P. and J.B. Marius. 1969. Source Areas of Storm Runoff. Water Resour Res 5: 574-582. doi:doi:10.1029/WR005i003p00574.

Beven, K. 1984. Infiltration into a class of vertically non-uniform soils. Hydrological Sciences Journal 29: 425-434.

Beven, K. and P. Germann. 1982. Macropores and water flow in soils. Water Resour Res 18: 1311-1325.

Beven, K.J. and M.J. Kirkby. 1979. A physically based, variable contributing area model of basin hydrology. Hydrological Scineces - Bulletin 24: 43-69.

Bierkens, M.F.P. 2015. Global hydrology 2015: State, trends, and directions. Water Resour Res 51: 4923-4947. doi:10.1002/2015wr017173.

Bisal, F. and K.F. Nielsen. 1967. Efect of frost action on the size of soil aggregates. Soil Science 104: 268-272.

Bonan, G.B. 1998. The land surface climatology of the NCAR Land Surface Model coupled to the NCAR Community Climate Model. J Climate 11: 1307-1326. doi:10.1175/1520-0442(1998)011<1307:Tlscot>2.0.Co;2.

Bonan, G.B., S. Levis, L. Kergoat and K.W. Oleson. 2002a. Landscapes as patches of plant functional types: An integrating concept for climate and ecosystem models. Global Biogeochem Cy 16. doi:Artn 1021

10.1029/2000gb001360.

Bonan, G.B., K.W. Oleson, M. Vertenstein, S. Levis, X.B. Zeng, Y.J. Dai, R.E. Dickinson and Z.L. Yang. 2002b. The land surface climatology of the community land model coupled to the NCAR community climate model. J Climate 15: 3123-3149. doi:Doi 10.1175/1520-0442(2002)015<3123:Tlscot>2.0.Co;2.

Boone, A., V. Masson, T. Meyers and J. Noilhan. 2000. The Influence of the Inclusion of Soil Freezing on Simulations by a Soil–Vegetation–Atmosphere Transfer Scheme. Journal of Applied Meteorology 39: 1544-1569. doi:10.1175/1520-0450(2000)039<1544:Tiotio>2.0.Co;2.

Boone, A. and P.J. Wetzel. 1999. A simple method for modeling sub-grid soil texture variability for use in an atmospheric climate model. Journal of the Meteorological Society of Japan 77: 317-333.

Boussetta, S., G. Balsamo, A. Beljaars, A.-A. Panareda, J.-C. Calvet, C. Jacobs, B. Hurk, P. Viterbo, S. Lafont, E. Dutra, L. Jarlan, M. Balzarolo, D. Papale and G. Werf. 2013. Natural land carbon dioxide exchanges in the ECMWF integrated forecasting system: Implementation and offline validation. Journal of Geophysical Research: Atmospheres 118: 5923-5946. doi:doi:10.1002/jgrd.50488.

Bouwer, H. 1964. Unsaturated flow in ground-water hydraulics. Journal of Hydraulic Engineering 90 (HY5): 121-144.

Brakensiek, D.L. and W.J. Rawls. 1983. Agricultural management effects on water processes, II, Green and Ampt parameters for crusting soils. Transactions of the American Society of Agricultural Engineers 26: 1753-1757.

Bresler, E. 1973. Simultaneous transport of solutes and water under transient unsaturated flow conditions. Water Resour Res 9: 975-986. doi:doi:10.1029/WR009i004p00975.

Bresler, E. and R. Hanks. 1969. Numerical method for estimating simultaneous flow of water and salt in unsaturated soils. Soil Science Society of America Journal 33: 827-832.

Bresler, E., B.L. McNeal and D.L. Carter. 1982. Saline and sodic soils: Principles-dynamics-modeling. Springer-Verlag, Berlin, Germany.

Bronick, C.J. and R. Lal. 2005. Soil structure and management: a review. Geoderma 124: 3-22. doi:https://doi.org/10.1016/j.geoderma.2004.03.005.

Bronswijk, J.J.B. 1991. Relation between Vertical Soil Movements and Water-Content Changes in Cracking Clays. Soil Science Society of American Journal 55: 1220-1226.

Brooks, R. and A. Corey. 1964. Hydraulic properties of porous media. Hydrology Papers. Colorado State University. p. 1-27.

Brown, G.G., I. Barois and P. Lavelle. 2000. Regulation of soil organic matter dynamics and microbial activityin the drilosphere and the role of interactionswith other edaphic functional domains§§Paper presented at the 16th World Congress of Soil Science, 20–26 August 1998, Montpellier, France. European Journal of Soil Biology 36: 177-198. doi:https://doi.org/10.1016/S1164-5563(00)01062-1.

Brutsaert, W. 2005. Hydrology – An introduction. Cambridge University Press, Cambridge UK.

Buckingham, E.B.U., Bureau of Soils, Washington D.C. 1907. Studies on the movement of soil moisture. Bureau of Soil Bulletin.

Busscher, W. 2011. Hardpan Soils: Management. Springer, Dordrecht; The Netherlands.

Cai, X.T., Z.L. Yang, Y.L. Xia, M.Y. Huang, H.L. Wei, L.R. Leung and M.B. Ek. 2014. Assessment of simulated water balance from Noah, Noah-MP, CLM, and VIC over CONUS using the NLDAS test bed. J Geophys Res-Atmos 119: 13751-13770. doi:10.1002/2014jd022113.

Campbell, G.S. 1974. Simple method for determineing unsaturated conductivity from moisture retention data. Soil Science 117: 311-314. doi:10.1097/00010694-197406000-00001.

Carsel, R.F. and R.S. Parrish. 1988. Developing joint probability-distributions of soil-water rentention characteristics. Water Resour Res 24: 755-769. doi:10.1029/WR024i005p00755.

Celia, M.A., E. T. Bouloutas and R.L. Zarba. 1990. A general mass ‐ conservative numerical solution for the unsaturated flow equationA general mass ‐ conservative numerical solution for the unsaturated flow equation. Water Resour Res 26: 1483-1496.

Chadburn, S., E. Burke, R. Essery, J. Boike, M. Langer, M. Heikenfeld, P. Cox and P. Friedlingstein. 2015a. An improved representation of physical permafrost dynamics in the JULES land-surface model. Geosci. Model Dev. 8: 1493-1508. doi:10.5194/gmd-8-1493-2015.

Chadburn, S.E., E.J. Burke, R.L.H. Essery, J. Boike, M. Langer, M. Heikenfeld, P.M. Cox and P. Friedlingstein. 2015b. Impact of model developments on present and future simulations of permafrost in a global land-surface model. Cryosphere 9: 1505-1521. doi:10.5194/tc-9-1505-2015.

Chamberlain, E.J. and A.J. Gow. 1979. Effect of Freezing and Thawing on the Permeability and structure of Soils. Engineering Geology 13: 73-92.

Chen, J. and P. Kumar. 2001. Topographic influence on the seasonal and interannual variation of water and energy balance of basins in North America. J Climate 14: 1989-2014. doi:Doi 10.1175/1520-0442(2001)014<1989:Tiotsa>2.0.Co;2.

Childs, E.C. 1969. An Introduction to the physical basis of soil water phenomena. John Wiley, New York, USA.

Childs, E.C. and M. Bybordi. 1969. The vertical movement of water in stratified porous material, 1. Infiltration. Water Resour Res 5: 446-459.

Choi, H.I., P. Kumar and X.Z. Liang. 2007. Three-dimensional volume-averaged soil moisture transport model with a scalable parameterization of subgrid topographic variability. Water Resour Res 43. doi:10.1029/2006wr005134.

Chow, V.T., D.R. Maidment and L.W. Mays. 1988. Applied Hydrology. McGraw-Hill Inc, Singapore.

Chu, S.T., C.A. Onstad and W.J. Rawls. 1986. Field evaluation of layered Green-Ampt model for transient crust conditions. Transactions of the American Society of Agricultural Engineers 29: 1268-1272.

Chu, X. and M.A. Marino. 2005. Determination of ponding condition and infiltration in layered soils under unsteady rainfall. J Hydrol 313: 195-207.

Clapp, R.B. and G.M. Hornberger. 1978. Empirical equations for some soil hydraulic properties. Water Resour Res 14: 601-604.

Clark, D.B. and N. Gedney. 2008. Representing the effects of subgrid variability of soil moisture on runoff generation in a land surface model. J Geophys Res-Atmos 113. doi:10.1029/2007jd008940.

Clark, D.B., L.M. Mercado, S. Sitch, C.D. Jones, N. Gedney, M.J. Best, M. Pryor, G.G. Rooney, R.L.H. Essery, E. Blyth, O. Boucher, R.J. Harding, C. Huntingford and P.M. Cox. 2011. The Joint UK Land Environment Simulator (JULES), model description - Part 2: Carbon fluxes and vegetation dynamics. Geosci Model Dev 4: 701-722. doi:10.5194/gmd-4-701-2011.

Clark, M.P., Y. Fan, D.M. Lawrence, J.C. Adam, D. Bolster, D.J. Gochis, R.P. Hooper, M. Kumar, L.R. Leung, D.S. Mackay, R.M. Maxwell, C.P. Shen, S.C. Swenson and X.B. Zeng. 2015. Improving the representation of hydrologic processes in Earth System Models. Water Resour Res 51: 5929-5956. doi:10.1002/2015wr017096.

Clothier, B.E. 2001. Infiltration. Soil and Environmental Analysis, . In: K. A. Smith and C. E. Mullins, editors, Physical Methods. Second Edition, Revised and Expanded. Marcel Dekker, Inc., New York. p. 239-280.

Colman, E.A. and G.B. Bodman. 1945. Moisture and energy conditions during downward entry of water into moist and layered soils. Soil Science of America Proceedings 9: 3-11.

Corradini, C., A. Flammini, R. Morbidelli and R.S. Govindaraju. 2011. A conceptual model for infiltration in two-layered soils with a more permeable upper layer: From local to field scale. J Hydrol 410: 62-72.

Corradini, C., R.S. Govindaraju and R. Morbidelli. 2002. Simplified modelling of areal average infiltration at the hillslope scale. Hydrol Process 16: 1757-1770. doi:doi:10.1002/hyp.394.

Corradini, C., F. Melone and R.E. Smith. 1994. Modeling Infiltration during Complex Rainfall Sequences. Water Resour Res 30: 2777-2784.

Corradini, C., F. Melone and R.E. Smith. 1997. A unified model for infiltration and redistribution during complex rainfall patterns. J Hydrol 192: 104-124. doi:https://doi.org/10.1016/S0022-1694(96)03110-1.

Cosby, B.J., G.M. Hornberger, R.B. Clapp and T.R. Ginn. 1984. A Statistical Exploration of the Relationships of Soil Moisture Characteristics to the Physical Properties of Soils. Water Resour Res 20: 682-690. doi:doi:10.1029/WR020i006p00682.

Cosh, M.H., J.R. Stedinger and W. Brutsaert. 2004. Variability of surface soil moisture at the watershed scale. Water Resour Res 40. doi:doi:10.1029/2004WR003487.

Craig, J.R., G. Liu and E.D. Soulis. 2010. Runoff–infiltration partitioning using an upscaled Green–Ampt solution. Hydrol Process 24: 2328-2334. doi:doi:10.1002/hyp.7601.

Crockford, H., S. Topalidis and D.P. Richardson. 1991. Water repellency in a dry sclerophyll eucalypt forest — measurements and processes. Hydrol Process 5: 405-420. doi:doi:10.1002/hyp.3360050408.

Cueto-Felgueroso, L. and R. Juanes. 2009. A phase field model of unsaturated flow. Water Resour Res 45. doi:10.1029/2009wr007945.

Cuntz, M. and V. Haverd. 2018. Physically Accurate Soil Freeze-Thaw Processes in a Global Land Surface Scheme. J Adv Model Earth Sy 10: 54-77. doi:doi:10.1002/2017MS001100.

Cuntz, M., J. Mai, L. Samaniego, M. Clark, V. Wulfmeyer, O. Branch, S. Attinger and S. Thober. 2016. The impact of standard and hard-coded parameters on the hydrologic fluxes in the Noah-MP land surface model. J Geophys Res-Atmos 121: 10676-10700. doi:10.1002/2016jd025097.

d'Orgeval, T., J. Polcher and P. de Rosnay. 2008. Sensitivity of the West African hydrological cycle in ORCHIDEE to infiltration processes. Hydrol. Earth Syst. Sci. 12: 1387-1401. doi:10.5194/hess-12-1387-2008.

Dagan, G. and E. Bresler. 1983. Unsaturated flow in spatially variable fields: 1. Derivation of models of infiltration and redistribution. Water Resour Res 19: 413-420. doi:doi:10.1029/WR019i002p00413.

Dahan, O., B. Tatarsky, Y. Enzel, C. Kulls, M. Seely and G. Benito. 2008. Dynamics of Flood Water Infiltration and Ground Water Recharge in Hyperarid Desert. Groundwater 46: 450-461. doi:doi:10.1111/j.1745-6584.2007.00414.x.

Darcy, H. 1856. Les Fontaines Publiques de la Ville de Dijon: Exposition et Application des Principes a Suivre et des Formulesa Employer dans les Questions de Distribution d'Eau. In: V. Dalmont, editor Paris,. p. 647.

Das, N.N., B.P. Mohanty and E.G. Njoku. 2008. A Markov chain Monte Carlo algorithm for upscaled soil-vegetation-atmosphere-transfer modeling to evaluate satellite-based soil moisture measurements. Water Resour Res 44. doi:doi:10.1029/2007WR006472.

Davidson J, Nielsen D and B. J. 1963. The measurement and description of water flow through Columbia silt loam and Hesperia sandy loam. Hilgardia 34: 601-617. doi:DOI:10.3733/hilg.v34n15p601.

Davidson, S.E. and J.B. Page. 1956. Factors Influencing Swelling and Shrinking in Soils. Soil Science Society of American Journal S20: 320-324.

de Boer, F. 2016. HiHydroSoil: A High Resolution Soil Map of Hydraulic Properties, Version 1.2 In: FutureWater, editor Report FutureWater. Wageningen, The Netherlands.

de Lannoy, G.J.M., R.D. Koster, R.H. Reichle, S.P.P. Mahanama and Q. Liu. 2014. An updated treatment of soil texture and associated hydraulic properties in a global land modeling system. J Adv Model Earth Sy 6: 957-979. doi:10.1002/2014ms000330.

de Rosnay, P., J. Polcher, M. Bruen and K. Laval. 2002. Impact of a physically based soil water flow and soil-plant interaction representation for modeling large-scale land surface processes. Journal of Geophysical Research: Atmospheres 107: ACL 3-1-ACL 3-19. doi:doi:10.1029/2001JD000634.

Decharme, B., A. Boone, C. Delire and J. Noilhan. 2011. Local evaluation of the Interaction between Soil Biosphere Atmosphere soil multilayer diffusion scheme using four pedotransfer functions. J Geophys Res-Atmos 116. doi:Artn D20126

10.1029/2011jd016002.

Decharme, B., E. Brun, A. Boone, C. Delire, P. Le Moigne and S. Morin. 2016. Impacts of snow and organic soils parameterization on northern Eurasian soil temperature profiles simulated by the ISBA land surface model. The Cryosphere 10: 853-877. doi:doi:10.5194/tc-10-853-2016.

Decharme, B. and H. Douville. 2006. Introduction of a sub-grid hydrology in the ISBA land surface model. Clim Dynam 26: 65-78. doi:https://doi.org/10.1007/s00382-005-0059-7.

Decharme, B., E. Martin and S. Faroux. 2013. Reconciling soil thermal and hydrological lower boundary conditions in land surface models. Jorrnal of geophysical Research: Atmospheres 118: 7819-7834. doi:doi:10.1002/jgrd.50631.

Decker, M. 2015. Development and evaluation of a new soil moisture and runoff parameterization for the CABLE LSM including subgrid-scale processes. J Adv Model Earth Sy 7: 1788-1809. doi:10.1002/2015ms000507.

Delleur, J.W. 2006. The handbook of groundwater engineering. CRC press.

Demaria, E.M., B. Nijssen and T. Wagener. 2007. Monte Carlo sensitivity analysis of land surface parameters using the Variable Infiltration Capacity model. J Geophys Res-Atmos 112. doi:10.1029/2006jd007534.

DiCarlo, D.A. 2004. Experimental measurements of saturation overshoot on infiltration. Water Resour Res 40. doi:doi:10.1029/2003WR002670.

DiCarlo, D.A. 2013. Stability of gravity-driven multiphase flow in porous media: 40 Years of advancements. Water Resour Res 49: 4531-4544. doi:10.1002/wrcr.20359.

Dinka, T.M. and R.J. Lascono. 2012. Review Paper: Challenges and Limitations in Studying the Shrink-Swell and Crack Dynamics of Vertisol Soils. Open Journal of Soil Science 2: 82-90.

Dirmeyer, P.A. and F.R.J. Zeng. 1999. Precipitation infiltration in the simplified SiB land surface scheme. Journal of the Meteorological Society of Japan 77: 291-303.

Doerr, S.H., R.A. Shakesby and R.P.D. Walsh. 2000. Soil water repellency: its causes, characteristics and hydro-geomorphological significance. Earth-Science Reviews 51: 33-65. doi:https://doi.org/10.1016/S0012-8252(00)00011-8.

Doerr, S.H. and A. Thomas. 2000. The role of soil moisture in controlling water repellency: New evidence from forest soils in Portugal.

Ducharne, A., R.D. Koster, M.J. Suarez, M. Stieglitz and P. Kumar. 2000. A catchment-based approach to modeling land surface processes in a general circulation model: 2. Parameter estimation and model demonstration. Journal of Geophysical Research: Atmospheres 105: 24823-24838. doi:doi:10.1029/2000JD900328.

Ducharne, A., K. Laval and J. Polcher. 1998. Sensitivity of the hydrological cycle to the parameterization of soil hydrology in a GCM. Climate Dynamics 14. doi: https://doi.org/10.1007/s003820050226.

Ducharne, A., C. Ottlé, F. Maignan, N. Vuichard, J. Ghattas, F. Wang, P. Peylin, J. Polcher, M. Guimberteau, P. Maugis, S. Tafasca, A. Tootchi, A. Verhoef and H. Mizuochi. 2017. The hydrol module of ORCHIDEE: Scientic documentation [rev 3977] and on, work in progress, towards CMIP6v1.

Dümenil, L. and E. Todini. 1992. A rainfall-runoff scheme for the use in the Hamburg climate model. In: J. P. O'Kane editor Advances in Theoretical Hydrology: A tribute to James Dooge. Elsevier Science Publishers B.V, Amsterdam. p. 129-157.

Dunkerley, D. 2012. Effects of rainfall intensity fluctuations on infiltration and runoff: rainfall simulation on dryland soils, Fowlers Gap, Australia. Hydrol Process 26: 2211-2224. doi:doi:10.1002/hyp.8317.

Dunkerley, D. 2017. An approach to analysing plot scale infiltration and runoff responses to rainfall of fluctuating intensity. Hydrol Process 31: 191-206. doi:doi:10.1002/hyp.10990.

Dunne, T. 1978. Field studies of hillslope flow processes and their significance. In: M. J. Kirkby, editor Hillslope Hydrology. Wiley-Interscience, New York. p. 227-293.

Dunne, T. and R.D. Black. 1970. An Experimental Investigation of Runoff Production in Permeable Soils. Water Resour Res 6: 478-490. doi:doi:10.1029/WR006i002p00478.

Edwards, L.M. 1991. The effect of alternate freezing and thawing on aggregate stability and aggregate size distribution of some Prince Edward Island soils. Journal of Soil Science 42: 193-204. doi:doi:10.1111/j.1365-2389.1991.tb00401.x.

Egorov, A.G., R.Z. Dautov, J.L. Nieber and A.Y. Sheshukov. 2003. Stability analysis of gravity-driven infiltrating flow. Water Resour Res 39. doi:10.1029/2002wr001886.

Eigenbrod, K.D. 1996. Effects of cyclic freezing and thawing on volume changes and permeabilities of soft fine-gained soils. Canadian Geotechnical Journal 33: 529-537. doi:10.1139/t96-079-301.

Eliassi, M. and R.J. Glass. 2002. On the porous-continuum modeling of gravity-driven fingers in unsaturated materials: Extension of standard theory with a hold-back-pile-up effect. Water Resour Res 38. doi:10.1029/2001wr001131.

Entekhabi, D. and P.S. Eagleson. 1989. Land Surface Hydrology Parameterization for Atmospheric General Circulation Models Including Subgrid Scale Spatial Variability. J Climate 2: 816-831. doi:10.1175/1520-0442(1989)002<0816:lshpfa>2.0.co;2.

Everett, D.H. 1955. A general approach to hysteresis, 4, an alternative formulation of the domain model. Transactions of Faraday Society 51: 1551-1557.

Eyring, V., S. Bony, G.A. Meehl, C.A. Senior, B. Stevens, R.J. Stouffer and K.E. Taylor. 2016. Overview of the Coupled Model Intercomparison Project Phase 6 (CMIP6) experimental design and organization. Geosci Model Dev 9: 1937-1958.

FAO. 1988. Food and Agriculture Organization - UNESCO soil map of the world, revised legend. World Resources Report 60: 138 pp.

FAO. 2003. The Digitized Soil Map of the World and Derived Soil Properties. FAO Land and Water Digital Media Series 1.

FAO. 2009. FAO/IIASA/ISRIC/ISS-CAS/JRC - Harmonized World Soil Database (version 1.1). FAO, , Rome, Italy and IIASA, Laxenburg, Austria.

Farrell, D.A. and W.E. Larson. 1972. Dynamics of the soil-water system during a rainstorm. Soil Science 113: 88-95.

Feddes, R.A., E. Bresler and S.P. Neuman. 1974. Field test of a modified numerical model for water uptake by root systems. Water Resour Res 10: 1199-1206. doi:doi:10.1029/WR010i006p01199.

Flowers, M.D. and R. Lal. 1998. Axle load and tillage effects on soil physical properties and soybean grain yield on a mollic ochraqualf in northwest Ohio. Soil and Tillage Research 48: 21-35. doi:https://doi.org/10.1016/S0167-1987(98)00095-6.

Fouli, Y., B.J. Cade-Menun and H.W. Cutforth. 2013. Freeze–thaw cycles and soil water content effects on infiltration rate of three Saskatchewan soils. Canadian Journal of Soil Science 93: 485-496. doi:10.4141/cjss2012-060.

Franzluebbers, A. 2002. Water infiltration and soil structure related to organic matter and its stratification with depth.

Frauenfeld, B. and C. Truman. 2004. Variable Rainfall Intensity Effects on Runoff and Interrill Erosion From Two Coastal Plain Ultisols in Georgia. Soil Science 169: 143-154. doi:10.1097/01.ss.0000117784.98510.46.

Freeze, R.A. 1980. A stochastic-conceptual analysis of rainfall-runoff processes on a hillslope. Water Resour Res 16: 391-408. doi:doi:10.1029/WR016i002p00391.

Frenkel, H., J.O. Goertzen and J.D. Rhoades. 1978. Effects of Clay Type and Content, Exchangeable Sodium Percentage, and Electrolyte Concentration on Clay Dispersion and Soil Hydraulic Conductivity1. Soil Science Society of America Journal 42: 32-39. doi:10.2136/sssaj1978.03615995004200010008x.

Furman, A., A. Warrick, D. Zerihun and C. Sanchez. 2006. Modified Kostiakov Infiltration Function: Accounting for Initial and Boundary Conditions. Journal of Irrigation and Drainage Engineering 132: 587-596. doi:10.1061/(ASCE)0733-9437(2006)132:6(587).

Gao, H. and M. Shao. 2015. Effects of temperature changes on soil hydraulic properties. Soil and Tillage Research 153: 145-154. doi:10.1016/j.still.2015.05.003.

Gardner, R. 1955. Relations of temperature to moisture tension of soils. Soil Science 79: 257-265.

Gardner, W.R. 1960. Soil water relations in arid and semi-arid conditions. Plant-water relationships in arid and semi-arid conditions: Reviews of Research. Arid Zone Research XV. UNESCO.

Garrote, L. and R.L. Bras. 1995. A distributed model for real-time flood forecasting using digital elevation models. J Hydrol 167: 279-306. doi:https://doi.org/10.1016/0022-1694(94)02592-Y.

Gedney, N. and P.M. Cox. 2003. The Sensitivity of Global Climate Model Simulations to the Representation of Soil Moisture Heterogeneity. J Hydrometeorol 4: 1265-1275. doi:10.1175/1525-7541(2003)004<1265:Tsogcm>2.0.Co;2.

Getirana, A., A. Boone, C. Peugeot, S. Boussetta, S. Ait-Mesbah, M. Anderson, G. Balsamo, E. Chan, J.-M. Cohard, A. Ducharne, E. Dutra, F. Favot, A. Getirana, S. Galle, T. Gascon, M. Gosset, Y. Gusev, C. Hain, P. Harris and T. Vischel. 2017. Streamflows over a West African basin from the ALMIP-2 model ensemble. J Hydrometeorol 18: 1831-1845. doi:10.1175/JHM-D-16-0233.1.

Getirana, A.C.V., E. Dutra, M. Guimberteau, J. Kam, H.-Y. Li, B. Decharme, Z. Zhang, A. Ducharne, A. Boone, G. Balsamo, M. Rodell, A.M. Toure, Y. Xue, C.D. Peters-Lidard, S.V. Kumar, K. Arsenault, G. Drapeau, L.R. Leung, J. Ronchail and J. Sheffield. 2014. Water Balance in the Amazon Basin from a Land Surface Model Ensemble. J Hydrometeorol 15: 2586-2614. doi:10.1175/jhm-d-14-0068.1.

Ghanbarian, B., V. Taslimitehrani, G.Z. Dong and Y.A. Pachepsky. 2015. Sample dimensions effect on prediction of soil water retention curve and saturated hydraulic conductivity. J Hydrol 528: 127-137. doi:10.1016/j.jhydrol.2015.06.024.

Giraldez, J.V. and G. Sposito. 1985. Infiltration in Swelling Soils. Water Resour Res 21: 33-44. doi:doi:10.1029/WR021i001p00033.

Glass, R.J., T.S. Steenhuis and J.-Y. Parlange. 1989. Mechanism for finger persistence in homogeneous, unsaturated, porous media: theory and verification. Soil Science 148: 60-70.

Gleeson, T., L. Smith, N. Moosdorf, J. Hartmann, H.H. Durr, A.H. Manning, L.P.H. van Beek and A.M. Jellinek. 2011. Mapping permeability over the surface of the Earth. Geophys Res Lett 38. doi:Artn L02401

10.1029/2010gl045565.

Govindaraju, R.S., C. Corradini and R. Morbidelli. 2006. A semi-analytical model of expected areal-average infiltration under spatial heterogeneity of rainfall and soil saturated hydraulic conductivity. J Hydrol 316: 184-194. doi:https://doi.org/10.1016/j.jhydrol.2005.04.019.

Govindaraju, R.S., C. Corradini and R. Morbidelli. 2012. Local- and field-scale infiltration into vertically non-uniform soils with spatially-variable surface hydraulic conductivities. Hydrol Process 26: 3293-3301.

Govindaraju, R.S., R. Morbidelli and C. Corradini. 2001. Areal Infiltration Modeling over Soils with Spatially Correlated Hydraulic Conductivities. Journal of Hydrologic Engineering 6: 150-158. doi:doi:10.1061/(ASCE)1084-0699(2001)6:2(150).

Grant, S.A. and J. Bachmann. 2002. Effect of Temperature on Capillary Pressure. In: P. A. C. Raats, D. E. Smiles and A. W. Warrick, editors, Environmental Mechanics, Water, Mass and Energy Transfer in the Biosphere, Geophysical Monograph Series v. 129. American Geophysical Union, Washington, D. C. p. 199-212.

Grant, S.A. and A. Salehzadeh. 1996. Calculation of Temperature Effects on Wetting Coefficients of Porous Solids and Their Capillary Pressure Functions. Water Resour Res 32: 261-270. doi:doi:10.1029/95WR02915.

Green, W.H. and G. Ampt. 1911. Studies on Soil Phyics. The Journal of Agricultural Science 4: 1-24.

Greene, R.S.B. and P.B. Hairsine. 2004. Elementary processes of soil–water interaction and thresholds in soil surface dynamics: a review. Earth Surf Proc Land 29: 1077-1091. doi:doi:10.1002/esp.1103.

Gudmundsson, L., L.M. Tallaksen, K. Stahl, D.B. Clark, E. Dumont, S. Hagemann, N. Bertrand, D. Gerten, J. Heinke, N. Hanasaki, F. Voss and S. Koirala. 2012. Comparing Large-Scale Hydrological Model Simulations to Observed Runoff Percentiles in Europe. J Hydrometeorol 13: 604-620. doi:10.1175/jhm-d-11-083.1.

Habets, F., J. Noilhan, C. Golaz, J.P. Goutorbe, P. Lacarrère, E. Leblois, E. Ledoux, E. Martin, C. Ottlé and D. Vidal-Madjar. 1999. The ISBA surface scheme in a macroscale hydrological model applied to the Hapex-Mobilhy area: Part II: Simulation of streamflows and annual water budget. J Hydrol 217: 97-118. doi:https://doi.org/10.1016/S0022-1694(99)00020-7.

Habets, F. and G.M. Saulnier. 2001. Subgrid runoff parameterization. Physics and Chemistry of the Earth, Part B: Hydrology, Oceans and Atmosphere 26: 455-459. doi:https://doi.org/10.1016/S1464-1909(01)00034-X.

Hagemann, S. and L.D. Gates. 2003. Improving a subgrid runoff parameterization scheme for climate models by the use of high resolution data derived from satellite observations. Clim Dynam 21: 349-359. doi:10.1007/s00382-003-0349-x.

Hagemann, S. and T. Stacke. 2015. Impact of the soil hydrology scheme on simulated soil moisture memory. Clim Dynam 44: 1731-1750. doi:10.1007/s00382-014-2221-6.

Hailegeorgis, T.T., Y.S. Abdella, K. Alfredsen and S. Kolberg. 2015. Evaluation of Regionalization Methods for Hourly Continuous Streamflow Simulation Using Distributed Models in Boreal Catchments. Journal of Hydrologic Engineering 20. doi:10.1061/(asce)he.1943-5584.0001218.

Haines, W.B. 1930. Studies in the physical properties of soil. V. The hysteresis effect in capillary properties, and the modes of moisture distribution associated therewith. Journal of Agricultural Science 20: 97-116. doi:10.1017/S002185960008864X.

Hamza, M.A. and W.K. Anderson. 2005. Soil Compaction in Cropping Systems. A Review of the Nature, Causes and Possible Solutions. Soil & Tillage Research 82: 121-145.

Hanks, R.J. and S.A. Bowers. 1962. Numerical solution of the moisture flow equation for infiltration into layered soils. Soil Science of America Proceedings 26: 530-534.

Hanks, R.J., A. Klute and E. Bresler. 1969. A numeric method for estimating infiltration, redistribution, drainage, and evaporation of water from soil. Water Resour Res 5: 1064-1069. doi:doi:10.1029/WR005i005p01064.

Hannes, M., U. Wollschläger, T. Wöhling and H.-J. Vogel. 2016. Revisiting hydraulic hysteresis based on long-term monitoring of hydraulic states in lysimeters. Water Resour Res 52: 3847-3865. doi:doi:10.1002/2015WR018319.

Hansen, S., P. Abrahamsen, C. T. Petersen and M. Styczen. 2012. Daisy: Model Use, Calibration, and Validation. Transactions of the ASABE 55: 1317. doi:https://doi.org/10.13031/2013.42244.

Haverd, V. and M. Cuntz. 2010a. Soil-Litter-Iso: A one-dimensional model for coupled transport of heat, water and stable isotopes in soil with a litter layer and root extraction. J Hydrol 388: 438-455. doi:10.1016/j.jhydrol.2010.05.029.

Haverd, V. and M. Cuntz. 2010b. Soil–Litter–Iso: A one-dimensional model for coupled transport of heat, water and stable isotopes in soil with a litter layer and root extraction. J Hydrol 388: 438-455. doi:https://doi.org/10.1016/j.jhydrol.2010.05.029.

Haverd, V., M. Cuntz, L.P. Nieradzik and I.N. Harman. 2016. Improved representations of coupled soil–canopy processes in the CABLE land surface model (Subversion revision 3432). Geosci. Model Dev. 9: 3111-3122. doi:10.5194/gmd-9-3111-2016.

Haverkamp, R., J.-Y. Parlange, S.J. L., G. Schmitz and C. Fuentes. 1990. Infiltration under ponded conditions: 3. A predictive equation based on physical parameters. Soil Science 149: 292-300.

Haverkamp, R., J.Y. Parlange, R. Cuenca, P.J. Ross and T.S. Steenhuis. 1998. Scaling of the Richards Equation and its application to watershed modelling. In: G. Sposito, editor Scale dependence and scale invariance in hydrology. Cambridge University Press, Cambridge, UK. p. 190-223.

Healy, R.W. 2008. Simulating Water, Solute, and Heat Transport in the Subsurface with the VS2DI Software Package. Vadose zone journal 7: 632-639. doi:10.2136/vzj2007.0075.

Hengl, T., J.M. de Jesus, G.B.M. Heuvelink, M.R. Gonzalez, M. Kilibarda, A. Blagotic, W. Shangguan, M.N. Wright, X.Y. Geng, B. Bauer-Marschallinger, M.A. Guevara, R. Vargas, R.A. MacMillan, N.H. Batjes, J.G.B. Leenaars, E. Ribeiro, I. Wheeler, S. Mantel and B. Kempen. 2017. SoilGrids250m: Global gridded soil information based on machine learning. Plos One 12. doi:10.1371/journal.pone.0169748.

Hengl, T., J.M. de Jesus, R.A. MacMillan, N.H. Batjes, G.B.M. Heuvelink, E. Ribeiro, A. Samuel-Rosa, B. Kempen, J.G.B. Leenaars, M.G. Walsh and M.R. Gonzalez. 2014. SoilGrids1km-Global Soil Information Based on Automated Mapping. Plos One 9. doi:10.1371/journal.pone.0105992.

Herbst, M., B. Diekkrüger and J. Vanderborght. 2006. Numerical experiments on the sensitivity of runoff generation to the spatial variation of soil hydraulic properties. J Hydrol 326: 43-58. doi:10.1016/j.jhydrol.2005.10.036.

Hillel, D. 1980. Fundamentals of Soil Physics. Academic Press, New York, London, Toronto, Sydney, San Francisco.

Hillel, D. 1998. Environmental soil physics. Academic Press, San Diego, CA.

Hillel, D. and W.R. Gardner. 1969. Steady infiltration into crust topped profiles. Soil Science 108: 137-142.

Hillel, D. and W.R. Gardner. 1970. Transient infiltration into crust topped profiles. Soil Science 109: 69-76.

Hirmas, D., R., D. Giménez, A. Nemes, R. Kerry, N.A. Brunsell and C.J. Wilson. 2018. Climate-induced changes in continental-scale soil macroporosity may intensify water cycle Nature 516. doi:https://doi.org/10.1038/s41586-018-0463-x.

Hogarth, W.L., J. Hopmans, J.Y. Parlange and R. Haverkamp. 1988. Application of a simple soil-water hysteresis model. J Hydrol 98: 21-29. doi:https://doi.org/10.1016/0022-1694(88)90203-X.

Hogue, T.S., L.A. Bastidas, H.V. Gupta and S. Sorooshian. 2006. Evaluating model performance and parameter behavior for varying levels of land surface model complexity. Water Resour Res 42. doi:10.1029/2005wr004440.

Hopmans, J. 1989. Stochastic description of field-measured infiltration data. American Society of Agricultural Engineers 32: 1987-1993.

Hopmans, J.W. and J.H. Dane. 1986. Temperature Dependence of Soil Hydraulic Properties1. Soil Science Society of America Journal 50: 4-9. doi:10.2136/sssaj1986.03615995005000010001x.

Hopmans, J.W., J.-Y. Parlange and S. Assouline. 2007. Infiltration. In: J. W. Delleur, editor The Handbook of Groundwater Engineering, 2nd Edition. CRC press, Taylor and Francis Group.

Horton, R.E. 1933. The role of infiltration in the hydrologic cycle. Eos, Transactions American Geophysical Union 14: 446-460.

Horton, R.E. 1940. The infiltration ‐ theory of surface ‐ runoff. Eos, Transactions American Geophysical Union 21: 541-541. doi:doi: 10.1029/TR021i002p00541-1.

Horton, R.E. 1941. An approach toward a physical interpretation of infiltration-capacity. Soil Science Society of America Journal 5 (C): 399-417.

Huang, H.-C., Y.-C. Tan, C.-W. Liu and C.-H. Chen. 2005. A novel hysteresis model in unsaturated soil. Hydrol Process 19: 1653-1665. doi:doi:10.1002/hyp.5594.

Huang, M., X. Liang and Y. Liang. 2003. A transferability study of model parameters for the variable infiltration capacity land surface scheme. J Geophys Res-Atmos 108. doi:10.1029/2003jd003676.

Huang, S.C., R. Kumar, M. Florke, T. Yang, Y. Hundecha, P. Kraft, C. Gao, A. Gelfan, S. Liersch, A. Lobanova, M. Strauch, F. van Ogtrop, J. Reinhardt, U. Haberlandt and V. Krysanova. 2017. Evaluation of an ensemble of regional hydrological models in 12 large-scale river basins worldwide. Climatic Change 141: 381-397. doi:10.1007/s10584-016-1841-8.

Hugelius, G., C. Tarnocai, G. Broll, J.G. Canadell, P. Kuhry and D.K. Swanson. 2013. The Northern Circumpolar Soil Carbon Database: spatially distributed datasets of soil coverage and soil carbon storage in the northern permafrost regions. Earth Syst. Sci. Data 5: 3-13. doi:10.5194/essd-5-3-2013.

Huyakorn, P.S., E.P. Springer, V. Guvanasen and T.D. Wadsworth. 1986. A three-dimensional finite-element model for simulating water flow in variably saturated porous media. Water Resour Res 22: 1790-1808. doi:doi:10.1029/WR022i013p01790.

Ibrahim, H.A. and W. Brutsaert. 1968. Intermittent infiltration into soils with hysteresis. Journal of the Hydraulics Devision, Proceedings of the American Society of Civil Engineers 94 (HY1): 113-137.

IGBP. 2000. Global Soil Data Task.

Imeson, A.C., J.M. Verstraten, E.J. van Mulligen and J. Sevink. 1992. The effects of fire and water repellency on infiltration and runoff under Mediterranean type forest. CATENA 19: 345-361. doi:https://doi.org/10.1016/0341-8162(92)90008-Y.

Jame, Y.-W. 1977. Heat and mass transfer in freezing unsaturated soil. University of Saskatchewan, Saskatoon, SK.

Jana, R. and B. Mohanty. 2011. Enhancing PTFs with remotely sensed data for multi-scale soil water retention estimation. J Hydrol 399: 201-211. doi:10.1016/j.jhydrol.2010.12.043.

Jana, R. and B. Mohanty. 2012a. On topographic controls of soil hydraulic parameter scaling at hillslope scales. Water Resour Res 48: 2518. doi:10.1029/2011WR011204.

Jana, R.B. and B.P. Mohanty. 2012b. A comparative study of multiple approaches to soil hydraulic parameter scaling applied at the hillslope scale. Water Resour Res 48. doi:doi:10.1029/2010WR010185.

Jana, R.B. and B.P. Mohanty. 2012c. A topography-based scaling algorithm for soil hydraulic parameters at hillslope scales: Field testing. Water Resour Res 48. doi:doi:10.1029/2011WR011205.

Jana, R.B., B.P. Mohanty and E.P. Springer. 2008. Multiscale Bayesian neural networks for soil water content estimation. Water Resour Res 44. doi:doi:10.1029/2008WR006879.

Jansson, P.E. 2012. CoupModel: Model Use, Calibration, and Validation. Transactions of the ASABE 55: 1337. doi:https://doi.org/10.13031/2013.42245.

Jarvis, N.J. 2007. A review of non-equilibrium water flow and solute transport in soil macropores: principles, controlling factors and consequences for water quality. European Journal of Soil Science 58: 523-546. doi:10.1111/j.1365-2389.2007.00915.x.

Jorda, H., M. Bechtold, N. Jarvis and J. Koestel. 2015. Using boosted regression trees to explore key factors controlling saturated and near-saturated hydraulic conductivity. European Journal of Soil Science 66: 744-756.

Jury, W.A., W.R. Gardner and W.H. Gardner. 1991. Soil physics, 5th Edition. John Wiley & Sons Inc., New York.
Jury, W.A., Z. Wang and A. Tuli. 2003. A Conceptual Model of Unstable Flow in Unsaturated Soil during Redistribution. Vadose Zone Journal 2: 61-67. doi:10.2113/2.1.61.
Kale, R. and B. Sahoo. 2011. Green-Ampt Infiltration Models for Varied Field Conditions: A Revisit. Water Resources Management 25: 3505-3536. doi:10.1007/s11269-011-9868-0.
Keune, J., F. Gasper, K. Goergen, A. Hense, P. Shrestha, M. Sulis and S. Kollet. 2016. Studying the influence of groundwater representations on land surface-atmosphere feedbacks during the European heat wave in 2003. J Geophys Res-Atmos 121: 13301-13325.
Kim, D., R.L. Ray and M. Choi. 2017. Simulations of energy balance components at snow-dominated montane watershed by land surface models. Environmental Earth Sciences 76: 337. doi:10.1007/s12665-017-6655-0.
Kim, J. and B. Mohanty. 2017. A physically-based hydrological connectivity algorithm for describing spatial patterns of soil moisture in the unsaturated zone: Hydrologic Connectivity in Soil Moisture. Journal of Geophysical Research Atmospheres 122: 2096-2114. doi:10.1002/2016JD025591.
Kim, K.H. and W.P. Miller. 1996. Effect of rainfall electrolyte concentration and slope on infiltration and erosion. Soil Technology 9: 173-185. doi:https://doi.org/10.1016/S0933-3630(96)00011-6.
King, P.M. 1981. Comparison of methods for measuring severity of water repellence of sandy soils and assessment of some factors that affect its measurement. Australian Journal of Soil Research 19: 275-285.
Kishné, A.S., C.L.S. Morgan, Y. Ge and W.L. Miller. 2010. Antecedent soil moisture affecting surface cracking of a Vertisol in field conditions. Geoderma 157: 109-117. doi:https://doi.org/10.1016/j.geoderma.2010.03.020.
Kollet, S.J. and R.M. Maxwell. 2006. Integrated surface-groundwater flow modeling: A free-surface overland flow boundary condition in a parallel groundwater flow model. Adv Water Resour 29: 945-958. doi:10.1016/j.advwatres.2005.08.006.
Kollet, S.J. and R.M. Maxwell. 2008a. Capturing the influence of groundwater dynamics on land surface processes using an integrated, distributed watershed model. Water Resour Res 44. doi:Artn W02402

10.1029/2007wr006004.
Kollet, S.J. and R.M. Maxwell. 2008b. Demonstrating fractal scaling of baseflow residence time distributions using a fully-coupled groundwater and land surface model. Geophys Res Lett 35.
Koren, V., J. Schaake, K. Mitchell, Q.Y. Duan, F. Chen and J.M. Baker. 1999. A parameterization of snowpack and frozen ground intended for NCEP weather and climate models. J Geophys Res-Atmos 104: 19569-19585.
Koster, R.D., M.J. Suarez, A. Ducharne, M. Stieglitz and P. Kumar. 2000. A catchment-based approach to modeling land surface processes in a general circulation model 1. Model structure. J Geophys Res-Atmos 105: 24809-24822. doi:10.1029/2000jd900327.
Kostiakov, A.N. 1932. On the Dynamics of the Coefficients of Water Percolation in Soils and on the Necessity of Studying It from a Dynamic Point of View for Purpose of Amelioration. Transactions of 6th Committee International Society of Soil Science, Russia Part A: 17-21.
Kowalczyk, E.A., L. Stevens, R.M. Law , M.R. Dix, Y.P. Wang, I.N. Harman, H. Srbinovsky, B. Pak and T. Ziehn. 2013. The land surface model component of ACCESS: Description and impact on the simulated surface climatology. Australian Meteorological and Oceanographic Journal 63: 65-82.
Kowalczyk, E.A., Y.P. Wang, R.M. Law, H.L. Davies, J.L. McGregor and G. Abramowitz. 2006a. The CSIRO Atmosphere Biosphere Land Exchange (CABLE) model for use in climate models and as an offline model CSIRO Marine and Atmospheric Research paper 013

Kowalczyk, E.A., Y.P. Wang, R.M. Law, H.L. Davies, J.L. McGregor and G.S. Abramowitz. 2006b. The CSIRO Atmosphere Biosphere Land Exchange (CABLE) model for use in climate models and as an offline model. CSIRO Marine and Atmospheric Research Paper. CSIRO Marine and Atmospheric Research, Aspendale, Vic.

Kutilek, M., V. Kuraz and M. Krejca. 1993. Measurement time and spatial variability of field infiltration. International Agrophysics 7: 133-140.

Kværnø, S.H. and L. Øygarden. 2006. The influence of freeze–thaw cycles and soil moisture on aggregate stability of three soils in Norway. CATENA 67: 175-182. doi:https://doi.org/10.1016/j.catena.2006.03.011.

Laliberte, G.E., A.T. Corey and R.H. Brooks. 1966. Properties of unsaturated porous media. Hydrology Papers. Colorado State University, Fort Collins.

Lange, B., P. Lüescher and P.F. Germann. 2009. Significance of tree roots for preferential infiltration in stagnic soils. Hydrol. Earth Syst. Sci. 13: 1809-1821. doi:10.5194/hess-13-1809-2009.

Lawrence, D.M., K.W. Oleson, M.G. Flanner, P.E. Thornton, S.C. Swenson, P.J. Lawrence, X. Zeng, Z.-L. Yang, S. Levis, K. Sakaguchi, G.B. Bonan and A.G. Slater. 2011. Parameterization improvements and functional and structural advances in Version 4 of the Community Land Model. J Adv Model Earth Sy 3. doi:doi:10.1029/2011MS00045.

Lawrence, D.M. and A.G. Slater. 2008. Incorporating organic soil into a global climate model. Clim Dynam 30: 145-160. doi:10.1007/s00382-007-0278-1.

Le Vine, N., A. Butler, N. McIntyre and C. Jackson. 2016. Diagnosing hydrological limitations of a land surface model: application of JULES to a deep-groundwater chalk basin. Hydrol. Earth Syst. Sci. 20: 143-159. doi:10.5194/hess-20-143-2016.

Lehmann, P. and D. Or. 2012. Hydromechanical triggering of landslides: From progressive local failures to mass release. Water Resour Res 48.

Lehrsch, G.A. 1998. Freeze-thaw cycles increase near-surface aggregate stability. Soil Science 163: 63-70.

Lehrsch, G.A., R.E. Sojka, D.L. Carter and P.M. Jolley. 1991. Freezing Effects on Aggregate Stability Affected by Texture, Mineralogy, and Organic Matter. Soil Science Society of America Journal 55: 1401-1406. doi:10.2136/sssaj1991.03615995005500050033x.

Letts, M.G., N.T. Roulet, N.T. Comer, M.R. Skarupa and D.L. Verseghy. 2000. Parametrization of peatland hydraulic properties for the Canadian Land Surface Scheme. Atmosphere-Ocean 38: 141-160.

Levy, G.J., H.J.C. Smith and M. Agassi. 1989. Water temperature effect on hydraulic conductivity and infiltration rate of soils. South African Journal of Plant and Soil 6: 240-244. doi:10.1080/02571862.1989.10634520.

Lewis, M. 1937. The rate of infiltration of water in irrigation ‐ practice. Eos, Transactions American Geophysical Union 18: 361-368.

Li, Q., S.F. Sun and Y.K. Xue. 2010. Analyses and development of a hierarchy of frozen soil models for cold region study. J Geophys Res-Atmos 115. doi:Artn D03107

10.1029/2009jd012530.

Liang, X., D.P. Lettenmaier, E.F. Wood and S.J. Burges. 1994. A Simple hydrologically Based Model of Land Surface Water and Energy Fluxes for GSMs. Journal of Geophysical Research 99: 415-428.

Liang, X. and Z. Xie. 2001. A new surface runoff parameterization with subgrid-scale soil heterogeneity for land surface models. Adv Water Resour 24: 1173-1193. doi:https://doi.org/10.1016/S0309-1708(01)00032-X.

Lin, H.S., K.J. Mclnnes, L.P. Wilding and C.T. Hallmark. 1998. Macroporosity and initial moisture effects on infiltration rates in Vertisols and vertic intergrades. Soil Science 163: 2-8.

Loague, K. and G.A. Gander. 1990. R-5 revisited: 1. Spatial variability of infiltration on a small rangeland catchment. Water Resour Res 26: 957-971. doi:doi:10.1029/WR026i005p00957.

Logsdon, S.D. and D.B. Jaynes. 1996. Spatial Variability of Hydraulic Conductivity in a Cultivated Field at Different Times. Soil Science Society of America Journal 60. doi:10.2136/sssaj1996.03615995006000030003x.

MacDonald, M.K., J.W. Pomeroy and R.L.H. Essery. 2017. Water and energy fluxes over northern prairies as affected by chinook winds and winter precipitation. Agricultural and Forest Meteorology 2017: 372-385. doi:10.1016/j.agrformet.2017.10.025.

Mantoglou, A. and L.W. Gelhar. 1987a. Capillary tension head variance, mean soil moisture content, and effective specific soil moisture capacity of transient unsaturated flow in stratified soils. Water Resour Res 23: 47-56.

Mantoglou, A. and L.W. Gelhar. 1987b. Effective hydraulic conductivity of transient unsaturated flow in stratified soils. Water Resour Res 23: 57-67.

Materia, S., P.A. Dirmeyer, Z.C. Guo, A. Alessandri and A. Navarra. 2010. The Sensitivity of Simulated River Discharge to Land Surface Representation and Meteorological Forcings. J Hydrometeorol 11: 334-351. doi:10.1175/2009jhm1162.1.

McGhie, D.A. and A.M. Posner. 1981. The effect of plant top material on the water repellence of fired sands and water repellent soils. Australian Journal of Agricultural Research 32: 609–620. doi:10.1071/AR9810609.

McNeal, B.L. and N.T. Coleman. 1966. Effect of Solution Composition on Soil Hydraulic Conductivity1. Soil Science Society of America Journal 30: 308-312. doi:10.2136/sssaj1966.03615995003000030007x.

Mein, R.G. and C.L. Larson. 1973. Modeling infiltration during a steady rain. Water Resour Res 9: 384-394. doi:doi:10.1029/WR009i002p00384.

Meng, H., J.D. Salas, T. Green and L. Ahuja. 2006. Scaling analysis of space-time infiltration based on the universal multifractal model. J Hydrol 322: 220-235. doi:10.1016/j.jhydrol.2005.03.016.

Mertens, J., D. Raes and J. Feyen. 2002. Incorporating rainfall intensity into daily rainfall records for simulating runoff and infiltration into soil profiles. Hydrol Process 16: 731-739. doi:doi:10.1002/hyp.1005.

Mezencev, V. 1948. Theory of formation of the surface runoff. Meteorologia e Hidrologia 3: 33-40.

Miller, D.E. and W.H. Gardner. 1962. Water Infiltration into Stratified Soil. Soil Science Society of America Journal 26: 115-119. doi:10.2136/sssaj1962.03615995002600020007x.

Miller, E.E. and R.D. Miller. 1956. Physical Theory for Capillary Flow Phenomena. Journal of Applied Physics 27: 324-332. doi:10.1063/1.1722370.

Milly, P.C.D. and P.S. Eagleson. 1988. Effect of storm scale on surface runoff volume. Water Resour Res 24: 620-624. doi:doi:10.1029/WR024i004p00620.

Milovac, J., J. Ingwersen and K. Warrach-Sagi. 2014. Soil texture forcing data for the whole world for the Weather Research and Forecasting (WRF) Model of the University of Hohenheim (UHOH) based on the Harmonized World Soil Database (HWSD) at 30 arc-second horizontal resolution. World Data Center for Climate (WDCC) at DKRZ.

Mis, J. 1982. Formulation and solution of fundamental problems of vertical infiltration. Czech/. Vodohosp. Gas 30: 304-311.

Mohammed, A., B. Kurylyk, E. Cey and M. Hayashi. 2018. Snowmelt infiltration and macropore flow in frozen soils: Overview, knowldedge and a conceptual framework. Vadose Zone Journal. doi:doi: 10.2136/vzj2018.04.0084.

Mohanty, B.P. 1999. Scaling hydraulic properties of a macroporous soil. Water Resour Res 35: 1927-1931. doi:doi:10.1029/1999WR900050.

Mohanty, B.P. and J. Zhu. 2007. Effective Hydraulic Parameters in Horizontally and Vertically Heterogeneous Soils for Steady-State Land–Atmosphere Interaction. J Hydrometeorol 8: 715-729. doi:10.1175/jhm606.1.

Montzka, C., M. Herbst, L. Weihermüller, A. Verhoef and H. Vereecken. 2017. A global data set of soil hydraulic properties and sub-grid variability of soil water retention and hydraulic conductivity curves. Earth Syst. Sci. Data 9: 529-543. doi:10.5194/essd-9-529-2017.

Moore, I.D. 1981a. Effect of surface sealing on infiltration. Transactions of the American Society of Agricultural Engineers 24: 1546-1553.

Moore, I.D. 1981b. Infiltration equations modified for surface effect. Journal of the Irrigation and Drainage Division 107: 71-86.

Moore, R.J. 1985. The probability-distributed principle and runoff production at point and basin scales. Hydrological Sciences Journal 30: 273-297. doi:10.1080/02626668509490989.

Morbidelli, R., C. Corradini and R.S. Govindaraju. 2006. A field-scale infiltration model accounting for spatial heterogeneity of rainfall and soil saturated hydraulic conductivity. Hydrol Process 20: 1465-1481. doi:doi:10.1002/hyp.5943.

Morbidelli, R., C. Saltalippi, A. Flammini and R.S. Govindaraju. 2018. Role of slope on infiltration: A review. J Hydrol 557: 878-886. doi:https://doi.org/10.1016/j.jhydrol.2018.01.019.

Mualem, Y. 1974. A conceptual model of hysteresis. Water Resour Res 10: 514-520. doi:doi:10.1029/WR010i003p00514.

Mualem, Y. 1976. A new model for predicting the hydraulic conductivity of unsaturated porous media. Water Resour Res 12: 513-522. doi:doi:10.1029/WR012i003p00513.

Mualem, Y. and S. Assouline. 1989. Modeling soil seal as a nonuniform layer. Water Resour Res 25: 2101-2108. doi:doi:10.1029/WR025i010p02101.

Mualem, Y. and S. Assouline. 1996. Soil sealing, infiltration and runoff. In: A. S. Issar and S. D. Resnick, editors, Runoff, infiltration and subsurface flow of water in arid and semi-arid regions. Water Science and Technology Library. Kluwer Academic Publishers. p. 131-181.

Mualem, Y. and S. Assouline. 1992. Flow processes in sealing soils: Conceptions and solutions. In: M. E. Sumner and B. A. Stewart, editors, Soil Crusting: Chemical and Physical Processes. Lewis Publishers, Boca Raton, Florida.

Mualem, Y. and A. Beriozkin. 2009. General scaling rules of the hysteretic water retention function based on Mualem's domain theory. European Journal of Soil Science 60: 652-661. doi:doi:10.1111/j.1365-2389.2009.01130.x.

Mualem, Y. and G. Dagan. 1975. A dependent domain model of capillary hysteresis. Water Resour Res 11: 452-460. doi:doi:10.1029/WR011i003p00452.

Mueller, A., E. Dutra, H. Cloke, A. Verhoef, G. Balsamo and F. Pappenberger. 2016. Water infiltration and redistribution in Land Surface Models. In: E. C. f. M.-R. W. Forecasts, editor ECMWF Technical Memoranda. Research Department University of Reading, UK.

Neuman, S.P. 1973. Saturated-unsaturated seepage by finite elements. Journal of the Hydraulics Division 99: 2233-2250.

Neuman, S.P. 1976. Wetting front pressure head in the infiltration model of Green and Ampt. Water Resour Res 12: 564-566. doi:doi:10.1029/WR012i003p00564.

Neuman, S.P., R.A. Feddes and E. Bresler. 1974. Finite element simulation of flow in saturated-unsaturated soils considering water uptake by plants. Third Annual Report. Hydraulic Engineering Lab., Technion, Haifa, Israel.

Nielsen, D., J. Biggar and K. Erh. 1973. Spatial variability of field-measured soil-water properties. Hilgardia 42: 215-259. doi:DOI:10.3733/hilg.v42n07p215

Nielsen, D.R., J.W. Hopmans and K. Reichardt. 1998. An emerging technology for scaling field soil-water behavior. In: G. Sposito, editor Scale dependence and scale invariance in hydrology. Cambridge University Press, Cambridge, UK. p. 136-166.

Nimmo, J., K. Perkins, K. M. Schmidt, D. Miller, J. D. Stock and K. Singha. 2009. Hydrologic Characterization of Desert Soils with Varying Degrees of Pedogenesis: 1. Field Experiments Evaluating Plant-Relevant Soil Water Behavior. Vadose Zone Journal 8: 480-495. doi:10.2136/vzj2008.0052.

Nimmo, J.R. 1992. Semiempirical model of soil water hysteresis. Soil Science Society of America Journal 56: 1723-1730.

Nimmo, J.R. and E.E. Miller. 1986. The temperature dependence of isothermal moisture vs. potential characteristics of soils. Soil Science Society of America Journal 50: 1105-1113.

Nissen, T.M. and M.M. Wander. 2003. Management and soil-quality effects on fertilizer-use efficiency and leaching. Soil Science Society of America Journal 67: 1524-1532.

Niu, G.-Y. and Z.-L. Yang. 2007. An observation-based formulation of snow cover fraction and its evaluation over large North American river basins. Journal of Geophysical Research: Atmospheres 112. doi:doi:10.1029/2007JD008674.

Niu, G.-Y., Z.-L. Yang, K.E. Mitchell, F. Chen, M.B. Ek, M. Barlage, A. Kumar, K. Manning, D. Niyogi, E. Rosero, M. Tewari and Y. Xia. 2011a. The community Noah land surface model with multiparameterization options (Noah-MP): 1. Model description and evaluation with local-scale measurements. Journal of Geophysical Research: Atmospheres 116. doi:doi:10.1029/2010JD015139.

Niu, G.Y., Z.L. Yang, R.E. Dickinson and L.E. Gulden. 2005. A simple TOPMODEL-based runoff parameterization (SIMTOP) for use in global climate models. J Geophys Res-Atmos 110. doi:10.1029/2005jd006111.

Niu, G.Y., Z.L. Yang, K.E. Mitchell, F. Chen, M.B. Ek, M. Barlage, A. Kumar, K. Manning, D. Niyogi, E. Rosero, M. Tewari and Y.L. Xia. 2011b. The community Noah land surface model with multiparameterization options (Noah-MP): 1. Model description and evaluation with local-scale measurements. J Geophys Res-Atmos 116. doi:10.1029/2010jd015139.

Noilhan, J. and P. Lacarrère. 1995. GCM gridscale evaporation from mesoscale modelling. J Climate 8: 206-223.

Nuth, M. and L. Laloui. 2008. Advances in modelling hysteretic water retention curve in deformable soils. Computers and Geotechnics 35: 835-844. doi:https://doi.org/10.1016/j.compgeo.2008.08.001.

Ogden, F.L., W. Lai, R.C. Steinke, J. Zhu, C.A. Talbot and J.L. Wilson. 2015. A new general 1-D vadose zone flow solution method. Water Resour Res 51: 4282-4300.

Oleson, K.W., D.M. Lawrence, G.B. Bonan, B. Drewniak, M. Huang, C.D. Koven, S. Levis, F. Li, W.J. Riley, Z.M. Subin, S.C. Swenson and P.E. Thornton. 2013. Technical description of version 4.5 of the community land model (CLM). NCAR Technical Note NCAR/TN-503+STR. National Center for Atmospheric Research, Boulder, CO. p. 422.

Oleson, K.W., G.-Y. Niu, Z.-L. Yang, D.M. Lawrence, P.E. Thornton, P.J. Lawrence, R. Stöckli, R.E. Dickinson, G.B. Bonan, S. Levis, A. Dai and T. Qian. 2008. Improvements to the Community Land Model and their impact on the hydrological cycle. Journal of Geophysical Research: Biogeosciences 113. doi:doi:10.1029/2007JG000563.

Or, D. 2008. Scaling of capillary, gravity and viscous forces affecting flow morphology in unsaturated porous media. Adv Water Resour 31: 1129-1136. doi:https://doi.org/10.1016/j.advwatres.2007.10.004.

Or, D., F.J. Leij, V. Snyder and T.A. Ghezzehei. 2000. Stochastic model for posttillage soil pore space evolution. Water Resour Res 36: 1641-1652. doi:doi:10.1029/2000WR900092.

Pachepsky, Y. and R.L. Hill. 2017. Scale and scaling in soils. Geoderma 287: 4-30. doi:https://doi.org/10.1016/j.geoderma.2016.08.017.

Paniconi, C. and M. Putti. 1994. A comparison of Picard and Newton iteration in the numerical solution of multidimensional variably saturated flow problems. Water Resour Res 30: 3357-3374. doi:doi:10.1029/94WR02046.

Paniconi, C. and M. Putti. 2015. Physically based modeling in catchment hydrology at 50: Survey and outlook. Water Resour Res 51: 7090-7129. doi:10.1002/2015wr017780.

Parhi, P.K., S.K. Mishra and R. Singh. 2007. A Modification to Kostiakov and Modified Kostiakov Infiltration Models. Water Resources Management 21: 1973-1989. doi:10.1007/s11269-006-9140-1.

Park, S.-E., A. Bartsch, D. Sabel, W. Wagner, V. Naeimi and Y. Yamaguchi. 2011. Monitoring freeze/thaw cycles using ENVISAT ASAR Global Mode. Remote Sensing of Environment 115: 3457-3467. doi:https://doi.org/10.1016/j.rse.2011.08.009.

Parlange, J.-Y. 1980. Water transport in soils. Annual Review of Fluid Mechanics 12: 77-102.

Parlange, J.-Y., W.L. Hogarth and M.B. Parlange. 1984. Optimal Analysis of the Effect of a Surface Crust1. Soil Science Society of America Journal 48: 494-497. doi:10.2136/sssaj1984.03615995004800030004x.

Parlange, J.-Y., T.S. Steenhuis, R. Haverkamp, D.A. Barry, P.J. Culligan, W.L. Hogarth, M.B. Parlange, P. Ross and F. Stagnitti. 1999. Soil properties and water movement. In: M. B. Parlange and J. W. Hopmans, editors, Vadose zone hydrology: Cutting across disciplines. Oxford University Press, New York. p. 99-129.

Parlange, J.Y. 1976. Capillary hysteresis and relationship between drying and wetting curves. Water Resour Res 12: 224-228. doi:10.1029/WR012i002p00224.

Parlange, J.Y., R. Haverkamp and J. Touma. 1985. Infiltration Under Ponded Conditions: 1. Optimal Analytical Solution and Comparison With Experimental Observations. Soil Science 139: 305-311. doi:10.1097/00010694-198504000-00003.

Parlange, J.Y. and D.E. Hill. 1976. Theoretical Analysis of Wetting Front Instability in Soils. Soil Science 122: 236-239. doi:10.1097/00010694-197610000-00008.

Parlange, J.Y., I.G. Lisle, R.D. Braddock and R.E. Smith. 1982. The Three-Parameter Infiltration Equation. Soil Science 133: 337-341. doi:10.1097/00010694-198206000-00001.

Parlange, M.B., A.T. Cahill, D.R. Nielsen, J.W. Hopmans and O. Wendroth. 1998. Review of heat and water movement in field soils. Soil and Tillage Research 47: 5-10. doi:https://doi.org/10.1016/S0167-1987(98)00066-X.

Peck, A.J. 1983. Field variability of soil physical properties. In: D. Hillel, editor Advances in Irrigation Vol. 2. Academic, San Diego, CA. p. 189-221.

Philip, J.-R. 1957. The theory of infiltration: 1. The infiltration equation and its solution. Soil science 83: 345-358.

Philip, J.R. 1967. Sorption and infiltration in heterogeneous media. Soil Research 5: 1-10. doi:https://doi.org/10.1071/SR9670001.

Philip, J.R. 1969. Theory of Infiltration. Advances in Hydroscience. p. 215-296.

Philip, J.R. 1970. Flow in Porous Media. Annual Review of Fluid Mechanics 2: 177-204. doi:10.1146/annurev.fl.02.010170.001141.

Philip, J.R. 1975. Stability analysis of infiltration. Soil Science of America Proceedings 39: 1042-1049.

Philip, J.R. and D.A. de Vries. 1957. Moisture movement in porous materials under temperature gradients. Eos, Transactions American Geophysical Union 38: 222-232. doi:doi:10.1029/TR038i002p00222.

Philip, J.R. and J.H. Knight. 1974. On solving the unsaturated flow equation: 3. New quasi-analytical technique. Soil Science 117: 1-13.

Poesen, J., J. Nachtergaele, G. Verstraeten and C. Valentin. 2003. Gully Erosion and Environmental Change: Importance and Research Needs. CATENA 50: 91-133. doi:10.1016/S0341-8162(02)00143-1.

Poulovassilis, A. 1962. Hysteresis of pore water, an application of the concept of independent domains. Soil Science 93: 405-412.

Prasad, S.N. and M.J.M. Römkens. 1982. An approximate integral solution of vertical infiltration under changing boundary conditions. Water Resour Res 18: 1022-1028. doi:doi:10.1029/WR018i004p01022.

Pruess, K. 1991. TOUGH2: A general-purpose numerical simulator for multiphase fluid and heat flow. Lawrence Berkeley Lab, Berekeley, California.

Puigdefabregas, J. 2005. The role of vegetation patterns in structuring runoff and sediment fluxes in drylands. Earth Surf Proc Land 30: 133-147. doi:10.1002/esp.1181.

Qi, J., P.A. Vermeer and G. Cheng. 2006. A review of the influence of freeze ‐ thaw cycles on soil geotechnical properties. Permafrost and Periglacial Processes 17: 245-252. doi:10.1002/ppp.559.

Qu, W., H.R. Bogena, J.A. Huisman, J. Vanderborght, M. Schuh, E. Priesack and H. Vereecken. 2015. Predicting subgrid variability of soil water content from basic soil information. Geophys Res Lett 42: 789-796. doi:doi:10.1002/2014GL062496.

Quirk, J.P. 1994. Interparticle Forces: A basis for the interpretation of soil physical behaviour. Advances in Agronomy 53: 121-183.

Quirk, J.P. and R.K. Schofield. 1955. The effect of electrolyte concentration of soil permeability. Journal of Soil Science 6: 163-178. doi:doi:10.1111/j.1365-2389.1955.tb00841.x.

Raats, P.A.C. 1973. Unstable Wetting Fronts in Uniform and Nonuniform Soils. Soil Science Society of America Journal 37: 681-685. doi:10.2136/sssaj1973.03615995003700050017x.

Raats, P.A.C. 2001. Developments in soil–water physics since the mid 1960s. Geoderma 100: 355-387. doi:https://doi.org/10.1016/S0016-7061(01)00028-3.

Raats, P.A.C. and A. Klute. 1969. One-dimensional simultaneous motion of the aqueous phase and the solid phase of saturated and partially saturated porous media. Soil Science 107: 329-333.

Raats, P.A.C., D. Smiles and A.W. Warrick. 2002. Environmental mechanics: water, mass and energy transfer in biosphere. American Geophysical Union, Published in cooperation with CSIRO, Australia, Washington, D.C.

Rahman, M. and R. Rosolem. 2017. Towards a simple representation of chalk hydrology in land surface modelling. Hydrology and Earth System Sciences 21: 459-471. doi: https://doi.org/10.5194/hess-21-459-2017.

Rahmati, M., L. Weihermüller, J. Vanderborght, Y.A. Pachepsky, L. Mao, S.H. Sadeghi, N. Moosavi, H. Kheirfam, C. Montzka, K. Van Looy, B. Toth, Z. Hazbavi, W. Al Yamani, A.A. Albalasmeh, M.Z. Alghzawi, R. Angulo-Jaramillo, A.C.D. Antonino, G. Arampatzis, R.A. Armindo, H. Asadi, Y. Bamutaze, J. Batlle-Aguilar, B. Béchet, F. Becker, G. Blöschl, K. Bohne, I. Braud, C. Castellano, A. Cerdà, M. Chalhoub, R. Cichota, M. Císlerová, B. Clothier, Y. Coquet, W. Cornelis, C. Corradini, A.P. Coutinho, M.B. de Oliveira, J.R. de Macedo, M.F. Durães, H. Emami, I. Eskandari, A. Farajnia, A. Flammini, N. Fodor, M. Gharaibeh, M.H. Ghavimipanah, T.A. Ghezzehei, S. Giertz, E.G. Hatzigiannakis, R. Horn, J.J. Jiménez, D. Jacques, S.D. Keesstra, H. Kelishadi, M. Kiani-Harchegani, M. Kouselou, M. Kumar Jha, L. Lassabatere, X. Li, M.A. Liebig, L. Lichner, M.V. López, D. Machiwal, D. Mallants, M.S. Mallmann, J.D. de Oliveira Marques, M.R. Marshall, J. Mertens, F. Meunier, M.H. Mohammadi, B.P. Mohanty, M. Pulido-Moncada, S. Montenegro, R. Morbidelli, D. Moret-Fernández, A.A. Moosavi, M.R. Mosaddeghi, S.B. Mousavi, H. Mozaffari, K. Nabiollahi, M.R. Neyshabouri, M.V. Ottoni, T.B. Ottoni Filho, M.R. Pahlavan-Rad, A. Panagopoulos, S. Peth, P.E. Peyneau, T. Picciafuoco, J. Poesen, M. Pulido, D.J. Reinert, S. Reinsch, M. Rezaei, F.P. Roberts, D. Robinson, J. Rodrigo-Comino, O.C. Rotunno Filho, T. Saito, H. Suganuma, C. Saltalippi, R. Sándor, B. Schütt, M. Seeger, N. Sepehrnia, E. Sharifi Moghaddam, M. Shukla, S. Shutaro, R. Sorando, A.A. Stanley, P. Strauss, Z. Su, R. Taghizadeh-Mehrjardi, E. Taguas, W.G. Teixeira, A.R. Vaezi, M. Vafakhah, T. Vogel, I. Vogeler, J. Votrubova, S. Werner, T. Winarski, D. Yilmaz, M.H. Young, S. Zacharias, Y. Zeng, Y. Zhao, H. Zhao and H. Vereecken. 2018. Development and analysis of the Soil Water Infiltration Global database. Earth Syst. Sci. Data 10: 1237-1263. doi:10.5194/essd-10-1237-2018.

Regalado, C.M. and A. Ritter. 2008. Cokriging Spatial Interpolation of Soil Water Dependent Repellency Parameters Determined with Two Different Tests. Soil Science Society of America Journal 72: 1683-1693. doi:10.2136/sssaj2008.0008.

Rengasamy, P. and K. Olsson. 1991. Sodicity and soil structure. Australian Journal of Soil Research 29: 935-952. doi:10.1071/SR9910935.

Reynolds, C.A., T.J. Jackson and W.J. Rawls. 2000. Estimating soil water-holding capacities by linking the Food and Agriculture Organization Soil map of the world with global pedon databases and continuous pedotransfer functions. Water Resour Res 36: 3653-3662. doi:doi:10.1029/2000WR900130.

Reynolds, W.D. and D.E. Eldrick. 1985. In-situ measurements of field saturated hydraulic conductivity, sorptivity and α-parameter using the Guelph permeameter. Soil Science 140: 292-302.

Richards, L.A. 1931. Capillary conduction of liquids through porous mediums. Physics 1: 318-333. doi:10.1063/1.1745010.

Ritsema, C.J. and L.W. Dekker. 1998. Three-dimensional patterns of moisture, water repellency, bromide and pH in a sandy soil. Journal of Contaminant Hydrology 31: 295-313. doi:https://doi.org/10.1016/S0169-7722(97)00067-3.

Roeckner, E., G. Bäuml, L. Bonaventura, R. Brokopf, M. Esch, M. Giorgetta, S. Hagemann, I. Kirchner, L. Kornblueh, E. Manzini, A. Rhodin, U. Schlese, U. Schulzweida and A. Tompkins. 2003. The atmospheric general circulation model ECHAM 5. PART I: Model description. MPI Report 349.

Römkens, M.J.M., R.L. Baumhardt, J.-Y. Parlange, F.D. Whisler, M.B. Parlange and S.N. Prasad. 1986. Effect of rainfall characteristics on seal hydraulic conductance. In: F. Callebaut, D. Gabriels and M. De Boodt, editors, Assessment of soil surface sealing and crusting. Ghent University Press, Ghent, Belgium. p. 228-235.

Romkens, M.J.M., R.L. Baumhardt, M. Parlange, F.D. Whisler, J.Y. Parlange and S.N. Prasad. 1986. Rain-induced surface seals: Their effect on ponding and infiltration. Annales Geophysicae 4: 417-424.

Römkens, M.J.M. and S.N. Prasad. 1992. A spectral series approach to infiltration for crusted and non-crusted soils. In: M. E. Sumner and B. A. Stewart, editors, Soil Crusting: Chemical and Physical Processes. S. Lewis Publishers, Boca Raton, Florida.

Ross, P.J., R. Haverkamp and J.-Y. Parlange. 1996. Calculating parameters for infiltration equations from soil hydraulic functions. Transport in Porous Media 24: 315-339. doi:10.1007/bf00154096.

Rubin, J. and R. Steinhardt. 1964. Soil Water Relations During Rain Infiltration: III. Water Uptake at Incipient Ponding1. Soil Science Society of America Journal 28: 614-619. doi:10.2136/sssaj1964.03615995002800050013x.

Russo, D. 2005. Physical aspects of soil salinity. In: D. Hillel, editor Encyclopedia of Soils in the Environment 3. Elsevier Ltd, Oxford, UK. p. 442-453.

Russo, D., I. Russo and A. Laufer. 1997. On the spatial variability of parameters of the unsaturated hydraulic conductivity. Water Resour Res 33: 947-956. doi:doi:10.1029/96WR03947.

Sadeghi, M., B. Ghahraman, A.N. Ziaei, K. Davary and K. Reichardt. 2012. Additional scaled solutions to Richards' equation for infiltration and drainage. Soil and Tillage Research 119: 60-69. doi:https://doi.org/10.1016/j.still.2011.12.004.

Sahoo, A.K., P.A. Dirmeyer, P.R. Houser and M. Kafatos. 2008. A study of land surface processes using land surface models over the Little River Experimental Watershed, Georgia. J Geophys Res-Atmos 113. doi:10.1029/2007/jd009671.

Samaniego, L., R. Kumar and S. Attinger. 2010. Multiscale parameter regionalization of a grid-based hydrologic model at the mesoscale. Water Resour Res 46. doi:doi:10.1029/2008WR007327.

Samaniego, L., R. Kumar, S. Thober, O. Rakovec, M. Zink, N. Wanders, S. Eisner, H. Müller Schmied, E.H. Sutanudjaja, K. Warrach-Sagi and S. Attinger. 2017. Toward seamless hydrologic predictions across spatial scales. Hydrol. Earth Syst. Sci. 21: 4323-4346. doi:10.5194/hess-21-4323-2017.

Sato, N., S. P.J., D.A. Randall, E.K. Schneider, J. Shukla, J.L. Kinter III, Y.-T. Hou and E. Albertazzi. 1989. Effects of Implementing the Simple Biosphere Model in a General Circulation Model. J Atmos Sci 46: 2757-2782. doi:10.1175/1520-0469(1989)046<2757:Eoitsb>2.0.Co;2.

Saulnier, G.M. and R. Datin. 2004. Analytical solution to a bias in the TOPMODEL framework balance. Hydrol Process 18: 1195-1218.

Scanlon, B. 2004. Review of HYDRUS-1D. Southwest Hydrology 3: 1.

Schaake, J.C., V.I. Koren, Q.Y. Duan, K. Mitchell and F. Chen. 1996. Simple water balance model for estimating runoff at different spatial and temporal scales. J Geophys Res-Atmos 101: 7461-7475. doi:10.1029/95jd02892.

Schaap, M.G. and F.J. Leij. 1998. DATABASE-RELATED ACCURACY AND UNCERTAINTY OF PEDOTRANSFER FUNCTIONS. Soil Science 163: 765-779.

Schaap, M.G., F.J. Leij and M.T. van Genuchten. 2001. ROSETTA: A computer program for estimating soil hydraulic parameters with hierarchical pedotransfer functions. J Hydrol 251: 163-176. doi:https://doi.org/10.1016/S0022-1694(01)00466-8.

Schlüter, S., J. Vanderborght and H.J. Vogel. 2012. Hydraulic non-equilibrium during infiltration induced by structural connectivity. Adv Water Resour 44: 101-112. doi:10.1016/j.advwatres.2012.05.002.

Scott, P.S., G.J. Farquhar and N. Kouwen. 1983. Hysteretic effects on net infiltration. Advances in Infiltration, Proceedings of the National Conference on Advances in Infiltration. American Society of Agricultural Engineers, St Joseph, MI. p. 163-170.

Selker, J.S. and S. Assouline. 2017. An explicit, parsimonious, and accurate estimate for ponded infiltration into soils using the Green and Ampt approach. Water Resour Res 53: 7481-7487. doi:doi:10.1002/2017WR021020.

Selker, J.S., J. Duan and J.-Y. Parlange. 1999. Green and Ampt infiltration into soils of variable pore size with depth. Water Resour Res 35: 1685-1688. doi:doi:10.1029/1999WR900008.

Sellers, P.J., Y. Mintz, Y.C. Sud and A. Dalcher. 1986. A Simple Biosphere Model (Sib) for Use within General-Circulation Models. J Atmos Sci 43: 505-531. doi:Doi 10.1175/1520-0469(1986)043<0505:Asbmfu>2.0.Co;2.

Sellers, P.J., D.A. Randall, Collatz.G.J., J.A. Berry, C.B. Field, D.A. Dazlich, C. Zhang, G.D. Collelo and L. Bounoua. 1996. A Revised Land Surface Parameterization (SiB2) for Atmospheric GCMS. Part I: Model Formulation. J Climate 9: 676-705. doi:10.1175/1520-0442(1996)009<0676:Arlspf>2.0.Co;2.

Seneviratne, S.I., T. Corti, E.L. Davin, M. Hirschi, E.B. Jaeger, I. Lehner, B. Orlowsky and A.J. Teuling. 2010. Investigating soil moisture-climate interactions in a changing climate: A review. Earth-Sci Rev 99: 125-161.

Sharma, M.L., G.A. Gander and C.G. Hunt. 1980. Spatial variability of infiltration in a watershed. J Hydrol 45: 101-122. doi:https://doi.org/10.1016/0022-1694(80)90008-6.

Sharma, M.L. and E. Seely. 1979. Spatial variability and its effects on areal infiltration. Proceedings Hydrology and Water Resources Symposium. Inst. Eng., Australia, Perth, W.A. p. 69-73.

Sharma, S.K., B.P. Mohanty and J. Zhu. 2006. Including Topography and Vegetation Attributes for Developing Pedotransfer Functions. Soil Science Society of America Journal 70: 1430-1440. doi:10.2136/sssaj2005.0087.

She, H.Y. and B.E. Sleep. 1998. The effect of temperature on capillary pressure-saturation relationships for air-water and perchloroethylene-water systems. Water Resour Res 34: 2587-2597. doi:doi:10.1029/98WR01199.

Shellito, P.J., E.E. Small and M.H. Cosh. 2016. Calibration of Noah Soil Hydraulic Property Parameters Using Surface Soil Moisture from SMOS and Basinwide In Situ Observations. J Hydrometeorol 17: 2275-2292. doi:10.1175/jhm-d-15-0153.1.

Shi, Y.N., K.J. Davis, F.Q. Zhang and C.J. Duffy. 2014. Evaluation of the Parameter Sensitivities of a Coupled Land Surface Hydrologic Model at a Critical Zone Observatory. J Hydrometeorol 15: 279-299. doi:10.1175/jhm-d-12-0177.1.

Shouse, P.J. and B.P. Mohanty. 1998. Scaling of near-saturated hydraulic conductivity measured using disc infiltrometers. Water Resour Res 34: 1195-1205. doi:doi:10.1029/98WR00318.

Silva, V.R., D.J. Reinert and J.M. Reichert. 2000. Densidade do solo, atributos químicos e sistema radicular do milho afetados pelo pastejo e manejo do solo (Soil density, chemical attributes and maize root distribution as affected by grazing and soil management). Revista Brasileira de Ciência do Solo 24: 191-199.

Simunek, J., N.J. Jarvis, M.T. van Genuchten and A. Gardenas. 2003. Review and comparison of models for describing non-equilibrium and preferential flow and transport in the vadose zone. J Hydrol 272: 14-35.

Šimůnek, J. and M.T. van Genuchten. 2008. Modeling Nonequilibrium Flow and Transport Processes Using HYDRUS. Vadose Zone Journal 7: 782-797. doi:10.2136/vzj2007.0074.

Šimůnek, J., M.T. van Genuchten and M. Šejna. 2008. Development and Applications of the HYDRUS and STANMOD Software Packages and Related Codes. Vadose Zone Journal 7: 587-600. doi:10.2136/vzj2007.0077.

Šimůnek, J., M.T. van Genuchten and M. Šejna. 2016. Recent Developments and Applications of the HYDRUS Computer Software Packages. Vadose Zone Journal 15. doi:10.2136/vzj2016.04.0033.

Sisson, J.B. and P.J. Wierenga. 1981. Spatial Variability of Steady-State Infiltration Rates as a Stochastic Process. Soil Science Society of America Journal 45: 699-704. doi:10.2136/sssaj1981.03615995004500040005x.

Sivapalan, M. and E.F. Wood. 1986. Spatial heterogeneity and scale in the infiltration response of Catchments. In: V. K. Gupta, I. Rodriguez-Iturbe and E. F. Wood, editors, Scale Problems in Hydrology. Reidel, Hingham, Mass. p. 81-106.

Sivapalan, M. and R.A. Woods. 1995. Evaluation of the effects of general-circulation models subgrid varability and patchiness of rainfall and soil-moisture on land-surface water-balance fluxes. Hydrol Process 9: 697-717. doi:10.1002/hyp.3360090515.

Skaggs, R.W. 1982. Infiltration. In: C. T. Haan, H. P. Johnson and D. L. Brakensiek, editors, Hydrologic modeling of small watersheds, ASAE Monograph Nr. 5, ASAE. St. Joseph, MI. p. 121-166.

Smiles, D.E. 1974. Infiltration into a swelling material. Soil Science 117: 140-147.

Smith, R.E. 1972. The infiltration envelope: Results from a theoretical infiltrometer. J Hydrol 17: 1-22. doi:https://doi.org/10.1016/0022-1694(72)90063-7.

Smith , R.E. 1990. Analysis of infiltration through a two-layer soil profile. Soil Science Society of America Journal 54: 1219-1227.

Smith, R.E., C. Corradini and F. Melone. 1999. A conceptual model for infiltration and redistribution in crusted soils. Water Resour Res 35: 1385-1393. doi:doi:10.1029/1998WR900046.

Smith, R.E. and D.C. Goodrich. 2000. Model For Rainfall Excess Patterns on Randomly Heterogeneous Areas. Journal of Hydrologic Engineering 5: 355-362. doi:doi:10.1061/(ASCE)1084-0699(2000)5:4(355).

Smith, R.E. and R.H.B. Hebbert. 1979. A Monte Carlo Analysis of the hydrologic effects of spatial variability of infiltration. Water Resour Res 15: 419-429. doi:doi:10.1029/WR015i002p00419.

Smith, R.E., K.R.J. Smettem, P. Broadbridge and D.A. Woolhiser. 2002. Infiltration theory for hydrologic applications. Water Resources Monograph. AGU, Washington DC.

Soet, M., R.J. Ronda, J.N.M. Stricker and A.J. Dolman. 2000. Land surface scheme conceptualisation and parameter values for three sites with contrasting soils and climate. Hydrology and Earth System Sciences 4: 283-294.

Sposito, G. 1975. Steady vertical flows in swelling soils. Water Resour Res 11: 461-464. doi:doi:10.1029/WR011i003p00461.

Stange, C. and R. Horn. 2005. Modeling the Soil Water Retention Curve for Conditions of Variable Porosity. Vadose Zone Journal 4: 602-613. doi:10.2136/vzj2004.0150.

Strudley, M.W., T.R. Green and J.C. Ascough. 2008. Tillage effects on soil hydraulic properties in space and time: State of the science. Soil & Tillage Research 99: 4-48. doi:10.1016/j.still.2008.01.007.

Sun, S. and Y. Xue. 2001a. Implementing a new snow scheme in Simplified Simple Biosphere Model. Adv Atmos Sci 18: 335-354. doi:10.1007/bf02919314.

Sun, S.F. and Y.K. Xue. 2001b. Implementing a new snow scheme in simplified simple biosphere model. Adv Atmos Sci 18: 335-354.

Swartzendruber, D. 1987. Rigorous derivation and interpretation of the Green and Ampt equation. In: Y. S. Fok, editor Infiltration Development and application. Water Resources Research Center, University of Hawaii, Honolulu, Hawaii, USA.

Talsma, T. and J.Y. Parlange. 1972. One dimensional vertical infiltration. Australian Journal of Soil Research 10: 143-150. doi:10.1071/SR9720143.

Täumer, K., H. Stoffregen and G. Wessolek. 2005. Determination of repellency distribution using soil organic matter and water content. Geoderma 125: 107-115. doi:https://doi.org/10.1016/j.geoderma.2004.07.004.

Thomas, P.J., J.C. Baker, L.W. Zelazny and D.R. Hatch. 2000. Relationship of Map Unit Variability to Shrink-Swell Indicators. Soil Science Society of America Journal 64: 262-268.

Tillotson, P.M. and D.R. Nielsen. 1984. Scale Factors in Soil Science. Soil Science Society of America Journal 48: 953-959. doi:10.2136/sssaj1984.03615995004800050001x.

Topp, G.C. 1971. Soil-Water Hysteresis: the Domain Theory Extended to Pore Interaction Conditions. Soil Science Society of America Journal 35: 219-225. doi:10.2136/sssaj1971.03615995003500020017x.

Tyler, S.W. and S.W. Wheatcraft. 1990. Fractal processes in soil water retention. Water Resour Res 26: 1047-1054. doi:doi:10.1029/WR026i005p01047.

Unger, P.W. 1991. Overwinter Changes in Physical Properties of No-Tillage Soil. Soil Science Society of America Journal 55: 778-782. doi:10.2136/sssaj1991.03615995005500030024x.

van Dam, J.C., P. Groenendijk, R.F.A. Hendriks and J.G. Kroes. 2008. Advances of modeling water flow in variably saturated soils with SWAP. Vadose Zone J 7: 640-653.

Van Dam, J.C., J.M.H. Hendrickx, H.C. Van Ommen, M.H. Bannink, M.T. Van Genuchten and L.W. Dekker. 1990. Water and solute movement in a coarse-textured water-repellent field soil. J Hydrol 120: 359-379. doi:https://doi.org/10.1016/0022-1694(90)90159-U.

van den Hurk, B. and P. Viterbo. 2003. The Torne-Kalix PILPS 2(e) experiment as a test bed for modifications to the ECMWF land surface scheme. Global Planet Change 38: 165-173. doi:10.1016/s0921-8181(03)00027-4.

Van Genuchten, M., Th. 1980. A Closed-form Equation for Predicting the Hydraulic Conductivity of Unsaturated Soils. Soil Science Society of America Journal 44: 892–898. doi:10.2136/sssaj1980.03615995004400050002x.

Van Looy, K., J. Bouma, M. Herbst, J. Koestel, B. Minasny, U. Mishra, C. Montzka, A. Nemes, Y.A. Pachepsky, J. Padarian, M.G. Schaap, B. Tóth, A. Verhoef, J. Vanderborght, M.J. Ploeg, L. Weihermüller, S. Zacharias, Y. Zhang and H. Vereecken. 2017. Pedotransfer Functions in Earth System Science: Challenges and Perspectives. Reviews of Geophysics 55: 1199-1256. doi:doi:10.1002/2017RG000581.

Vandervaere, J.-P., M. Vauclin, R. Haverkamp, C. Peugeot, J.-L. Thony and M. Gilfedder. 1998. Prediction of Crust-Induced Surface Runoff With Disc Infiltrometer Data. Soil Science 163: 9-21. doi:10.1097/00010694-199801000-00003.

Vaught, R., K.R. Brye and D.M. Miller. 2006. Relationships among Coefficient of Linear Extensibility and Clay Fractions in Expansive, Stoney Soils. Soil Science Society of America journal 70: 1983-1990. doi:10.2136/sssaj2006.0054.

Vereecken, H., R. Kasteel, J. Vanderborght and T. Harter. 2007a. Upscaling Hydraulic Properties and Soil Water Flow Processes in Heterogeneous Soils. Vadose Zone Journal 6: 1-28. doi:10.2136/vzj2006.0055.

Vereecken, H., R. Kasteel, J. Vanderborght and T. Harter. 2007b. Upscaling hydraulic properties and soil water flow processes in heterogeneous soils: A review Vadose Zone Journal 6: 1-28. doi:DOI: 10.2136/vzj2006.0055

Vereecken, H., J. Maes and J. Feyen. 1990. Estimating Unsaturated Hydraulic Conductivity From Easily Measured Soil Properties. Soil Science 149: 1-12. doi:10.1097/00010694-199001000-00001.

Vereecken, H., J. Maes, J. Feyen and P. Darius. 1989. Estimating the soil-moisture retention characteristics from testure, bulk-density, and carbon content. Soil Science 148: 389-403. doi:10.1097/00010694-198912000-00001.

Vereecken, H., M. Weynants, M. Javaux, Y. Pachepsky, M.G. Schaap and M.T. van Genuchten. 2010. Using Pedotransfer Functions to Estimate the van Genuchten-Mualem Soil Hydraulic Properties: A Review. Vadose Zone Journal 9: 795-820. doi:10.2136/vzj2010.0045.

Verhoef, A. and G. Egea-Cegarra. 2013. Soil Water and its Management. In: P. Gregory and S. Nortcliff, editors, Soil Conditions and Plant Growth. Blackwell Publishing:. p. 321-387.

Vieira, S.R., D.R. Nielsen and J.W. Biggar. 1981. Spatial Variability of Field-Measured Infiltration Rate. Soil Science Society of America Journal 45: 1040-1048. doi:10.2136/sssaj1981.03615995004500060007x.

Viterbo, P. and A.C.M. Beljaars. 1995. An improved land-surface parameterization scheme in the ECMWF model and its validation. J Climate 8: 2716-2748. doi:10.1175/1520-0442(1995)008<2716:ailsps>2.0.co;2.

Vogel, H.-J. and O. Ippisch. 2008. Estimation of a Critical Spatial Discretization Limit for Solving Richards' Equation at Large Scales. Vadose Zone Journal 7: 112-114. doi:10.2136/vzj2006.0182.

Vogel, H.J., I. Cousin, O. Ippisch and P. Bastian. 2006. The dominant role of structure for solute transport in soil: experimental evidence and modelling of structure and transport in a field experiment. Hydrology and Earth System Sciences 10: 495-506.

Vogel, H.J. and K. Roth. 1998. A new approach for determining effective soil hydraulic functions. European Journal of Soil Science 49: 547-556. doi:doi:10.1046/j.1365-2389.1998.4940547.x.

Vrugt, J.A., C.J.F. ter Braak, C.G.H. Diks, B.A. Robinson, J.M. Hyman and D. Higdon. 2009. Accelerating Markov Chain Monte Carlo Simulation by Differential Evolution with Self-Adaptive Randomized Subspace Sampling. Int J Nonlin Sci Num 10: 273-290.

Walko, R.L. and R. Avissar. 2008a. The Ocean-Land-Atmosphere Model (OLAM). Part I: Shallow-Water Tests. Mon Weather Rev 136: 4033-4044.

Walko, R.L. and R. Avissar. 2008b. The Ocean–Land–Atmosphere Model (OLAM). Part I: Shallow-Water Tests. Mon Weather Rev 136: 4033-4044. doi:10.1175/2008mwr2522.1.

Walko, R.L., L.E. Band, J. Baron, T.G.F. Kittel, R. Lammers, T.J. Lee, D. Ojima, R.A. Pielke Sr., C. Taylor, C. Tague, C.J. Tremback and P.L. Vidale. 2000. Coupled Atmosphere–Biophysics–Hydrology Models for Environmental Modeling. Journal of Applied Meteorology 39: 931-944. doi:10.1175/1520-0450(2000)039<0931:Cabhmf>2.0.Co;2.

Wang, L.L., D.H. Chen and H.J. Bao. 2016. The improved Noah land surface model based on storage capacity curve and Muskingum method and application in GRAPES model. Atmos Sci Lett 17: 190-198. doi:10.1002/asl.642.

Wang, Y.P., E. Kowalczyk, R. Leuning, G. Abramowitz, M.R. Raupach, B. Pak, E. van Gorsel and A. Luhar. 2011. Diagnosing errors in a land surface model (CABLE) in the time and frequency domains. J Geophys Res-Biogeo 116. doi:Artn G01034

10.1029/2010jg001385.

Wang, Z., J. Feyen, M.T. van Genuchten and D.R. Nielsen. 1998. Air entrapment effects on infiltration rate and flow instability. Water Resour Res 34: 213-222. doi:10.1029/97wr02804.

Wang, Z., A. Tuli and W.A. Jury. 2003a. Unstable Flow during Redistribution in Homogeneous Soil. Vadose Zone J 2: 52-60. doi:10.2113/2.1.52.

Wang, Z., L.S. Wu, T. Harter, J.H. Lu and W.A. Jury. 2003b. A field study of unstable preferential flow during soil water redistribution. Water Resour Res 39.

Warrick, A.W. 2003. Soil Water Dynamics. Oxford Univ. Press, New York. p. 416.

Warrick, A.W. and A.A. Hussen. 1993. Scaling of Richards' Equation for Infiltration and Drainage. Soil Science Society of America Journal 57: 15-18. doi:10.2136/sssaj1993.03615995005700010004x.

Warrick, A.W. and T.C. Jim Yeh. 1990. One-dimensional, steady vertical flow in a layered soil profile. Adv Water Resour 13: 207-210. doi:https://doi.org/10.1016/0309-1708(90)90042-3.

Warrick, A.W. and D.R. Nielsen. 1980. Spatial variability of soil physical properties in the field. Applications of Soil Physics. Academic, San Diego, CA. p. 319-344.

Warrilow, D.A., A.B. Sangster and A. Slingo. 1986. Modelling of land surface processes and their influence on european climate. Dynamical Climatology DCTN38,. Meteorological Office, Bracknell, UK.

Weynants, M., H. Vereecken and M. Javaux. 2009. Revisiting Vereecken Pedotransfer Functions: Introducing a Closed-Form Hydraulic Model Vadose Zone Journal 8: 86-95. doi:10.2136/vzj2008.0062.

Whisler, F.D., A.A. Curtis, A. Niknam and M.J.M. Römkens. 1979. Modeling infiltration as affected by soil crusting. Proc. Fort Collins Third International Hydrol. Sympos. Fort Collins, Colorado. p. 400-413.

White, I. and M.J. Sully. 1992. On the variability and use of the hydraulic conductivity alpha parameter in stochastic treatments of unsaturated flow. Water Resour Res 28: 209-213. doi:doi:10.1029/91WR02198.

Williams, P.J. and T.P. Burt. 1974. Measurement of Hydraulic Conductivity of Frozen Soils. Canadian Geotechnical Journal 11: 647-650. doi:10.1139/t74-066.

Witter, J.V., P.D. Jungerius and M.J. ten Harkel. 1991. Modelling water erosion and the impact of water repellency. CATENA 18: 115-124. doi:https://doi.org/10.1016/0341-8162(91)90011-L.

Wood, E.F., D.P. Lettenmaier, X. Liang, D. Lohmann, A. Boone, S. Chang, F. Chen, Y. Dai, R.E. Dickinson, Q. Duan, M. Ek, Y.M. Gusev, F. Habets, P. Irannejad, R. Koster, K.E. Mitchel, O.N. Nasonova, J. Noilhan, J. Schaake, A. Schlosser, Y. Shao, A.B. Shmakin, D. Verseghy, K. Warrach, P. Wetzel, Y. Xue, Z.-L. Yang and Q.-c. Zeng. 1998. The Project for Intercomparison of Land-surface Parameterization Schemes (PILPS) Phase 2(c) Red–Arkansas River basin experiment:: 1. Experiment description and summary intercomparisons. Global Planet Change 19: 115-135. doi:https://doi.org/10.1016/S0921-8181(98)00044-7.

Woolhiser, D.A., R.E. Smith and J.-V. Giraldez. 1996. Effects of Spatial Variability of Saturated Hydraulic Conductivity on Hortonian Overland Flow. Water Resour Res 32: 671-678. doi:doi:10.1029/95WR03108.

Wösten, J.H.M., A. Lilly, A. Nemes and C. Le Bas. 1999. Development and use of a database of hydraulic properties of European soils. Geoderma 90: 169-185. doi:https://doi.org/10.1016/S0016-7061(98)00132-3.

Wösten, J.H.M., Y.A. Pachepsky and W.J. Rawls. 2001. Pedotransfer functions: bridging the gap between available basic soil data and missing soil hydraulic characteristics. J Hydrol 251: 123-150. doi:https://doi.org/10.1016/S0022-1694(01)00464-4.

Xue, Y., P.J. Sellers, J.L. Kinter and J. Shukla. 1991. A Simplified Biosphere Model for Global Climate Studies. J Climate 4: 345-364. doi:10.1175/1520-0442(1991)004<0345:Asbmfg>2.0.Co;2.

Xue, Y.K., F.J. Zeng and C.A. Schlosser. 1996. SSiB and its sensitivity to soil properties - A case study using HAPEX-Mobilhy data. Global Planet Change 13: 183-194. doi:Doi 10.1016/0921-8181(95)00045-3.

Yager, R.R. 2001. The power average operator. IEEE Transactions on Systems, Man, and Cybernetics - Part A: Systems and Humans 31: 724-731. doi:10.1109/3468.983429.

Yang, K., T. Koike, B.S. Ye and L. Bastidas. 2005. Inverse analysis of the role of soil vertical heterogeneity in controlling surface soil state and energy partition. J Geophys Res-Atmos 110. doi:10.1029/2004jd005500.

Yang, Z.-L. and R.E. Dickinson. 1996. Description of the Biosphere-Atmosphere Transfer Scheme (BATS) for the Soil Moisture Workshop and evaluation of its performance. Global Planet Change 13: 117-134. doi:https://doi.org/10.1016/0921-8181(95)00041-0.

Yang, Z.L. and G.Y. Niu. 2003. The versatile integrator of surface and atmosphere processes - Part 1. Model description. Global Planet Change 38: 175-189. doi:10.1016/s0921-8181(03)00028-6.

Young, I.M. and J.W. Crawford. 2004. Interactions and Self-Organization in the Soil-Microbe Complex. Science 304: 1634-1637. doi:10.1126/science.1097394.

Zaslavsky, D. 1964. Theory of unsaturated flow into a non-uniform soil profile. Soil Science 97: 400-410.

Zhan, X.W., Y.K. Xue and G.J. Collatz. 2003. An analytical approach for estimating CO2 and heat fluxes over the Amazonian region. Ecol Model 162: 97-117. doi:10.1016/S0304-3800(02)00405-2.

Zhang, Y.Q., H.X. Zheng, F.H.S. Chiew, J. Pena-Arancibia and X.Y. Zhou. 2016. Evaluating Regional and Global Hydrological Models against Streamflow and Evapotranspiration Measurements. J Hydrometeorol 17: 995-1010. doi:10.1175/jhm-d-15-0107.1.

Zhao, W. and A. Li. 2015. A Review on Land Surface Processes Modelling over Complex Terrain. Adv Meteorol 2015: 17. doi:10.1155/2015/607181.

Zhou, X.Y., Y.Q. Zhang, Y.P. Wang, H.Q. Zhang, J. Vaze, L. Zhang, Y.H. Yang and Y.C. Zhou. 2012. Benchmarking global land surface models against the observed mean annual runoff from 150 large basins. J Hydrol 470: 269-279. doi:10.1016/j.jhydrol.2012.09.002.

Zhu, J. and B.P. Mohanty. 2002a. Spatial Averaging of van Genuchten Hydraulic Parameters for Steady-State Flow in Heterogeneous Soils: A Numerical Study. Vadose Zone Journal 1: 261-272.

Zhu, J. and B.P. Mohanty. 2002b. Upscaling of soil hydraulic properties for steady state evaporation and infiltration. Water Resour Res 38: 17-11-17-13. doi:doi:10.1029/2001WR000704.

Zhu, J. and B.P. Mohanty. 2003. Effective hydraulic parameters for steady state vertical flow in heterogeneous soils. Water Resour Res 39. doi:doi:10.1029/2002WR001831.

Zhu, J. and B.P. Mohanty. 2004. Soil Hydraulic Parameter Upscaling for Steady-State Flow with Root Water Uptake. Vadose Zone Journal 3: 1464-1470. doi:10.2113/3.4.1464.

Zhu, J. and B.P. Mohanty. 2006. Effective scaling factor for transient infiltration in heterogeneous soils. J Hydrol 319: 96-108. doi:https://doi.org/10.1016/j.jhydrol.2005.07.004.

Zhu, J., B.P. Mohanty and N.N. Das. 2006. On the Effective Averaging Schemes of Hydraulic Properties at the Landscape Scale. Vadose Zone Journal 5: 308-318. doi:10.2136/vzj2005.0035.

Zhu, J., B.P. Mohanty, A.W. Warrick and M.T. Van Genuchten. 2004. Correspondence and Upscaling of Hydraulic Functions for Steady-State Flow in Heterogeneous Soils. Vadose Zone Journal 3: 527-533. doi:10.2113/3.2.527.

Zobler, L. 1986. A World Soil File for Global Climate Modeling. NASA Technical Memorandum #87802. NASA.

Zobler, L. 1999. Global Soil Types, 1-Degree Grid (Zobler). ORNL Distributed Active Archive Center.

List of Symbols

a_s fitting parameter for each grid box to estimate F_{sat} (JULES)

a_{SSiB} constant in Eq. [A54] (-)

a_r fitting parameter in CLSM

b_r fitting parameter in CLSM

A fraction of an area for which the soil moisture capacity is less than or equal to I (-)

AC steady state infiltration (LT^{-1})

A_f fitting parameter

A_{gf} grid box fraction of soil water capacity (-)

A_1 fitting parameter (LT^{-1})

b parameter that reflects the grid cell heterogeneity (-)

b_{SSiB} constant in Eq. [A54] (-)

b_{BC} parameter in the Brooks Corey equation (Clapp and Hornberger, 1978) (-)

B potential infiltration rate shape parameter which is a measure for the spatial variability of the potential infiltration rate defined as the maximum infiltration rate of each point when the surface is ponded (Liang and Xie, 2001) (-)

B' parameter related to the BC exponent of the water retention characteristic (-)

B_{TW} exponent of the tension water capacity distribution curve (-)

C fraction of an area for which the potential infiltration rate is less than or equal to f (Liang and Xie, 2001) (-)

c water storage capacity at a certain location (L)

c_{SSiB} constant in Eq. [A54] (-)

c_{max} maximum water storage capacity (L),

C_{ice} ice impedance factor (-)

c_s fitting parameter for each grid box to estimate F_{sat} (JULES)

C_v tunable parameter (-)

D_b spatially averaged soil moisture storage deficit (-)

D_{bmax} maximum soil water storage (L)

D_x soil water storage (L)

D_θ average water table depth (L)

D_{sm} local soil moisture deficit (L)

D_t mean water storage deficit (L)

D_θ the amount of water stored between surface and groundwater (L)

d_o maximum local water deficit (L)

$\bar{d}$ mean water table depth (L)

dx length of the grid cell in km (L)

$\langle d_2 \rangle$ depth of the root zone (L)

F_{sat} saturated fraction of the catchment or grid cell in a LSM (-)

F_{max} fraction of pixels in a grid cell whose topographic index is larger than or equal to the grid cell mean topographic index (-)

F_{frz} fractional impermeable area as a function of soil ice content of the surface soil layer (-)

cumulative distribution of mean infiltrability (ORCHIDEE)

$F(c)$ standard reflected power cumulative distribution function of the spatial variation of the storage capacity, c

$F_S(z^*)$ cumulative distribution function of the scaled infiltration capacity Eq. [47]

f^* infiltrability of the first soil layer (LT^{-1})

$f_{.}$ pdf of the respective variables
f point potential infiltration rate (LT^{-1})
f_c is the final infiltration capacity (LT^{-1}),
f_d decay factor (L^{-1})
f_0 initial infiltration capacity (LT^{-1})
f_{h20sfc} fraction of the area that is inundated (-)
f_H Hortonian infiltration capacity at time t (LT^{-1})
f_m maximum potential infiltration rate (LT^{-1})
f_{mm} average potential infiltration rate (LT^{-1})
f_{sno} fraction of the grid cell covered by snow (-)
$f_{sc,i}$ fraction of soil carbon in layer *i*,
$f_{unf,i}$ pdf representing the spatial variability of the local maximum infiltration rate in a grid cell
$f_s(s)$ gamma function of the mean surface layer point soil water saturation
h_{sat} pressure head at air entry value (L)
I_{max} maximum infiltration rate (ML^2T^{-1} or LT^{-1}) or maximum soil moisture capacity (L)
$I_{c,t}$ cumulative infiltration capacity at a certain moment in time t (L)
$I_{unf,i}$ local maximum infiltration rates for unfrozen soil at soil layer I (LT^{-1})
i point soil moisture capacity (L)
i_c infiltration capacity (ML^2T^{-1})
I spatially averaged actual infiltration (LT^{-1})
$\langle I_m \rangle$ mean maximum infiltration rate over the grid cell
I_{roff} normalized runoff in SSiB (LT^{-1})
h matric potential (L)
h_A minimum (i.e., for evaporation) pressure head at the soil surface allowed under the prevailing soil conditions [L]
h_S maximum (i.e., for infiltration) pressure heads at the soil surface allowed under the prevailing soil conditions [L]
h_c matric potential at air entry (L)
h_f capillary pressure at the wetting front [L],
$h_o(t)$ matric potential at the soil surface at time t (l)
H total water head (L)
i_p maximum potential rate of infiltration or evaporation under the current atmospheric conditions [LT^{-1}]
i point scale water capacity (L)
$i^*(t)$ scaled infiltration rate (LT^{-1})
I^* scaled cumulative infiltration (L)
I_r infiltration rate for the whole soil column (LT^{-1})
$I_{unf,i}$ local maximum infiltration rates for unfrozen soil (LT^{-1})
J Darcian water flux (LT^{-1})
J_w precipitation rate [$L\,T^{-1}$]
K_i^{int} average of hydraulic conductivity at the wetting front and the deepest saturated node (LT^{-1})
$K_i^{int,*}$ scaled K_i^{int}(LT^{-1})
K_{dt} constant parameter set equal to 3.0 (-)
K_{ref} reference K value (2×10^{-6} m/s) (LT^{-1})
K_s saturated hydraulic conductivity (LT^{-1})
$K_{s,min,i}$ saturated hydraulic conductivity of the mineral phase of layer i (LT^{-1})
$K_{s,sc,i}$ saturated hydraulic conductivity of the organic soil carbon of layer i (LT^{-1})

K_o	hydraulic conductivity of the soil surface layer (LT^{-1})
l	tortuosity index in the Mualem model (-)
M_{se}	surface layer excess [L]
m	fitting parameter in the van Genuchten model (-)
n_{vg}	pore size distribution index in van Genuchten model (-)
n_K	fitting parameter in the Kostiakov Equation
P_{drop}	precipitation reaching surface after canopy interceptrion in SSiB (LT^{-1})
P_M	snowmelt (either L or ML^2T^{-1} or LT^{-1})
P_R	rainfall rate (LT^{-1})
P_T	throughfall precipitation (either L or ML^2T^{-1} or LT^{-1})
P_x	flux incident at the soil surface (ML^2T^{-1}),
q_{cap}	infiltration capacity of the soil (LT^{-1})
$q(t)$	infiltration flux (LT^{-1})
$q^*(t)$	scaled infiltration rate (LT^{-1})
q_f	final (constant) infiltration rate ($L\,T^{-1}$)
q_i	initial infiltration rate ($L\,T^{-1}$)
$q_{evapo,soil}$	water loss due to evaporation (LT^{-1})
$q_{in,soil}$	infiltration rate of water into the soil (LT^{-1})
q_s	surface runoff (ML^2T^{-1}) or (LT^{-1})
q_H	Hortonian excess infiltration runoff (LT^{-1})
q_D	Dunne saturation excess runoff (LT^{-1})
$q_{liq,o}$	moisture input into the grid cell (LT^{-1}) and is the sum of liquid precipitation reaching the surface and snowmelt
$q_{in,surface}$	surface moisture flux remaining after surface runoff has been removed (LT^{-1})
q_u	downslope subsurface flow rate per unit contour width (LT^{-1})
q_{re}	recharge rate (LT^{-1})
$Q(t)$	cumulative infiltration at time t [L]
Q_{wat}	input of water (rainfall, snowfall, dew) (LT^{-1})
$r(t)$	water supply rate (LT^{-1})
r_o	amount of water that needs to infiltrate (throughfall, snowmelt and ponded water) (LT^{-1})
$R(i)$	mean infiltration excess runoff (LT^{-1})
s	water content expressed as saturation (-)
$\langle s \rangle$	grid mean surface layer soil water saturation (-)
S	grid cell mean storage (-)
S_e	the effective saturation (-)
S_g	surface gradient (-)
S_{max}	maximum water depth over the basin (L)
S_o	minimum storage below which there is no surface saturation (L)
S_{op}	soil sorptivity [$L\,T^{-2}$],
SW	equilibrium root zone wetness index (-)
SW_o	minimum value of the soil wetness index distribution (-)
SWI	Soil water index (-)
Sl	mean slope in the grid-cells
Sl_{max}	maximum threshold slope
$S^*_{x_l}$	local terrain surface slope
t	time (T)
T	transmissivity (LT^{-1})

T_o transmissivity of the soil profile (LT^{-1})
t^* scaled time (T)
t_f time needed to infiltrate a certain amount of water (T)
t_p time to ponding (T)
$T(z_\nabla)$ transmissivity in Eq. [A38]
$tan\beta$ local surface topographic slope
$\check{v}$ depth averaged velocity vector [LT^{-1}],
v_K parameter describing the decrease of saturated hydraulic conductivity with depth
w_{min} minimal local subgrid soil water capacity
w_{max} maximum local soil water capacity
w_{act} subgrid water content that corresponds to the fractional saturation
W vertically integrated soil water content (θ) over the first 50 cm of the soil profile (L)
W_{sat} vertically integrated saturated soil water content (θ_{sat}) over the first 50 cm of the soil profile (L)
$\bar{x}$ mean catchment value of *ln*(*α/tanβ*)
X dimensionless time
z(i) thickness of soil layer *i* (L)
z_{pdm} depth over which soil moisture is considered (L)
Z soil profile depth to bedrock (L)
Z_g ground surface elevation (L)
Z_m maximum value of profile depth to bedrock (L)
z_∇ mean water table depth (L)
z_l local water table depth (L)
z_{bot} middle point of the bottom layer (1.5.m) (L)
z_{wt} water table depth (L)
α_{an} anisotropic factor accounting for differences in Ksat between vertical and horizontal direction
α_G parameter in the Gamma distribution
α_{GA} parameter proportional to the matric potential at the wetting front
β_G parameter in the Gamma distribution
α_{AC} Miller-Miller scaling factor for final infiltration capacity
α_K decay constant in Kostiakov equation
α_s shape parameter in the spatial distribution function of soil wetness
α_{sc} Miller-Miller similarity scaling factor
α_{Sop} Miller-Miller scaling factor for sorptivity
α_{opt} single Miller-Miller scaling factor for infiltration
α_T upstream area that contributes flow through a unit contour positioned at the point or specific catchment area
α_{wf} product of the absolute value of wetting front suction head and the difference between saturated water content and initial water content at the beginning of the infiltration event
β_T slope parameter
β parameter depending on grid resolution (-)
β_K fitting parameter in the Kostiakov equation
β_s correction parameter for Ks (-)
γ parameter related to topography (-)
γ_f fraction of surface runoff (-)
$\gamma_{1,2,3}$ fitting parameters
δ_t model time step (L)
ε dimensionless error (-)

θ	volumetric soil water content (-)
θ_l	the content of liquid water (-)
θ_{ice}	the content of ice (-)
θ_i	initial water content (-)
θ_s	saturated soil water content (-)
θ_r	residual moisture content (-)
θ_{rz}	mean diagnosed root zone moisture content [-]
θ_{wilt}	water content at wilting point (-)
κ_p	related to the standard deviation of the subgrid slope (-)
κ	scaling factor needed to redistribute the GCM grid scale precipitation over the scale of precipitation events (-)
λ	wetness index (-)
λ_{sc}	characteristic length of a Miller-Miller similar porous medium (L)
λ_{crit}	critical topographic index (-)
λ_p	dimensionless pore size distribution index [-]
λ_m	mean topographic or wetness index (-)
λ_s	subgrid heterogeneity of soil (-)
λ_r	characteristic length of Miller-Miller scaling reference soil (L)
ρ	correlation coefficient between the terrain slope and the soil water content (-)
σ_{or}	standard deviation of the orography
σ_{min}	minimum standard deviation of the orography
σ_{max}	maximum standard deviation of the orography
σ_{slope}	standard deviation of the subgrid slope variability (-)
σ_θ	standard deviation of soil water content (-)
$\sigma_{S_{x_l}}$	standard deviation of local surface slopes (-)
σ_{Ks}	standard deviation of saturated hydraulic conductivity (LT^{-1})
τ	time scale of transfer of surface layer moisture into the root zone (T)
a	fraction of surface runoff

Appendix

Appendix A1: The PDM of Moore (1985)

In the PDM-based scheme (Moore, 1985) for calculating Dunne runoff, F_{sat} was described as:

$$F_{sat} = 1 - \left(1 - \frac{\langle S \rangle - S_0}{S_{max} - S_0}\right)^{b/(b+1)} \quad \text{[A1]}$$

where $\langle S \rangle$ is the grid cell mean water storage [L], S_0 is the minimum water storage below which there is no water saturation at the surface [L], $S_{max}$is the maximum possible grid cell water storage [L], and *b* is a shape parameter proposed by Moore (1985) that reflects the heterogeinity in a lumped manner (see also Eq. 64). Parameters *b* and S_o were obtained from model calibration using catchment data and S_{max} was obtained from available data and calculated from:

$$S_{max} = \theta_{sat} z_{pdm} \quad \text{[A2]}$$

where z_{pdm} (L) is the soil depth over which the soil water content is considered for PDM modelling. Clark and Gedney (2008) assumed z_{pdm} to be 1 m.

Appendix A2: Description of maximum infiltration rate in different LSMs

Note that only those models using the maximum infiltration rate in their concept will be described here and that the last number of the label (e.g., A2.**3**) referes to the number given in Table 1 to facilitate reading. Additionally, I_{max} depends on F_{sat} for those models relying on the F_{sat} approach.

A2.3 ORCHIDEE

ORCHIDEE (Ducharne et al., 2017) includes a sub-grid distribution of infiltration, which reduces the effective infiltration rate into each successive layer of the wetting front. In practice, the mean infiltrability of a layer over the grid-cell is spatially distributed using an exponential pdf, then compared locally to the amount of water that needs to infiltrate (called r_o and comprised of throughfall, potentially increased by snowmelt and ponded water). As a result, infiltration-excess runoff is produced over the fraction of the grid-cell where r_o [L T^{-1}] is larger than the local K_i^{int} [L T^{-1}] defined by the exponential distribution of mean saturated hydraulic conductivity $\langle K_i^{int} \rangle$, applying the following cumulative distribution function (cdf):

$$F\left(K_i^{int}\right) = 1 - exp^{\left(-\frac{K_i^{int}}{\langle K_i^{int} \rangle}\right)} \quad \text{[A3]}$$

K_i^{int} is calculated as the average of the actual hydraulic conductivity at the wetting front and the deepest saturated node. A spatial integration is conducted for each soil layer that becomes saturated when the wetting front propagates, giving the mean infiltration excess runoff *Re,ᵢ* produced from the saturation of each soil layer *i*:

$$R_{e,i} = r_o - K_i^{int}(1 - \exp^{(-\frac{r_o}{K_i^{int}})}) \quad \text{[A4]}$$

By reducing the effective conductivity $K_i^{int,*} = K_i^{int}(1 - exp^{(-\frac{r_o}{K_i^{int}})})$ compared to the uniform case ($K_i^{int,*} = K_i^{int}$), this sub-grid distribution increases surface runoff, given by the sum of R_i from all the layers saturated during the time step. The model also considers the mean slope of the grid-cell, with a reinfiltration of excess water only possible at low slopes. This sub-grid distribution can be seen as the opposite to the parametrization of Warrilow et al. (1986), since the actual hydraulic conductivity *K* rather than the precipitation rate is spatially distributed within the grid-cells.

A2.4 CLSM

The Catchment Land Surface Model (CLSM) (Koster et al., 2000), the land model component of the NASA Goddard Earth Observing System (GEOS-5) coupled Earth system model, does not impose a priori a maximum infiltration rate in its formulation. The amount of water that can infiltrate over a certain time at the catchment scale is a function of the model's dynamically varying spatial moisture fields. Infiltration in CLSM is considered here in two steps: (i) precipitation throughfall into the near-surface soil layer (2 or 5 cm), and (ii) the subsequent transfer of this soil water into the root zone. It is important to recognize that CLSM is designed to emphasize a description of horizontal moisture variability that is linked to the simulation of a spatially-variable dynamic water table depth. This is discussed in more detail in Section 4.1.2. In effect, the land surface area in CLSM is divided into distinct (and dynamically changing) hydrological regimes. Regarding the throughfall into the near-surface layer, all rainwater runs off the surface in the 'saturated fraction' regime, effectively as Dunne runoff and without infiltration. In recent versions of CLSM, the other two regimes (the 'subsaturated-but-transpiring' and the 'wilting' regimes) allow all precipitation water in a given time step to infiltrate, and thereby, increase the surface soil moisture, though if the layer becomes fully saturated, the excess does run off the surface, effectively as Hortonian runoff.

The transfer of surface layer moisture into the root zone is controlled by a time scale, τ [T], computed with

$\tau=a_r/(\theta_{rz}+b_r\, M_{se})^3$. [A5]

here, a_r and b_r are fitted parameters, θ_{rz} is mean diagnosed root zone moisture content [$L^3\, L^{-3}$] and M_{se} is the surface layer excess [L] (see Section 4.1.2). With this timescale defined, the water transferred from the surface layer to the root zone, ΔM_{se} [L], is

$\Delta M_{se}=-M_{se}\,\Delta t/\tau$ [A6]

The empirical equation for the timescale τ was fitted to results from high resolution (1 cm) solutions of the vertical one-dimensional Richards equation, conducted off-line prior running climate or land surface simulations. The simulations behind these offline solutions used a comprehensive set of values for the CLSM's water prognostic variables (see Ducharne et al., 2000) appropriately downscaled to 1 cm vertical resolution, and a comprehensive set of soil classes parameterized by the Campbell (1974) equations, with corresponding hydraulic parameters based on lookup tables or using the pedotransfer functions (PTFs) of Wösten et al. (2001) (de Lannoy et al., 2014).

In CLSM, catchment-scale infiltration rate decreases by two mechanisms in which the actual groundwater level is crucial: 1) the non-saturated area into which rainfall can infiltrate at the catchment scale decreases for rising water levels, i.e. higher areal fractions of the saturated regime, and 2) the hydraulic gradient between surface and root zone in the non-saturated area decreases when the root zone fills up due to infiltration and rising water levels. The combination of both mechanisms results in a dynamical prediction of catchment scale maximum infiltration rates into the surface layer that range from high values (larger than K_s) under deep water level conditions to values that drop below K_s under shallow water level conditions.

A2.5 ISBA-SURFEX

In ISBA-SURFEX (Decharme and Douville, 2006), the local maximum infiltration rates for unfrozen soil are given by:

$$I_{unf,i} = K_{s,i}\left[\frac{b_{BC}h_c}{\Delta z}\left(\frac{\theta}{\theta_s}-1\right)+1\right] \qquad \text{[A7]}$$

where h_c is the matric potential at air entry [L], θ_s is the soil porosity or saturated water content [$L^3\, L^{-3}$], b_{BC} is the pore size distribution index from the the Brooks Corey equation [-] (see Eq. [4]), Δz is the top layer soil thickness of 0.1m, and $K_{s,i}$ is the saturated hydraulic conductivity at location i [$L\, T^{-1}$]. $I_{unf,i}$

comes from the equation presented in the paper by Abramopoulos et al. (1988) for calculating infiltration and evapotranspiraton in global climate models, whereby the maximum infiltration was defined as:

$$I_{max} = K_{s,i}\left[\frac{dh_i}{d\theta_i}\bigg|_{\theta_i=\theta_s}\left(\frac{\theta_i-\theta_s}{z_i}\right)+1\right] \qquad \text{[A8]}$$

where *i* refers to the top soil layer (*i* = 1), θ_i the volumetric soil water content of top soil layer [$L^3 L^{-3}$], and z_i the thickness of this layer [L]. The mean maximum infiltration rate, $\langle I_{max}\rangle$ is used to calculate the surface runoff generated by Hortonian overland flow as:

$$q_H = \mu\left[\int_0^1\int_{f^*}^{\infty}\left(P_{x,i}-I_{unf,i}\right)f_{Px,i}\left(P_{x,i}\right)dP_{x,i}f_{unf,i}\left(I_{unf,i}\right)dI_{unf,i}\right] \qquad \text{[A9]}$$

where P_x is the incident flux reaching the the soil surface and

$$f_{unf,i}\left(I_{unf,i}\right) = \frac{1}{\langle I\rangle}e^{-I_{max,i}/\langle I_{max}\rangle} \qquad \text{[A10]}$$

where $\langle I_{max}\rangle$ is the mean maximum infiltration rate over the grid cell [L T^{-1}]. Hereby, $f_{unf,i}\left(I_{unf,i}\right)$ represents the spatial variability of the local maximum infiltration rate in a grid cell.

The parameter μ in Eq. [58] is given by:

$$\mu = 1 - e^{-\beta\langle P_x\rangle} \qquad \text{[A11]}$$

where β is a parameter depending on the grid resolution according to:

$$\beta = 0.2 + 0.5e^{-0.01dx} \qquad \text{[A12]}$$

where *dx* is the length of the grid cell in km.

Combining all equations, we obtain:

$$q_H = \frac{\langle P_x\rangle}{1+\langle I_{unf}\rangle\frac{\mu}{\langle P_x\rangle}} \qquad \text{[A13]}$$

Overall, the infiltration rate is calculated from the difference between throughfall rate and surface runoff, whereby the throughfall rate has three components, namely interception, snowmelt, and dripping from the interception reservoir.

A2.6 Noah-MP

Wang et al. (2016) defined the maximum infiltration rate, I_{max} [L T^{-1}], for a grid cell in Noah-MP as:

$$I_{max} = \frac{P_x D_x[1-\exp(-kdt\delta_t]}{P_x+[1-exp(-kdt\delta_t]} \quad \text{[A14]}$$

where δ_t is the model time step [T]. D_x is incorrectly termed by Wang et al. (2016) as soil water diffusivity, when in fact it is simply the soil water storage in length units (L), calculated as:

$$D_x = \sum_{i=1}^{4} \Delta z_i(\theta_s - \theta_i) \quad \text{[A15]}$$

and

$$kdt = kdt_{ref}\frac{K_s}{K_{ref}} \quad \text{[A16]}$$

where P_x is defined as the precipitation rate [L T^{-1}], K_s is the saturated hydraulic conductivity [L T^{-1}], θ_s and θ_i are the volumetric saturated water content and the actual water content [L^3 L^{-3}] at time step *i*, respectively. *Kdt* is a parameter in Eq. [A14], K_{dtref} is constant parameter set equal to 3.0 (-), and K_{ref} is a reference *K* value (2x10^{-6} m s^{-1}).

In Noah-MP (Niu et al., 2005, Niu et al., 2011b) I_{max} is used to calculate Hortonian excess infiltration using the following equation:

$$q_s = F_{sat}Q_{wat} + (1 - F_{sat})\max(0, (Q_{wat} - I_{max})) \quad \text{[A17]}$$

where F_{sat} is calculated from the TOPMODEL (see below), Q_{wat}[L T^{-1}] is the input of water (rainfall, snowfall, dew) and I_{max} is the maximum soil infiltration capacity calculated according to Entekhabi and Eagleson (1989), where it is defined as infiltrability.

A2.7 JULES

In the JULES model (Best et al., 2011) the maximum surface infiltration rate is defined as I_{max} = β*s* K_s, where β*s* is the enhancement factor [-], generally set equal to 0.5 for bare soil, whereas larger values are used for vegetated grid cells (4 for trees, 2 for grasses and shubs), to account for infiltration enhancing factors such as root macropores, and K_s is the saturated hydraulic conductivity [L T^{-1}]. This approach may lead to an underestimation of the infiltration rate as sorptivity forces are not taken into account and essentially all the water reaching the soil surface will infiltrate. Hortonian runoff is calculated as the difference between throughfall plus snowmelt and infiltration. Runoff can increase under certain configurations to avoid supersaturation of the upper soil layer - thus explicitly representing Dunne runoff at the point scale. If the 'large scale hydrology' scheme is used, Dunne runoff is calculated in addition to Hortonian runoff, based on the surface saturated fraction, F_{sat} (see Appendix A3), according to:

$$q_{\mathrm{dunne}} = F_{sat}\, q(t) \quad \text{[A18]}$$

where *q(t)* is the infiltration rate [L T^{-1}], which is multiplied by 1 - F_{sat} to account for this additional runoff term. Note, that ponding is not simulated.

A2.8 CLM

The Community Land Model (CLM) 4.5 version (Oleson et al., 2013) calculates the maximum soil infiltration capacity as:

$$I_{max} = (1 - F_{sat})K_s C_{ice} \qquad \text{[A19]}$$

where K_s is the saturated hydraulic conductivity [L T^{-1}] , and $C_{ice}$is an ice impedance factor [-]. Hortonian excess infiltration runoff, q_H [L T^{-1}], is generated as:

$$q_H = \max(q_{in,soil} - \left(1 - f_{h20sfc}\right)I_{max}, 0) \qquad \text{[A20]}$$

where f_{h20sfc} is the fraction of the area where ponded water exists exists and thus equals F_{sat}. Note, that Hortonian excess infiltration runoff is only generated and ponded water only occurs on the diagnosed unsaturated fraction (1-Fsat) of the soil column. $q_{in,soil}$ refers to the infiltration rate of water into the soil, defined as:

$$q_{in,soil} = \left(1 - f_{h20sfc}\right)q_{in,surface} - q_H - (1 - f_{sno} - f_{h20sfc})q_{evapo,soil} \qquad \text{[A21]}$$

and

$$q_{in,surface} = (1 - F_{sat})q_{liq,o} \qquad \text{[A22]}$$

where $q_{liq,o}$ is the water input into the grid cell [L T^{-1}] that is the sum of liquid precipitation reaching the surface and snowmelt. $q_{evapo,soil}$ [L T^{-1}] is the water loss due to evaporation, $q_{in,surface}$ [L T^{-1}] is the surface water flux after surface runoff has been removed, and $f_{sno}$is the fraction of the grid cell covered by snow.

A2.11 H-TESSEL/CH-TESSEL

In H-TESSEL (Balsamo et al., 2009) or in the more recent CH-TESSEL both based on the same hydrological principles (Boussetta et al., 2013) the maximum infiltration rate is calculated using Eq. [A23] to calculate Hortonian overland flow.

$$I_{max} = (W_{sat} - W) + max\left(0, W_{sat}\left\{(1 - \frac{W}{W_{sat}})^{\frac{1}{b+1}} - (\frac{P_T + P_M}{(b+1)W_{sat}})\right\}^{b+1}\right) \qquad \text{[A23]}$$

where P_T is the throughfall precipitation [L], P_M is the snowmelt [L] leading to P_x as the total water reaching the surface ($P_x = P_T + P_M$) [L], and W and W_{sat} [L] are the vertically integrated soil water contents (equivalent to θ and θ_s, albeit with different units) over the first 50 cm of the soil profile. The b parameter reflects the grid cell heterogeneity (see Section 4.1.2). In H-TESSEL/CH-TESSEL $q_s = P_x - I_{max}$, where q_s is surface runoff (defined as R in Balsamo et al. (2009)). Notice that the units of I_{max} are length, although it is defined as a rate in Balsamo et al. (2009).

A3 Description of the saturated water fraction *F_{sat}*

Note that only those models using the maximum infiltration rate in their concept will be described here and that the last number of the label (e.g., A3.3) referes to the number given in Table 1 to facilitate reading. As the TOPMODEL concept to calculate F_{sat} is embedded in several LSMs presented in this appendix, we briefly present the basic equations and ways to calculate basic properties.

A3.0 TOPMODEL

In the TOPMODEL approach (Niu et al., 2005) F_{sat} can be defined as:

$$F_{sat} = \int_{\lambda \geq (\lambda_m + f_d z_\nabla)} pdf(\lambda) d\lambda \qquad \text{[A24]}$$

where f_d is the decay factor (L^{-1}), which is a measure for the decline of K_s with increasing depth, z_∇ is the mean water table depth, and the local water table depth z_l is given by:

$$z_l = z_\nabla - \frac{1}{f_d}(\lambda_m - \lambda) \qquad \text{[A25]}$$

Here, the mean topographic or wetness index λ_m is defined as:

$$\lambda_m = \langle ln(\alpha_T / tan\beta_T) \rangle \qquad \text{[A26]}$$

where α_T is the specific catchment area and $tan\beta_T$ is the local surface topographic slope.

In order to calculate the average water table depth Chen and Kumar (2001) proposed an iterative procedure where D_θ is the amount of water stored between surface and groundwater:

$$D_\theta = \int_0^{z_\nabla} (\langle \theta_s(z) \rangle - \langle \theta(z) \rangle) dz \qquad \text{[A27]}$$

where the water contents $\theta_S(Z)$ and $\theta(Z)$ denote the catchment or basin average [L^3 L^{-3}]. Further, D_θ is calculated from:

$$D_\theta = \sum_{i=1}^{NLAYERS} (\theta_s - \langle \theta(z) \rangle_i) \Delta z_i \qquad \text{[A28]}$$

The water content $\theta(z)$ is calculated using e.g. the Brooks Corey equation (Eq. [4-6]) and the assumption that the soil water content profile is an equilibrium with the groundwater by:

$$\langle\theta(z)\rangle = \theta_s \left(\frac{h_c-(z_\nabla-z)}{h_c}\right)^{-1/B\prime} \qquad \text{[A29]}$$

$$\langle\theta(z)\rangle = \langle\theta_s(z)\rangle \left(\frac{h_c-(z_\nabla-z)}{h_c}\right)^{-1/B\prime} \qquad \text{[A30]}$$

where *B'* is related to the Brooks Corey exponent of the water retention characteristic and $h_c$is the pressure head at air entry [cm]. This approach was used by Niu et al. (2005) to develop a runoff-scheme for global climate models and it has also been implemented in CLM (see A3.8)

A3.3 ORCHIDEE

The ORCHIDEE model does not use F_{sat} to generate surface runoff, which is the complement of upscaled local infiltration rates (see A2.3). In constrast, it uses the concept of ponded fraction, to reduce surface and enhance infiltration. A fraction of surface runoff, γ_f, is allowed to pond in flat areas, and it is kept to be infiltrated at the following time step with throughfall and snowmelt, to account for the effect of ponding on infiltration (d'Orgeval et al., 2008). This fraction γ is constant over time, but varies spatially, based on the mean slope *Sl* in the grid-cells and a threshold slope Sl_{max} (with a default value of 0.5%), such that the ponding fraction decreases from 1 when *Sl* = 0 to 0 when $Sl \geq Sl_{max}$:

$$\gamma_f = 1 - \min(1, Sl/Sl_{max}). \qquad \text{[A31]}$$

This leads to reduce grid-scale surface runoff by γ_f.

A3.4 Catchment Land Surface Model (CLSM)

In the Catchment Land Surface Model, the saturated land fraction at equilibrium conditions is effectively computed as the fraction of the area for which the water table depth lies “above” the ground surface, based on the TOPMODEL framework. The strategy for calculating the saturated land fraction was described above in Section 4.1.2.

A3.5 ISBA-SURFEX

In the ISBA-SURFEX model, the saturation excess runoff can also be computed using the TOPMODEL assumption instead of using the Arno scheme. So, only Dunne runoff is affected by F_{sat} (Decharme and

Douville, 2006) and it is described according to a corrected approach of the original TOPMODEL framework proposed by Saulnier and Datin (2004) and written as:

$$q_D = P_x F_{sat} \qquad [A32]$$

where F_{sat} is defined as the saturation fraction of a grid cell, being inversely proportional to the mean water storage deficit, D_t, of the grid cell, whereby D_t can be written as:

$$D_t = (\theta_s - \langle\theta\rangle)\langle d_2\rangle \qquad [A33]$$

D_t is bounded between 0 and d_o, the maximum local water deficit defined by:

$$d_o = (\theta_s - \theta_{wilt})\langle d_2\rangle \qquad [A34]$$

where θ_s and $\langle\theta\rangle$ are the saturated and mean volumetric water content averaged over the depth d_2 [L] at grid scale [L^3 L^{-3}] that can be, optionally, the depth of the entire root zone (Decharme and Douville, 2006) or the depth of the layer in which the cumulated root profile reached 90% (Decharme et al., 2013) and θ_{wilt} is the water content at wilting point [L^3 L^{-3}]. Hereby, D_t will be d_o when $F_{sat} = 0$ or vice versa

A3.6 Noah, Noah-MP

In this section we briefly describe the way infiltration is handled in NOAH and then present Noah-MP and the approaches used to calculate F_{sat}.

In the NOAH model (Schaake et al., 1996), the spatially averaged actual infiltration rate, *Ir*, depends on the cumulative infiltration capacity ($I_{c,t}$) at a certain moment in time *t*. $I_{c,t}$ is expressed as:

$$I_{c,t} = D_b[1 - \exp(-K_{dt}\Delta t] \qquad [A35]$$

where Δt is the model time step, K_{dt} is a constant, and D_b represents the spatially averaged soil water storage for the whole soil column. D_b in each soil layer is computed by:

$$D_b(i) = D_{bmax}(\mathrm{i})(1 - \frac{\theta_l(\mathrm{i}) + \theta_i(\mathrm{i}) - \theta_{wilt}(\mathrm{i})}{\theta_s(\mathrm{i}) - \theta_{wilt}(\mathrm{i})}) \qquad [A36]$$

where D_{bmax}(i), $\theta_l(\mathrm{i})$, $\theta_i(\mathrm{i})$, $\theta_{wilt}(\mathrm{i})$ and $\theta_s(\mathrm{i})$ are the maximum soil water storage, the content of liquid water and ice, wilting point, and soil porocity or saturated water content in soil layer *i*, respectively. D_{bmax}(*i*) is defined by the following equation:

$$D_{bmax}(i) = -\mathrm{z}(\mathrm{i})(\theta_s(\mathrm{i}) \; - \theta_{wilt}(\mathrm{i}) \,) \qquad [A37]$$

where z(*i*) is the thinkness of soil layer *i*.

Then, the infiltration rate for the whole soil column is given by:

$$I_r = (\frac{P_R * I_{c,t}}{P_R + I_{c,t}})/\Delta t \qquad [A38]$$

where *PX* is the precipitation input into the whole column.

Soil freezing has significant effect on the permeability of soils because ice impedes the infiltration rate. Noah computs the impermeable area factor *FC* to consider freezing influence on soil infiltration following Koren et al. (1999).

Soil freezing has significant effect on the permeability of soils because ice impedes the infiltration rate. Noah computs the impermeable area factor *FC* to consider freezing influence on soil infiltration following Koren et al. (1999).

Noah-MP is an improved version of Noah (Niu et al., 2011b), whereby Noah-MP (Niu et al., 2011b) offers four options for computing infiltration and surface-subsurface runoff. Option 1 is the TOPMODEL-based runoff scheme with the simple groundwater scheme (Niu and Yang, 2007) implemented by Cai et al. (2014), where the fraction of the gridbox that is saturated, F_{sat}, is given by:

$$F_{sat} = \left(1 - F_{frz}\right) F_{max} e^{-0.5 f_d (z_{\mathrm{wt}} - z_{bot})} + F_{frz} \qquad [A39]$$

where z_{bot} is the soil profile thickness (default = 2.0 m), z_{wt} (L) is the water table depth, F_{max} is set to a global mean value of 0.38, and F_{frz} is the fraction of impermeable area as a function of soil ice content of the surface soil layer. At urban areas F_{frz} is set to 0.95. The runoff decay factor, f_d, in Eq. [A39] equals 6 m^{-1}.

Option 2 is a simple TOPMODEL-based runoff scheme with an equilibrium water table (Niu et al., 2005). Like in Option 1, this scheme parameterizes both surface and subsurface runoff as functions of the water table depth but with a sealed bottom of the soil column (zero-flux lower boundary condition) in accordance with one of the TOPMODEL assumptions, i.e., the exponential decay of saturated hydraulic conductivity, F_{sat} is calculated as:

$$F_{sat} = \left(1 - F_{frz}\right) F_{max} e^{-0.5 f_d z_{\mathrm{wt}}} + F_{frz} \qquad [A40]$$

here, f_d is set to 2.0 m^{-1}.

Option 3 is an infiltration-excess-based surface runoff scheme with a gravitational free-drainage subsurface runoff scheme as used in the original Noah (Schaake et al., 1996). Surface runoff (R) is computed as the excess of precipitation (P_d) not infiltrated into the soil ($R = P_d - I_{max}$). The maximum infiltration rate, I_{max}, is computed as:

$$I_{max} = P_d \frac{D_x\left(1-e^{-kdt\Delta t}\right)}{P_d+D_x\left(1-e^{-kdt\Delta t}\right)} \qquad \text{[A41]}$$

with

$$D_x = \sum_{i=1}^{N} \Delta z_i(\theta_s - \theta_i) \qquad \text{[A42]}$$

and

$$kdt = kdt_{ref} \frac{K_S}{K_{ref}} \qquad \text{[A43]}$$

where Δt is the time step (T), and K_S (L T^{-1}) is the saturated hydraulic conductivity, which depends on soil texture and is prescribed in a lookup table. The symbol N stands for the number of layers. The parameters kdt_{ref} = 3.0 and K_{ref} = 2 x 10^{-6} m s^{-1} were determined in the framework of the PILPS2(c) experiments for the Red-Arkansas River basins in the Southern Great Plains region of the United States (Wood et al., 1998).

Finally, option 4 is the BATS runoff scheme, which parameterizes surface runoff as a 4^{th} power function of the top 2 m soil wetness (expressed as degree of saturation) and subsurface runoff as gravitational free drainage (Yang and Dickinson, 1996) described by:

$$F_{sat} = \left(1 - F_{frz}\right)\left(\frac{\theta_{tot}}{\theta_s}\right)^4 + F_{frz} \qquad \text{[A44]}$$

with

$$\theta_{tot} = \frac{1}{z_{bot}} \sum_{i=1}^{N} \Delta z_i \theta_i \qquad \text{[A45]}$$

A3.7 JULES

There are two options in JULES to account for spatial heterogeneity of soil water content and thus determine F_{sat}. The first option is based on a modified form of the TOPMODEL (Beven and Kirkby, 1979), described by Gedney and Cox (2003), where the assumption of an exponential decay of K_s with depth (leading to Eqs [A24-A25]) is relaxed. Gridbox mean water table depth, z_∇, is calculated using the approach described in A3.0 (Eqs [A27-A29]). This is used to estimate a critical topographic index λ_{crit} using the relation:

$$\lambda_{crit} = ln(\,T(0)\,/\,T(z_{\nabla})\,)\, + \lambda_m \qquad [A46]$$

where transmissivity $T(z_{\nabla})$ is given by:

$$T(z_{\nabla})\; = \int_z^{\infty} \quad K_s(z)\,dz \qquad [A47]$$

F_{sat} is then calculated as the fraction of the gridbox for which $\lambda > \lambda_{crit}$, assuming λ follows a gamma distribution with mean (λ_m) and standard deviation read in from observational datasets. In order to speed up the computation, the integral over the probability distribution of λ is calculated for a range of mean water table depths during model initialisation, and approximated by an exponential function by:

$$F_{sat} = a_s exp\,(-c_s\lambda_{crit}) \qquad [A48]$$

where a_s and c_s are fitted to approximate the full integral (i.e. Eq. [A24]). Recently, this scheme has been modified to account for the impact of frozen water in the soil by replacing K_s in Eq. [A49] by $(1\text{-}\theta_f)^{2b+3}K_s$ (where b is the Brooks-Corey parameter ,and θ_f is the frozen water content) and additionally correcting the gridbox mean water table depth (z_{∇}) to account for the fact that the profile of soil moisture above the water table will not follow the same equilibrium profile (assumed in Eq. [A29]) when ice is present. The second option for calculating F_{sat} is the use of the probability distributed model of Moore (1985) (see Eq. [38]).

A3.8 CLM 4.5

In CLM 4.5 (Lawrence et al., 2011, Oleson et al., 2013), the fraction of the saturated area, F_{sat} is calculated by:

$$F_{sat} = F_{max} exp(-0.5 f_d z_{\nabla}) \qquad [A49]$$

where F_{max} is the maximum value of F_{sat} and f_d is the decay factor (L^{-1}) F_{max} is defined as the fraction of sub-grid cells from a high-resolution digital elevation map (DEM) in a grid cell whose topographic index (the ratio of the upstream area to the slope, Niu et al. (2005)) is larger than or equal to the grid cell mean topographic index. It is the value of the discrete cumulative distribution function (CDF) of the topographic index when the grid cell mean water table depth is zero.

A3.9 CABLE

The original CABLE model (version 2, Kowalczyk et al., 2013) generates surface runoff from excess infiltration only when the first three soil layers are at least 95% saturated. There is no other surface runoff generation process. However, Decker (2015) implemented subgrid-scale soil water content variability, explicit runoff generation and ground water in CABLE. The fraction of the saturated area, F_{sat}, follows Entekhabi and Eagleson (1989) and is defined as:

$$F_{sat} = \int_{\kappa_p}^{\infty} f(s) ds \qquad \text{[A50]}$$

where *f(s)* is the Gamma-distribution of Eq. [42], and κ_p is defined by Eq. [A53]. One can solve this integral assuming a constant α_c in Eq. [42], which then links $s = \frac{\langle\theta\rangle - \langle\theta_r\rangle}{\langle\theta_s\rangle - \langle\theta_r\rangle}$, the mean of the vertically averaged relative saturation over the grid cell, with λ_s due to the properties of the Gamma-distribution (Eq. [42]):

$$\lambda_s = \frac{1}{2s} \qquad \text{[A51]}$$

For α_c = ½, one gets:

$$F_{sat} = 1 - erf\left(\sqrt{\frac{\kappa_p}{\lambda_s}}\right) \qquad \text{[A52]}$$

Finally, κ_p is parameterized by an empirical formulation as:

$$\kappa_p = C_v \sigma_{slope} \qquad \text{[A53]}$$

with C_v as a fitting parameter and σ_{slope} as the standard deviation of the subgrid slope.

Haverd et al. (2016) and Cuntz and Haverd (2018) recently implemented a new soil (Haverd and Cuntz, 2010b) and snow model with physically accurate freeze-thaw processes within CABLE, which is currently combined with the developments of (Decker, 2015).

A3.10 SSiB

In SSiB the model, the normalized runoff I_{roff} is spatially distributed as a function of fractional area of grid area x, (0 < x < 1) (Sato et al., 1989):

$$I_{roff}(x) = a_{SSiB} e^{-b_{SSiB} x} + c_{SSiB} \qquad \text{[A54]}$$

where a_{SSiB}, b_{SSiB}, c_{SSiB} are constants. This distribution has also been applied to the convective precipitation. The constants (*a*, *b*, and *c*) were obtained by comparison with the observational data and are normalized so that:

$$\int_0^1 I_{roff}(x) dx = 1 \qquad \text{[A55]}$$

Based the above two spatial distributions, the saturation fraction, F_{sat}, could be obtained (Sato et al., 1989) as:

$$F_{sat} = \frac{1}{b_{SSiB}} log\left(\frac{K_s \Delta t}{P_{drop} a_{SSiB}}\right) - \frac{c_{SSiB}}{a_{SSiB}} \qquad \text{[A56]}$$

where K_s is the saturated hydraulic conductivity [L T^{-1}], Δt is time interval [T], and P_{drop} is the precipitation reaching the surface after interception by canopy [L T^{-1}]. The spatial distribution of convective precipitation has also been applied to obtained the P_{drop} (Sellers et al., 1996).

A3.12 JSBACH

JSBACH uses the original Arno scheme (Dümenil and Todini, 1992) to determine surface runoff and infiltration. Accordingly, the saturated fraction is estimated for the grid box fraction for which soil water capacity of the rootzone is less than or equal to the gridbox mean rootzone soil moisture. The shape parameter *b* is being determined using Eq. [46].

A3 Use of PTF for the estimation of K_s

For soils with low organic carbon content, Noah-MP, and CLM 4.5 use the PTFs developed on point scale by Clapp and Hornberger (1978) and Cosby et al. (1984) to estimate K_s. In ISBA-SURFEX, K_s is related to the soil textural properties (clay and sand) using the Noilhan and Lacarrère (1995) continuous relationships derived from theses PTFs. These PTFs are basically class PTFs (Van Looy et al., 2017) that give average values of Brooks Corey parameters and the measured K_s for each textural class of the USDA classification and are also developed on point scale.

Soil classes in CLSM are parameterized by Campbell (1974) equations and the corresponding hydraulic parameters including K_s are based on lookup tables for twelve different soil textural classes or using the PTFs of Wösten et al. (2001), which are both developed on point scale. Campbell's method used the Brooks-Corey parameterization of the soil water retention curve and a single point measurement of *K* at a given water content to calculate the complete hydraulic conductivity function.

None of the models directly considers the effect of soil structure on saturated hydraulic conductivity. Only the OLAM-SOIL considers implicitly the impact of structural properties on K_s by linearly interpolating between the measured K_s value and the value of the hydraulic conductivity obtained at a pressure head of about -6 cm as proposed by Weynants et al. (2009). Based on the work of Jarvis (2007) this value was considered to delineate the saturation range that is controlled by structural properties.

In JSBACH, K_s values are assigned to 11 textural classes based on data presented in Beringer et al. (2001). However, the origin of the tabulated K_s values that appear to be mean measured values for a specific textural class is not clear. Most likely, they were derived from the dataset of Clapp and Hornberger (1978).

JULES uses sand and clay content to estimate the saturated hydraulic conductivity for the main soil column. Below the soil column is an additional `deep water store', within which K_s decreases exponentially with depth with a dampening factor set equal to 3 as proposed by Clark and Gedney (2008). K_s values can also be defined for each soil layer and can account for the presence of soil organic matter (Chadburn et al., 2015a). Rahman and Rosolem (2017) incorporated the effect of preferential flow into JULES (but note that this has not yet been adopted in the current 'official' UKMO version of JULES), to allow simulation of highly fractured unsaturated Chalk soils. Their bulk conductivity (BC) model introduces only two additional parameters (namely the macroporosity factor and the soil wetness threshold parameter for fracture flow activation) and uses the saturated hydraulic conductivity from the chalk matrix. The BC model was implemented into JULES and applied to a study area encompassing the Kennet catchment in the southern UK and the model performance at the catchment scale was evaluated against independent data sets (e.g., runoff and latent heat flux). The results demonstrated that the inclusion of the BC model in JULES improved the simulations of land surface water and energy fluxes over the chalk-dominated Kennet catchment. This simple approach to account for soil structure has potential for large-scale land surface modelling applications. ORCHIDEE uses VG soil parameters (K_s, n, α, θ_r, and θ_s) for each USDA class. In addition, a decay of K_s with depth is imposed (as also in JULES), as written in Appendix A2.7. With respect to the horizontal variability, ORCHIDEE uses an exponential PDF to describe horizontal heterogeneity.